

Theoretical and Experimental Investigations on Integrity Assessment of Pipes and Elbows

From the Faculty of Mechanical Engineering of the University of Stuttgart
for the attainment of the Honour of a Doctorate of Engineering Sciences
(Dr.-Ing.) Treatise Approved

Presented by
Jayanta Chattopadhyay, M.Tech., India

Main assessment :	Prof. Dr.-Ing.habil E.Roos
Second assessment :	Prof. Dr.-Ing. U.Gampe
Date of Oral Examination :	16 th November 2004

2004
Materials Testing Institute (MPA), University of Stuttgart

Preface

This work has been carried out by me while working as Scientific Officer in Bhabha Atomic Research Centre (BARC), Mumbai, India in collaboration with MPA, Stuttgart, Germany. I convey my acknowledgement to the concerned authorities in BARC and University of Stuttgart for granting me the permission to pursue Doctorate of Engineering in the University of Stuttgart under the Indo-German bilateral project.

I am extremely grateful to Prof. Dr.-Ing habil Eberhard Roos, Director, MPA, University of Stuttgart for helping me in every possible way to complete my Doctorate. Without this, my Doctorate would never have been possible.

I am thankful to Prof. Dr.-Ing. U.Gampe, University of Dresden for assessing my doctoral thesis.

I am also grateful to Mr. H.S.Kushwaha, Director, Health, Safety and Environment Group, BARC, India who has also helped in every possible way to facilitate my Doctorate.

I am thankful to Dr.U.Eisele, Dr.H.Silcher, Dr.K.Kerkhof, Dr.K.-H.Herter, Ms.S.Bisinger, Ms.C.Crane, Mrs.E.Kosthaus, all from MPA, Stuttgart for helping me in various ways during my stay here.

I am thankful to Dr. A.K.Ghosh, Head, Reactor Safety Division (RSD), BARC, India and Dr.B.K.Dutta, Head, Computational Mechanics Section , RSD, BARC for their help.

I am also thankful to my colleague Mr. T.V.Pavankumar, RSD, BARC for helping in some finite element analysis work, Dr. D.S. Ramachandra Murthy and his staff at Structural Engineering Research Centre (SERC), India for helping in experimental work.

I am immensely indebted to my mother Mrs. Mira Chattopadhyay and Late father Mr. Hrishikesh Chattopadhyay for their inspiration and encouragement throughout the course of my education including this Doctorate.

Last but not the least, I am extremely grateful to my wife, Mrs. Seema Chattopadhyay for her constant encouragement throughout the course of this Doctoral work, which has seen lots of ups and downs. Thanks also to my 5½ year old son, Upamanyu Chatterjee for inspiration through his innocence.

November, 2004

Jayanta Chattopadhyay

CONTENTS

Nomenclature	...	1
Abstract	...	5
Kurzfassung	...	8
1. Introduction	...	23
1.1 Problem definition	...	24
1.2 Aim of the present Work	...	25
2. Literature Review	...	26
2.1 Leak-Before-Break Concept and Integrity Assessment of Piping Components	...	27
2.2 Limit load of Un-cracked Pipes and Elbows	...	29
2.2.1 Limit load of un-cracked pipe	...	31
2.2.2 Limit load of un-cracked elbow	...	32
2.3 Integrity Assessment of Piping Components with Cracks	...	35
2.3.1 Elastic-plastic fracture mechanics methodology	...	36
2.3.2 Limit load equations of cracked pipes and elbows	...	40
2.3.2.1 Straight pipe	...	40
2.3.2.2 Elbow	...	42
2.3.3 Transferability of specimen fracture resistance data to components	...	42
2.4 Determination of J-R Curve from Experimental Data: η_{pl} and γ Functions	...	44
2.5 Measurement of Crack Growth during Fracture Experiment	...	49
3. Theoretical Investigations	...	52
3.1 Closed-form Collapse Moment Equations of Un-cracked Elbows Subjected to Combined Internal Pressure and In-plane Bending Moment	...	53

3.1.1	Scope of the work	...	53
3.1.2	Finite element analysis	...	53
3.1.2.1	Geometry	...	54
3.1.2.2	Material	...	55
3.1.2.3	Loading	...	55
3.1.2.4	Definition of collapse moment	...	56
3.1.2.5	Finite element model	...	57
3.1.3	Results and discussion	...	58
3.1.3.1	Moment versus end rotation curves	...	58
3.1.3.2	Variation of collapse moment with internal pressure	...	61
3.1.3.3	Variation of collapse moment with elbow factor	...	63
3.1.3.4	Deformed shape of elbow cross section	...	63
3.1.3.5	Proposed closed-form equations	...	65
3.1.3.6	Comparison of closed-form equation prediction with available results	...	66
3.2	Derivation of Limit Load Based General Expression of ' η_{pl} ' and ' γ ' Functions and Evaluating New ' η_{pl} ' and ' γ ' Functions for Piping Components	...	69
3.2.1	Scope of the work	...	69
3.2.2	Derivation of limit load based general expression of ' η_{pl} ' and ' γ ' functions	...	70
3.2.3	Validation of proposed general expression : Derivation of available ' η_{pl} ' and ' γ ' functions	...	73
3.2.3.1	TPB specimen	...	73
3.2.3.2	Pipe with throughwall circumferential crack under 4 point bending	...	73
3.2.3.3	Pipe with throughwall circumferential crack under axial tension	...	75
3.2.3.4	Pipe with constant depth part-throughwall circumferential crack under axial tension	...	76
3.2.4	Evaluation of new ' η_{pl} ' and ' γ ' functions for various geometry and loading condition	...	78
3.2.4.1	Throughwall circumferentially cracked thick pipe under combined bending and tension	...	78
3.2.4.2	Pipe with constant depth part-throughwall circumferential crack under combined bending moment and axial tension	...	82

3.2.4.3	Pipe with semi-elliptical part-through circumferential crack under axial tension	... 86
3.2.4.4	Pipe with semi-elliptical part-through circumferential crack under combined bending and axial tension	... 87
3.2.4.5	Pipe with full circumferential part-through crack under axial tension	... 88
3.2.4.6	Elbow with throughwall circumferential crack under in-plane bending moment	... 90
3.2.4.7	Elbow with throughwall axial crack under in-plane bending moment	... 93
3.2.4.7.1	Long radius elbow	... 93
3.2.4.7.2	Short radius elbow	... 96
3.3	Studying the Possibilities to Improve the Experimental Crack Growth Measurement	... 100
3.3.1	Scope of the Work	... 100
3.3.2	Methodology	... 101
3.3.2.1	TPB specimen	... 101
3.3.2.2	Straight pipe	... 102
3.3.3	Finite element analysis	... 103
3.3.3.1	TPB specimen	... 104
3.3.3.2	Straight Pipe	... 105
3.3.4	Results and discussion	... 108
3.3.4.1	TPB specimen	... 108
3.3.4.2	Straight Pipe	... 111
4.	Experimental Investigation	... 115
4.1	Experiments on Small Specimen	... 116
4.1.1	Scope of the work	... 116
4.1.2	Geometry of the specimen	... 116
4.1.3	Tensile properties	... 117
4.1.4	Fracture properties	... 119
4.2	Fracture Experiments on Full Scale Piping Components	... 120
4.2.1	Scope of the work	... 120

4.2.2	Fracture tests on straight pipes	... 121
4.2.2.1	Test specimens	... 121
4.2.2.2	Test arrangement	... 122
4.2.2.3	Instrumentation and data acquisition	... 123
4.2.2.4	Pipe fracture test results	... 124
4.2.3	Fracture tests on elbows	... 126
4.2.3.1	Test specimens and set-up	... 126
4.2.3.2	Experimental results	... 130
5.	Numerical and Theoretical Analysis of Experimental Results	... 133
5.1	Finite Element Analysis of TPB Specimens, Pipes and Elbows	... 134
5.1.1	Finite element model	... 134
5.1.2	Material parameters	... 137
5.1.3	Finite element analysis results	... 138
5.1.3.1	Load-deflection curves	... 138
5.1.3.2	Evaluation of stress triaxiality ahead of crack and transferability of J-R curve	... 140
5.2	Comparison of Crack Initiation Load	... 141
5.3	J-integral-Tearing Modulus (J-T) Analysis of Pipe Fracture Experimental Data	... 142
5.4	Limit Load Analysis	... 145
5.4.1	Carbon steel pipes	... 145
5.4.2	Carbon steel elbows	... 147
5.5	Determination of Component J-R Curve	... 148
5.5.1	Straight pipe with throughwall circumferential crack	... 148
5.5.2	Elbow with throughwall circumferential crack	... 149
6.	Integrity Assessment of Pipes and Elbows : Recommended Methodology	... 151
7.	Conclusions	... 155
8.	References	... 158
9.	Curriculum Vitae	... 167

NOMENCLATURE

a	Crack length per crack tip for through wall crack and crack depth for part-through crack
a_o	Initial crack length per crack tip for through wall crack and initial crack depth for part-through crack
A	Crack area
D	Outer diameter of pipe/elbow cross section
D_m	Mean diameter of pipe/elbow cross section
D_N	Nominal pipe diameter
E	Young's modulus
F_L	Limit load
h	$= tR_o/R^2$, Elbow factor or pipe bend characteristics
J	Total J-integral
J_{app}	Applied J-integral
J_e	Elastic component of total J-integral
J_i	Initiation toughness from stretched zone width
J_{Ic}	Initiation toughness from ASTM blunting line equation
J_{mat}	Material J-resistance (J-R)
J_p	Plastic component of total J-integral
m	$= M/M_L$, Normalised moment
M	Total applied moment
M_c	Critical moment which is lower of unstable ductile tearing and limit moment
M_L	Limit moment (collectively used to define instability or collapse moment)
m_L	$= M_L/4R^2t\sigma_y$, Normalised limit moment

P	Total applied load
P_r	Internal pressure
p	$= P_r R / t \sigma_y$, Normalised internal pressure
R	Mean radius of pipe/elbow cross section
R_i	Inside radius of pipe/elbow cross section
R_o	Outside radius of pipe/elbow cross section
R_b	Bend radius of elbow at crown
R_{bi}	Bend radius of elbow at intrados
R_{bo}	Bend radius of elbow at extrados
s	$= \frac{T}{2\pi R t \sigma_f}$ = Normalised axial tension
t	Wall thickness of pipe/elbow
T	Axial tension in pipe
T_{app}	Applied tearing modulus
T_{mat}	Material tearing modulus
U	Strain energy
U_{pl}	Plastic Strain energy
x	$= a/t$ for part-through crack

Greek Symbols

α	Half axial crack angle in elbow
α_o	Initial half axial crack angle in elbow
Δ	Total load-line-displacement
Δ_{pl}	Plastic load-line-displacement

ϕ_{pl}	Plastic load-point rotation
γ	A function to correct the J-integral evaluated by ' η ' function in crack growth situation
η	A function to multiply the area under the load vs. load-point-deflection curve to get the J-integral
η_{pl}	A function to multiply the area under the load vs. plastic load-point-deflection curve to get the plastic component of the J-integral
λ	Normalized unloading compliance
ν	Poisson's ratio
θ	Half circumferential crack angle
σ_y	Material yield stress
σ_f	Material flow stress defined as the average of yield and ultimate strength
ζ	$=t/R_o$

Abbreviations

BWR	Boiling Water Reactor
CMOD	Crack Mouth Opening Displacement
CT	Compact Tension
DEGB	Double Ended Guillotine Break
ECCS	Emergency Core Cooling System
J-T	J-integral – Tearing Modulus
LBB	Leak-Before-Break
LVDT	Linear Variable Displacement Transducer
NB	Nominal Bore diameter
NDE	Non-Destructive Examination

OD	Outer Diameter
PWR	Pressurized Water Reactor
PHWR	Pressurized Heavy Water Reactor
SIF	Stress Intensity Factor
TPB	Three Point Bend
USNRC	United States Nuclear Regulatory Commission
UTS	Ultimate Tensile Strength

Abstract

Integrity assessment of piping components is very essential for safe and reliable running of both conventional and nuclear power plants. It is especially important for nuclear power plants because the concept of leak-before-break (LBB) is now widely used to design the primary heat transport (PHT) piping system of nuclear power plants. The LBB concept basically demonstrates through fracture mechanics analysis that there is negligible chance of any catastrophic break of PHT pipes without giving prior indication of leakage. This involves detailed fracture mechanics studies of different piping components such as straight pipes, elbows and branch tees. LBB is ensured by demonstrating three levels of safety assessment against sudden Double Ended Guillotine Break (DEGB). Therefore, the application of LBB concept involves detailed integrity assessment of piping components with the postulated cracks subjected to maximum credible loading condition.

There are various issues in the integrity assessment of piping components that are unresolved or partially resolved and require experimental/analytical investigation. These issues include non-availability of closed-form collapse moment equation of elbows under combined internal pressure and bending moment, non-availability of general ' η_{pl} ' and ' γ ' functions to evaluate J-R curves from experimental data, measurements of crack growth in fracture experiments, transferability of the specimen fracture properties to component level and choice of proper failure stress in limit load analyses of pipes for quick and conservative design. The present work aims to address these issues.

The overall aim of this investigation is to define improved fracture assessment methods in order to better quantify the safety and integrity assessment of piping components and thus allow an optimised and economical operation of piping system.

This overall aim is achieved by doing the following analytical and experimental work :

Analytical Work

- Elbow is an important component in the piping system. It is very important to know the collapse load of elbow, because, the service load must be lower than the collapse load with a well-defined safety margin. The existing collapse moment equations of elbows are applicable for pure bending moment whereas the actual service load is often the combined internal pressure and bending moment. No collapse moment equation was available for this combined loading. In the present work, closed-form collapse moment equations have been proposed for elbow subjected to combined internal pressure and in-plane closing/opening bending moment through non-linear finite element analysis. The predictions of these new equations are consistent with the test data.
- Material fracture resistance (J-R curve) is an important input to all elastic-plastic fracture analyses of structures. J-R curve is evaluated through fracture test of the concerned specimen/component. However, J-integral cannot be directly measured in experiments. One evaluates J-integral from the test data of load vs. deflection and load vs. crack growth through ' η_{pl} ' and ' γ ' functions. These ' η_{pl} ' and ' γ ' functions are available in the literature for very limited geometry and loading conditions. No direct method is available to get these functions. In this work, a new limit load based general expression of ' η_{pl} ' and ' γ ' have been proposed to evaluate J-R curve from test results of load-deflection and load-crack growth data. It has been verified by deriving all the existing ' η_{pl} ' and ' γ ' functions. The implication of these new equations is that for any new specimen geometry and loading condition for which limit load formula is available, specimen/component J-R curve can be obtained from test data. Also new ' η_{pl} ' and ' γ ' functions for piping components with various crack configurations under different loading conditions have been derived.
- Crack growth measurement is one of the important tasks in any fracture experiments. There are various methods, for example, potential drop,

compliance and image processing techniques for this measurement. Compliance technique is quite common for crack growth measurement in small specimens for J-R tests. However, one equation correlating the unloading compliance with the crack length is a pre-requisite for this technique. The effect of deformation on the unloading compliance correlation has been investigated for accurate measurement crack growth during fracture tests. It has been shown that deformation of pipe significantly changes the compliance correlation and must be accounted for. However, it has also been shown that this effect is not so significant for the commonly used ASTM three point bend bar (TPBB) specimen.

Experimental Work

- Fracture tests have been carried out on full size (200 – 400 mm diameter) pipes and elbows with through wall circumferential cracks. Load, load-line-displacement and crack growth have been measured during these experiments. From these data, component J-R curve have been evaluated using the newly developed ' η_{pl} ' and ' γ ' functions.
- Tensile tests have been carried out on small tensile samples machined from these tested pipes to evaluate the pipe/elbow material tensile properties.
- Small TPBB specimens have also been machined from these tested pipes to conduct fracture tests and evaluate the small specimen J-R curve.
- Finally, elastic-plastic finite element analyses have been carried out on these tested specimens and components to evaluate the stress triaxiality (quantified by ' q ' parameter) ahead of crack tip and it has been shown that if stress triaxialities of specimen and component match, small laboratory specimen J-R curve can be transferred to full size real components.

Finally, with these new findings, the improved integrity assessment procedure of pipes and elbows have been proposed.

Kurzfassung

Einleitung

Rohrleitungen und Druckbehälter sind wesentliche Komponenten in thermischen Kraftwerken. Je nach Kraftwerkstyp wird in ihnen der Dampf erzeugt und generell zur Turbine transportiert, um durch Antrieb des Generators elektrische Energie zu erzeugen. In Kernkraftwerken sind sie darüber hinaus ein wesentliches Element der Kühlung des Kernes. Die Sicherheitsbewertung von Rohrleitungskomponenten ist somit für einen sicheren und zuverlässigen Betrieb konventioneller Kraftwerke und Kernkraftwerke von großer Bedeutung.

Dies ist besonders wichtig für Kernkraftwerke, bei denen die Kühlung unter allen Betriebs- und Störfallbedingungen aufrecht erhalten, d. h. der Abriss einer Rohrleitung vermieden werden muss. Hierfür wurde das Leck-vor-Bruch Konzept entwickelt. Das Leck-vor-Bruch Konzept bedeutet, dass Rohrleitungen und Druckbehälter nicht bersten, sondern lediglich durch Leckage versagen. Dies ist von besonderer Bedeutung, da damit die beim Bersten derartiger Komponenten möglichen Sekundärschäden ausgeschlossen werden können.

Dem Versagen voraus geht die Entstehung eines Risses, der nun je nach Werkstoff und Belastung begrenzt bis zum Leck oder unbegrenzt bis zum Abriss, d. h. Bruch, wachsen kann. Der Nachweis dieses sogenannten Leck-vor-Bruch Verhaltens erfolgt mit bruchmechanischen Ansätzen oder mit Grenzlastbeziehungen, deren Gültigkeit und Anwendbarkeit experimentell nachgewiesen werden muss. Die Erstellung und Verbesserung eines derartigen Nachweises für spezifische Komponenten ist Inhalt der vorliegenden Arbeit.

Problemstellung

Hinsichtlich der Sicherheitsabschätzung von Rohrleitungskomponenten verbleiben immer noch offene Teilfragen, die weitere experimentelle und analytische Untersuchungen erfordern.

Die Rohrleitungsbogen bzw. Rohrbogen sind wichtige Komponenten eines Rohrleitungssystems. Daher ist es sehr wichtig, dass man über geschlossene Beziehungen zur Bestimmung der Grenzbelastung umfassende Kenntnisse

besitzt, um die Rohrleitungssysteme schnell, sicher und benutzerfreundlich auszulegen bzw. zu analysieren. Die derzeit verfügbaren Beziehungen sind für reine Biegemomentbelastung zutreffend. Ein Rohrbogen ist aber in der Praxis in der Regel einer kombinierten Belastungen aus Innendruck und Biegemoment ausgesetzt. Dies bedeutet konservative Abschätzungen mit erhöhten Sicherheitsfaktoren.

Da die verwendeten Werkstoffe duktil sind, muss die elastisch-plastische Bruchmechanik oder eine entsprechende plastische Grenzlastbeziehung für die Sicherheitsbewertung dieser Rohrleitungen eingesetzt werden. Für eine elastisch-plastische Bruchmechanikanalyse werden Bruchmechanikennwerte benötigt, die den Beginn des Risswachstums charakterisieren und an J-Integral basierten Risswiderstandskurven (J-R-Kurven) abgeleitet werden. Die J-R Kurven werden gemäß Regelwerken (z. B. ASTM E-1820) i. Allg. an Kompaktzugproben (Compact-Tension, CT) und Dreipunkt-Biegeproben (Three-Point-Bend, TPB) durchgeführt und ausgewertet. Anfangs wurde angenommen, dass die so ermittelte J-R-Kurve eine Materialeigenschaft darstellt, die nur vom Werkstoff abhängig ist. Jedoch zeigten weiterführende Analysen, dass sich in realen Bauteilen andere J-R-Kurven einstellen. Dies wird auf den Spannungszustand in der Umgebung der Rissspitze zurückgeführt, d. h. es wurde erkannt, dass die J-R-Kurve nicht nur vom Werkstoff abhängig ist, sondern auch von der Mehrachsigkeit des Spannungszustandes in der Rissspitzenumgebung. Aus diesem Grund ist die Übertragbarkeit der J-R-Kurve auf Bauteile eine wichtige Frage der Bruchmechanik. An der MPA Universität Stuttgart, Deutschland wurde auf diesem Gebiet intensiv geforscht, um das Problem der Übertragbarkeit zu lösen. Es sind aber noch immer offene Punkte vorhanden, so dass weitere spezifische experimentelle und analytische Untersuchungen erforderlich sind.

Das Problem der Übertragbarkeit lässt sich eingrenzen, wenn J-R-Kurven verschiedener Bauteile mit verschiedenen Rissgeometrien und Belastungsarten vorliegen, um J-R-Kurven mit einem größeren Bereich von Mehrachsigkeiten in der Rissspitzenumgebung zu erhalten. Zur Ermittlung der bauteilspezifischen J-

R-Kurven aus den Versuchsdaten ist die experimentelle Belastung als Funktion der Verlängerung der Lastangriffslinie, aus der das J-Integral bestimmt wird, und des Risswachstums erforderlich. Das J-Integral wird aus einer elastischen und plastischen Komponente ermittelt. Die elastische Komponente wird aus dem Spannungsintensitätsfaktor berechnet. Hierzu gibt es geschlossene Lösungen in Form von Tabellen. Die Ermittlung des plastischen J-Integrals erfolgt aus den Versuchsdaten des plastischen Anteils des Last-Verlängerungs- und des Last-Risswachstums-Verlaufs. Hierfür sind Funktionen, die für die Rissgeometrie und Belastungsbedingungen spezifisch sind, erforderlich. Diese Funktionen gibt es für sehr limitierte Fälle spezifischer Rissgeometrie und Belastungsbedingungen und sind für die im Rahmen der Arbeit untersuchten Geometrien teilweise modifiziert bzw. entwickelt worden.

Diese Funktionen sind insofern wichtig, weil es damit möglich ist, die J-R-Kurve an einer einzigen Probe bzw. an einem einzigen Bauteil zu bestimmen. Damit ist dieselbe Vorgehensweise in Probe und Bauteil realisiert. Dabei wird das Risswachstum über die Änderung der Steifigkeit des Prüfkörpers bestimmt, wofür bei diskreten Verformungen partielle Entlastungen durchgeführt werden. In Abhängigkeit vom Bauteil- und Werkstoffverhalten können zusätzliche Verformungen auftreten, die in den Funktionen berücksichtigt werden müssen. Diese Art der Risslängenmessung kann mit derjenigen verglichen werden, die mit der Potentialsondenmethode durchgeführt wird, so dass für aufwändige Versuche 2 redundante Messverfahren zur Verfügung stehen.

Zielsetzung

Im Rahmen dieser Arbeit sollte ein abgesichertes Konzept zum Leck-vor-Bruch Verhalten von Rohrleitungen erstellt werden. Hierzu musste zunächst eine experimentell abgesicherte Basis geschaffen werden. Neben der Absicherung der plastischen Grenzlastgleichungen und der Angabe von Gültigkeitsgrenzen waren in diesem Zusammenhang Untersuchungen zur Übertragbarkeit bruchmechanischer Kennwerte und Werkstoffgesetze, wie die J-R-Kurve, auf Rohrleitungskomponenten erforderlich.

Mit numerischen Berechnungen der untersuchten Rohre konnten die Ansätze bestätigt werden. Darauf aufbauend wurden analytische Beziehungen entwickelt, die eine schnelle, effiziente und zuverlässige Leck-vor-Bruch Aussage erlauben.

Durchgeführte Untersuchungen

Wie schon erwähnt, sind die bekannten plastischen Grenzlastgleichungen für Rohrbogen entweder für reinen Innendruck und reine Biegebelastung gültig. Im Betrieb ist aber eine Überlagerung beider Belastungen gegeben. Deshalb wurden in dieser Arbeit neue geschlossene plastische Grenzlastgleichungen für Rohrbögen unter Innendruck- und Biegebelastung auf der Basis umfangreicher, nichtlinearer Finite Elemente Analysen entwickelt. Hierfür wurden sechs Rohrbogen unterschiedlicher relativer Dicke ($R/t = 5 - 12.5$) und den Rohrbogenkennwerten ($h = 0.24 - 6$) analysiert. Entsprechend der realen Belastungssituation wurden bei jedem Rohrbogen sowohl die Belastungsart „Zubiegen“ als auch „Aufbiegen“ betrachtet, wobei der Innendruck zusätzlich variiert wurde. Daher werden insgesamt jeweils 60 Lastfälle für „Zubiegen“ und 54 Lastfälle für „Aufbiegen“ berechnet. Bei jedem dieser Fälle wurde die Moment-Rotation der Bogenenden-Charakteristik bestimmt. Aus diesen Moment-Rotationskurven wurden die Kollapsmomente nach der Methode der Verdoppelung der Steigung der elastischen Anstiegsgeraden berechnet. Die Bilder Z-1 und Z-2 zeigen die Auswirkung des normalisierten Innendruckes auf das normalisierte Kollapsmoment ($m_L = M_L/(4R^2t\sigma_y)$) der Rohrbögen jeweils für „Zubiegen“ und „Aufbiegen“. In beiden Fällen wurde beobachtet, dass sich das Kollapsmoment mit dem Innendruck erhöht bis ein Maximum erreicht, ab dem es auch bei weiterer Erhöhung des Innendruckes wieder abfällt. Dies stimmt mit den Beobachtungen anderer Forscher überein. Die Ovalisierung des Querschnitts des Rohrbogens spielt im Kollapsverhalten eine wichtige Rolle. Der Kollapsvorgang wird durch den Innendruck verzögert, da die Ovalisierung des Rohrbogenquerschnitts behindert wird. Die Ovalisierung hat größere Bedeutung bei dünnwandigen Rohrbogen, da der Innendruck eine deutliche Erhöhung des

Kollapsmomentes bewirkt. Hat der Innendruck eine Höchstgrenze erreicht, verringert sich mit zunehmender Erhöhung des Innendruckes das Kollapsmoment. Im Falle des „Aufbiegens“ beginnt die Abnahme des Kollapsmoments bereits bei niedrigeren Werten des Innendruckes.

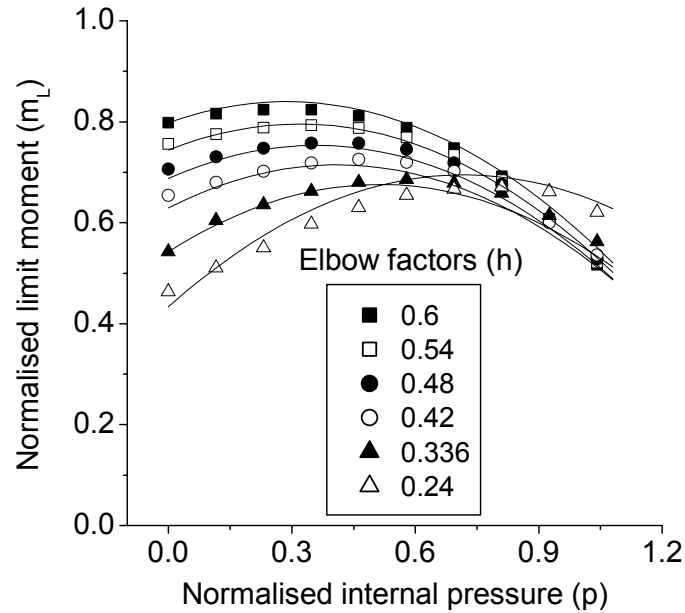


Bild Z-1 Normalisierte Grenzlastmomente für Zubiegen für unterschiedlich hohen Innendruck und Rohrbogenfaktoren (die Symbole zeigen die FE-Ergebnisse, die Linien zeigen die Ergebnisse analytischer Lösungen)

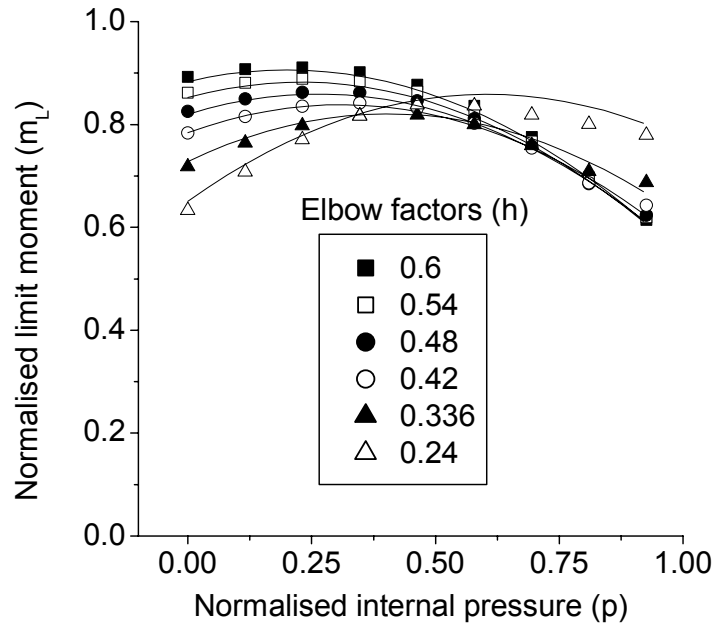


Bild Z-2 Normalisierte Grenzlastmomente für Aufbiegen für unterschiedlich hohen Innendruck und Rohrbogenfaktoren (die Symbole zeigen die FE-Ergebnisse, die Linien zeigen die Ergebnisse analytischer Lösungen)

Neben den plastischen Grenzlast- oder Kollapslastgleichungen sind bruchmechanische Analysen eine weitere Möglichkeit, kritische Zustände von Rohrbögen mit Anrissen zu identifizieren, insbesondere Aussagen zum Leck-vor-Bruchverhalten zu ermöglichen. Hierfür sind die entsprechenden Risswiderstandskurven, d. h. J-R-Kurven erforderlich.

Die Werkstoff J-R Kurve ist eine wichtige Vorgabe für alle elastisch-plastischen Bruchmechanikanalysen. Die J-R Kurve wird im Versuch an den jeweiligen Proben/Bauteilen/Komponenten ermittelt. Das J-Integral kann aber während des Experiments nicht direkt gemessen werden. Es wird aus den Versuchsdaten der Last-Verformungscharakteristik bzw. Last-Risswachstumscharakteristik ermittelt. Hierzu sind entsprechende Funktionen erforderlich. Dies sind die η_{pl} und γ Funktionen, die in Veröffentlichungen nur für sehr begrenzte Geometrien und Belastungsbedingungen aufgeführt sind. Es ist keine direkte Methode verfügbar, um diese Funktionen zu erhalten. Im Rahmen dieser Arbeit wird eine neue Grenzlastbeziehung für die genannten Belastungsfälle hergeleitet, die Basis für die η_{pl} und γ Funktionen bilden, die erforderlich sind, um die J-R-Kurve aus den Versuchsergebnissen auszuwerten.

Dies sind:

$$\eta_{pl} = - \frac{\partial F_L}{\partial A} \cdot \frac{1}{F_L} \quad (Z-1)$$

$$\gamma = \frac{\partial^2 F_L / \partial a^2}{\partial F_L / \partial a} \quad (Z-2)$$

wobei F_L die Grenzlast des angerissenen Bauteils in Abhängigkeit der Rissgröße und a die Risslänge (oder Risstiefe im Falle eines Oberflächenrisses) darstellt.

Die Rissfläche entspricht A .

Diese allgemein gültigen Ausdrücke haben den Vorteil, dass η_{pl} und γ Funktionen sehr leicht für jegliche Rissgeometrie bestimmt werden können, weil die plastische Grenzlast für viele Bauteile in Veröffentlichungen aufgeführt ist. Mit Hilfe dieser vorgeschlagenen neuen Methode kann man auch die bestehenden

' η_{pl} ' und ' γ ' Funktionen modifizieren, falls es bessere Grenzlastformeln in Zukunft geben wird. Mit diesen neuen, auf Grenzlastgleichungen basierten Funktionen, können ' η_{pl} ' und ' γ ' Funktionen für Rohrleitungskomponenten mit verschiedenen Risskonfigurationen unter unterschiedlicher Belastungsbedingungen abgeleitet werden. Diese Geometrien umfassen den Oberflächenriss mit konstanter Tiefe unter kombinierter Biege- und axialer Zugspannung, ein Rohr mit halb-elliptischem Riss unter kombinierter Biegung und axialer Zugspannung sowie einen wanddurchdringenden Axial- und Umfangsriss in einem Rohrbogen unter einem „in-plane“ Biegemoment. Einen typischen Fall eines Rohrbogens mit Axialriss und den entsprechenden Verläufen der ' η_{pl} ' und ' γ ' Funktionen sind in den Bildern Z-3 – Z-5 dargestellt.

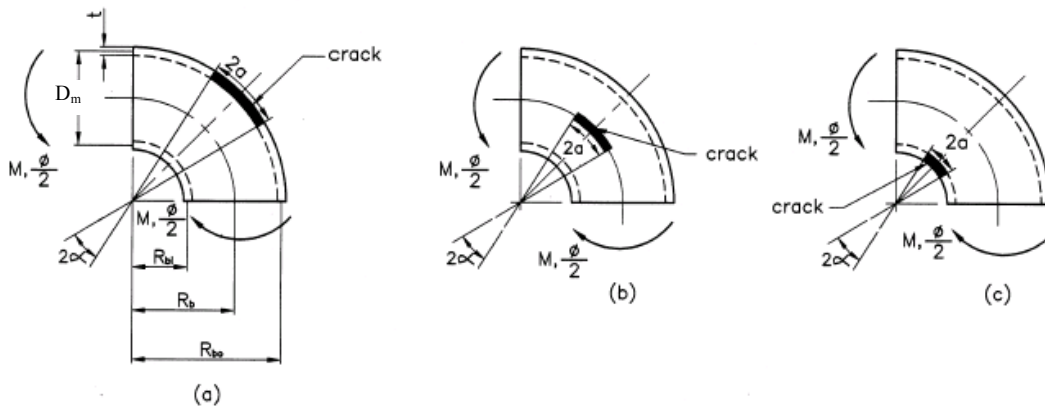


Bild Z-3 Rohrbogen mit wanddurchdringendem Axialriss (a) Extrados (b) Krone und (c) Intrados unter „in-plane“ Biegemomenten

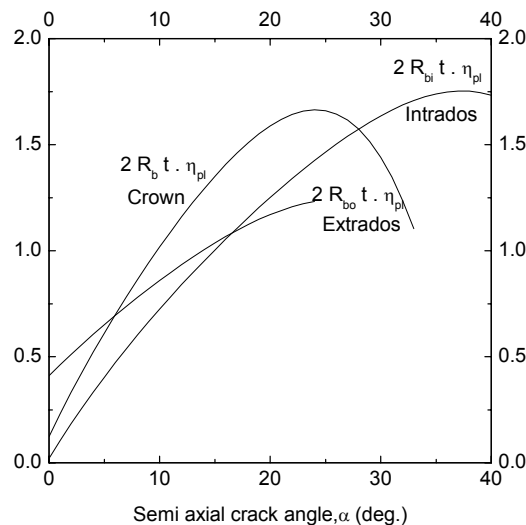


Bild Z-4 Variation von ' η_{pl} ' für Rohrbogen mit wanddurchdringendem Axialriss an verschiedenen Positionen unter „in-plane“ Biegemomenten

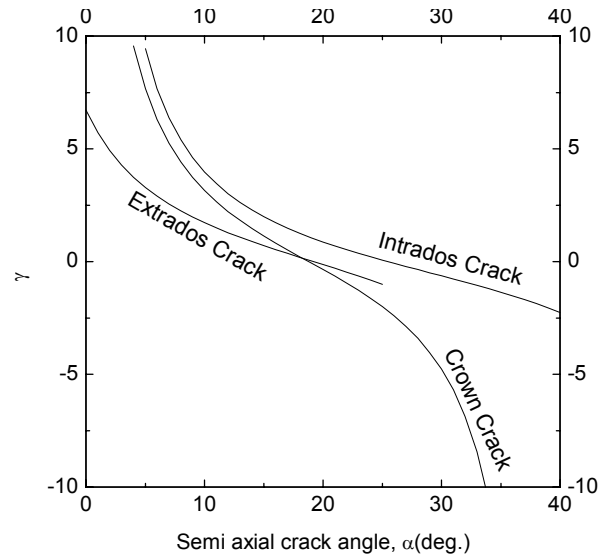


Bild Z-5 Variation von γ für Rohrbogen mit wanddurchdringendem Axialriss an verschiedenen Positionen unter "in-plane" Biegemomenten

Die Risswachstumsmessung ist eine der wichtigsten Aufgaben bei den Bruchmechanikexperimenten. Für diese Messungen gibt es verschiedene Methoden wie z. B. Potentialsondenmethode, Nachgiebigkeitstechnik und Bildanalysetechnik. Die Nachgiebigkeitstechnik ist die am meisten angewandte Messung zur Risswachstumsbestimmung an Kleinproben. Eine Voraussetzung für die Anwendung dieser Technik ist eine Gleichung, die die Korrelation der Nachgiebigkeit bei der Entlastung mit der Risslänge in Beziehung bringt. Solche Beziehungen sind für die am häufigsten eingesetzten Laborproben wie z. B. Kompaktzug- (CT-), Dreipunktbiegeprobe (TPB-) verfügbar. Allgemein wird die Nachgiebigkeit als Funktion der Risslänge durch eine linear-elastische Finite Element Berechnung ermittelt. Es ist aber nicht für die großen Verformungen anwendbar, die während der Probenbelastung auftreten können. Die dadurch hervorgerufene Änderung in der Grundgeometrie kann die Nachgiebigkeit bei der Entlastung beeinflussen. In diesem Fall hängt die Nachgiebigkeitsfunktion nicht nur von der Risslänge ab, sondern auch von der aktuellen Belastung. Um diesen Einfluss zu untersuchen, wurden nichtlineare Finite Elemente Analysen durchgeführt. Diese wurden für TPB-Proben sowie für Rohre mit wanddurchdringenden Umfangsrissen durchgeführt. Für TPB-Proben gibt es eine Nachgiebigkeitsfunktion in der Literatur, die jedoch die Verformung bei der

Belastung nicht berücksichtigt. Das Ziel dieser Untersuchung ist es festzustellen, ob die Verformung der TPB-Probe die Nachgiebigkeitsfunktion stark beeinflusst und ob dadurch Modifikationen der bestehenden Funktionen erforderlich werden.

Es existiert keine Nachgiebigkeitsfunktion für ein gerades Rohr mit wanddurchdringendem Umfangsriss unter Vierpunktbiegebelastung, das oft für Bruchmechanikversuche an Rohrbauteilen eingesetzt wird. Wegen der Ovalisierung des Rohrquerschnitts während der Verformung hängt die Nachgiebigkeit nicht nur von der aktuellen Risslänge, sondern auch von der aktuellen Belastung ab. Aus diesem Grunde wurden in dieser Arbeit elastisch-plastische Finite Elemente Analysen an Rohren mit verschiedenen Durchmessern, Wanddicken und wanddurchdringenden Umfangsrissen durchgeführt. Das Ziel dieser Studie war zu ermitteln wie die elastische Anfangsnachgiebigkeit durch die Verformung beeinflusst wird.

Aus dieser Untersuchung geht hervor, dass die Verformung des Rohres die Nachgiebigkeitsfunktion bedeutend ändert und daher in Betracht gezogen werden muss. Es wurde aber auch gezeigt, dass dieser Effekt keine so große Bedeutung für die oft eingesetzten TPB-Proben hat.

Durchgeführte Experimente

Die Experimente wurden mit dem Werkstoff SA 333 Gr. 6, einem Feinkornbaustahl, durchgeführt.

Versuche an Kleinproben

Die Rohrleitungs- bzw. Rohrbogenwerkstoffeigenschaften wurden ermittelt, indem Zugversuche an Normzugproben durchgeführt wurden. Die Zugproben wurden aus Werkstoff hergestellt, der den geprüften Rohren und Rohrbogen an wenig beanspruchten Stellen entnommen wurde. Die Fließkurven sind in Bild Z-6 enthalten. Um die J-R Kurve an Kleinproben zu bestimmen, wurden kleine TPB-Proben ebenfalls aus den geprüften Rohren und Rohrbogen herausgearbeitet.

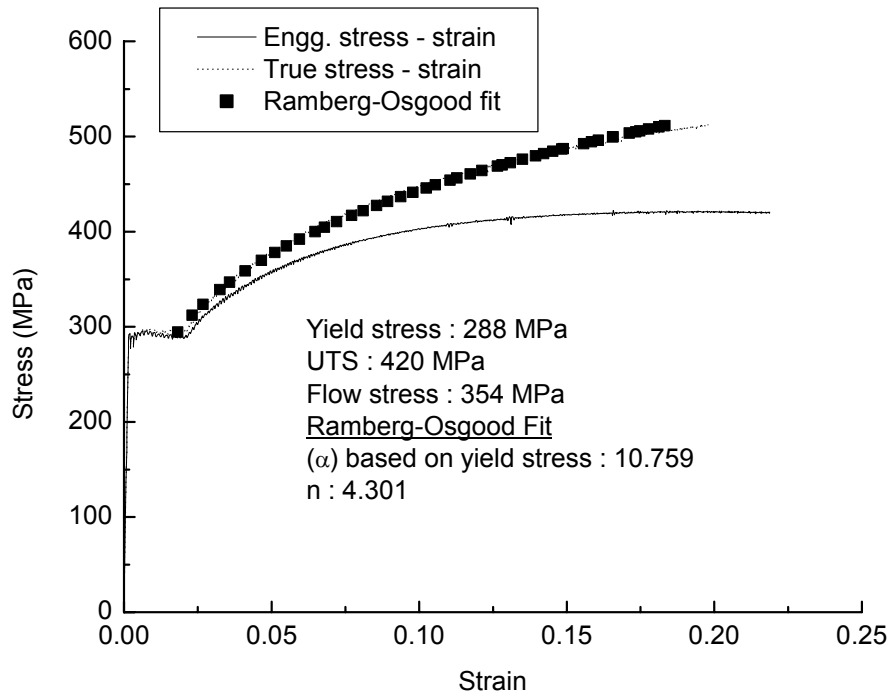


Bild Z-6 Spannungs-Dehnungs-Diagramm des Werkstoffs eines Rohrbogens

Versuche an Rohrleitungskomponenten

Bruchversuche wurden an großen Rohrleitungen und Rohrbogen (Nenndurchmesser 200 – 400 mm) mit wanddurchdringenden Umfangsrissen bei Raumtemperatur durchgeführt. Die Belastungen, die Verschiebung der Lastangriffslinie und das Risswachstum wurden während der Versuche gemessen. Mit Hilfe der im Rahmen dieser Arbeit neuentwickelten ' η_{pl} ' und ' γ ' Funktionen wurden die J-R Kurven der Bauteile aus diesen Daten generiert. In den Bildern Z-7 bis Z-11 sind die verschiedenen Aspekte der Rohrleitungs- bzw. Rohrbogenversuche dargestellt.

Numerische Analyse der geprüften Proben und Bauteile

Die elastisch-plastischen Finite Elemente Analysen wurden durchgeführt, um die Mehrachsigkeit des Spannungszustandes vor der Rissspitze an den geprüften Kleinproben und Rohren sowie Rohrbogen zu bestimmen. Die Bewertung der Mehr-achsigkeit erfolgte mittels des Mehrachsigkeitsquotienten q . Es konnte nachgewiesen werden, dass die J-R Kurve der kleinen Laborproben

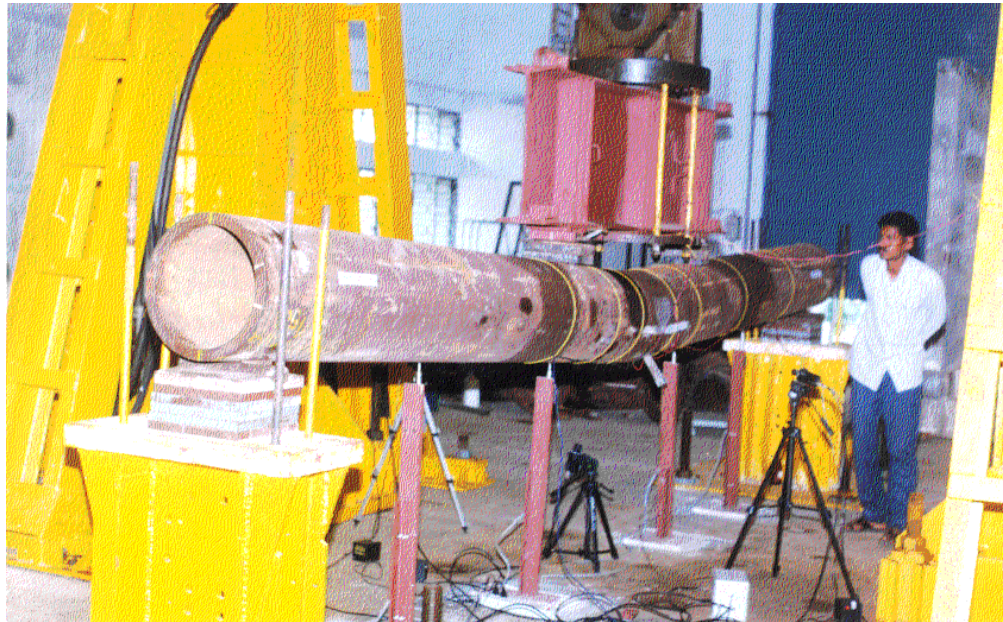


Bild Z-7 Testaufbau eines Rohrbiegeversuchs

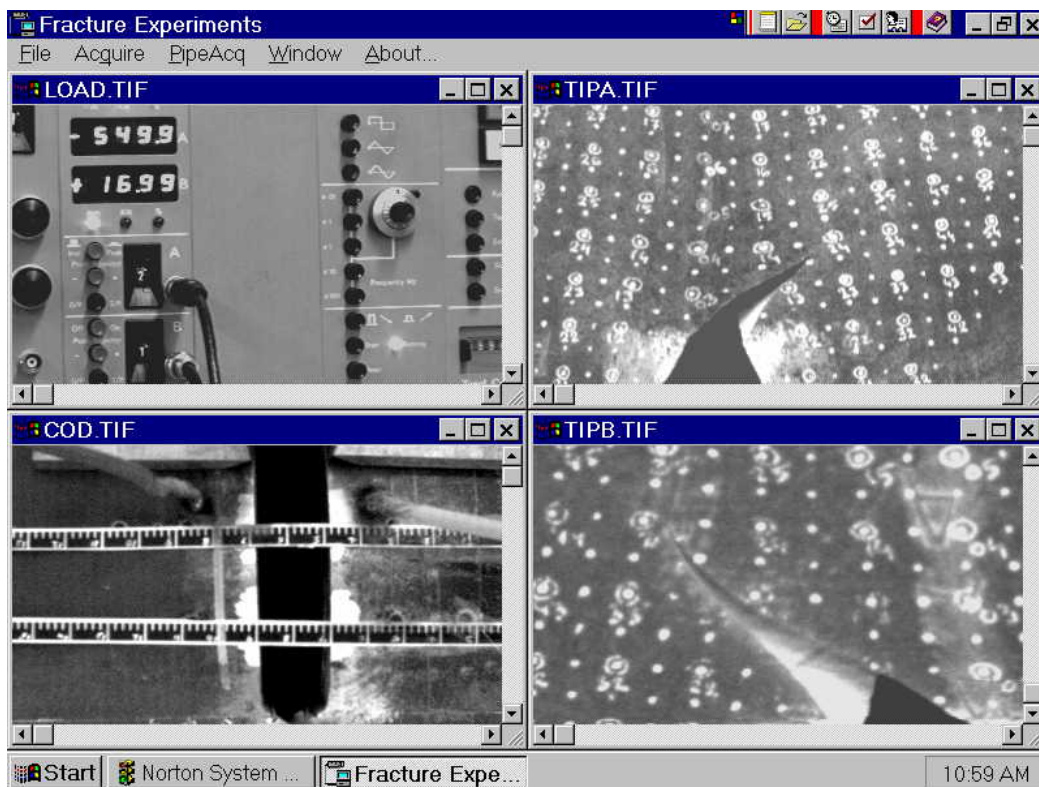


Bild Z-8 Typische Anzeigen am PC – Last, COD, TIPA, TIPB (Risspitze A + B)

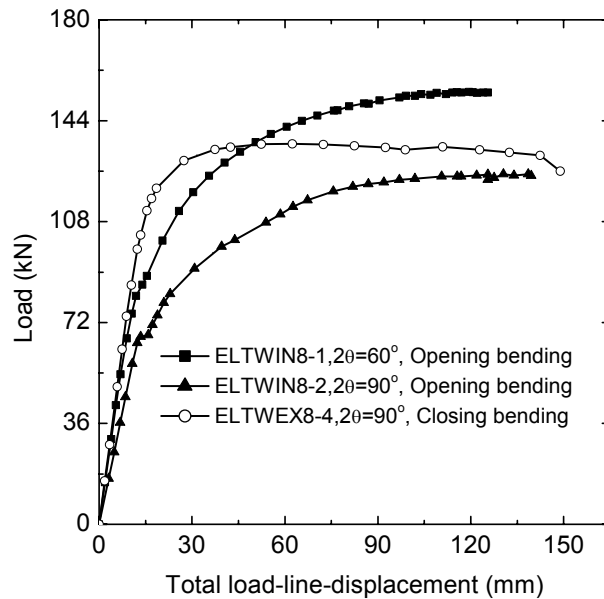


Bild Z-9 Testaufbau eines Rohrbiegeversuchs **Bild Z-10 Typische Rohrbogen-Testdaten**

auf die realen Komponente übertragen werden kann, wenn die Mehrachsigkeit des Spannungszustandes in Bereichen vor der Risspitze sowohl in Kleinproben als auch Komponente übereinstimmt. In Bild Z-12 ist ein typischer Vergleich der Versuchsdaten mit den numerischen Berechnungen für einen wanddurchdringenden Umfangsriss in einer Rohrleitung dargestellt. Den identische dreiachsige Spannungszustand, charakterisiert durch den Verlauf des Mehrachsigkeitsquotienten q in der Umgebung der Risspitze für TPB Proben und wanddurchdringenden, umfangsgerissenen Rohren, die unter Vierpunktbelastung geprüft wurden, zeigt Bild Z-13. Die identischen J-R Kurven aus demselben Probensatz und denselben Rohrleitungen sind aus Bild Z-14 ersichtlich. Hier wird die Bedeutung des mehrachsigen Spannungszustandes bei der Übertragung der J-R Kurve von Kleinproben auf reale Komponenten offensichtlich.

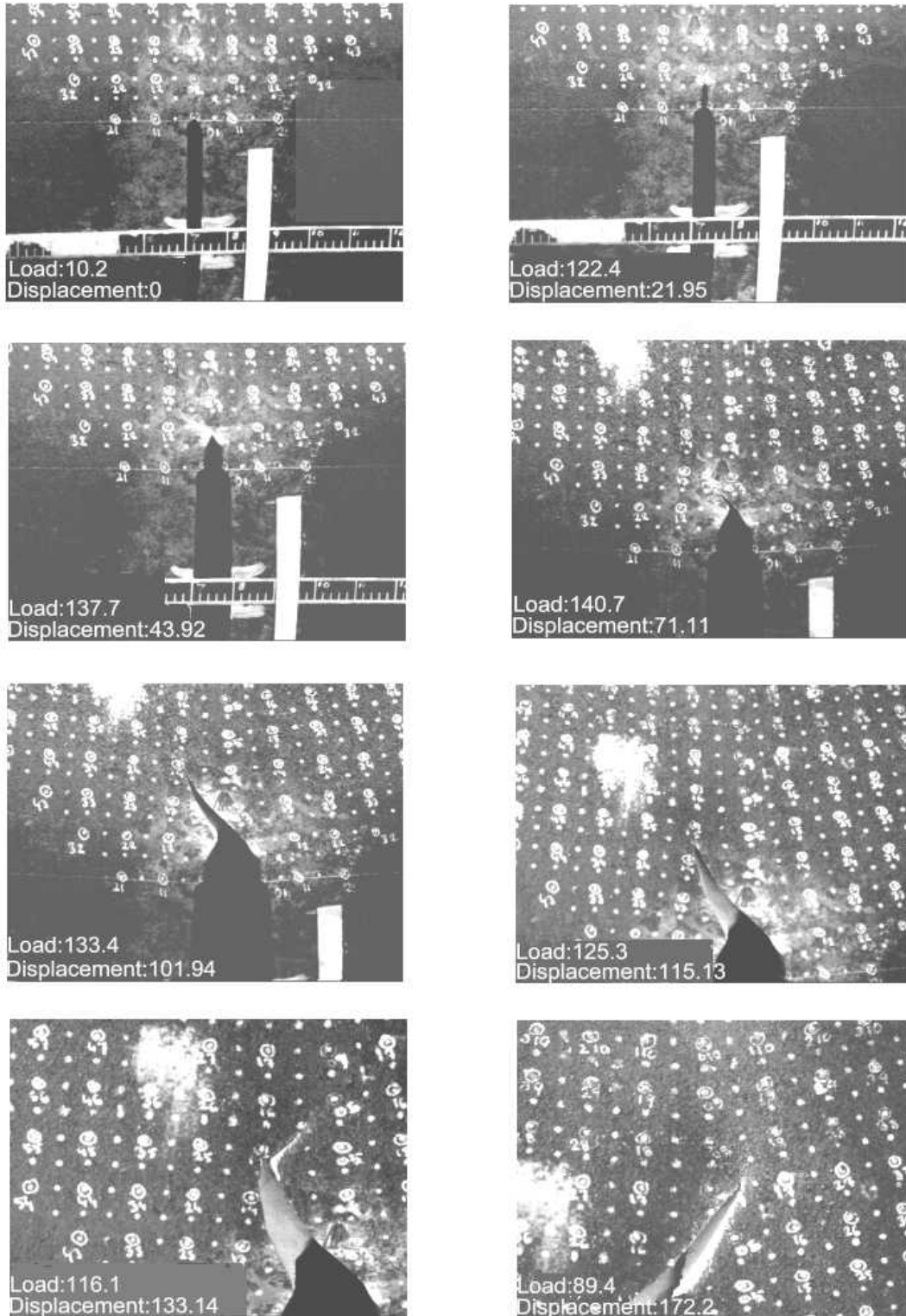


Fig. Z-11 Bilder des Risswachstums in verschiedenen Stadien eines Geradrohrs mit Schlitz unter Biegebeanspruchung

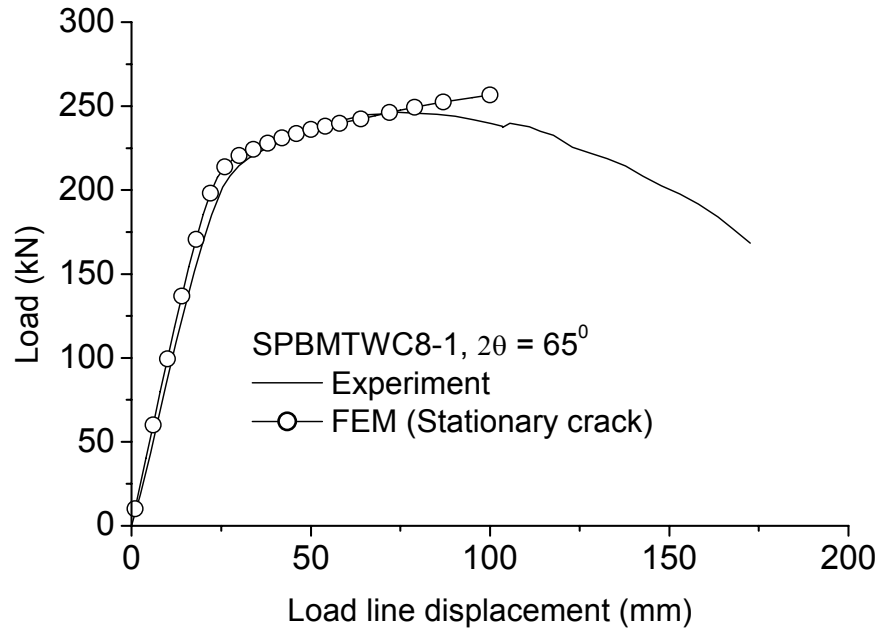


Bild Z-12 Vergleich von Testdaten mit numerischen Ergebnissen eines Geradrohrs

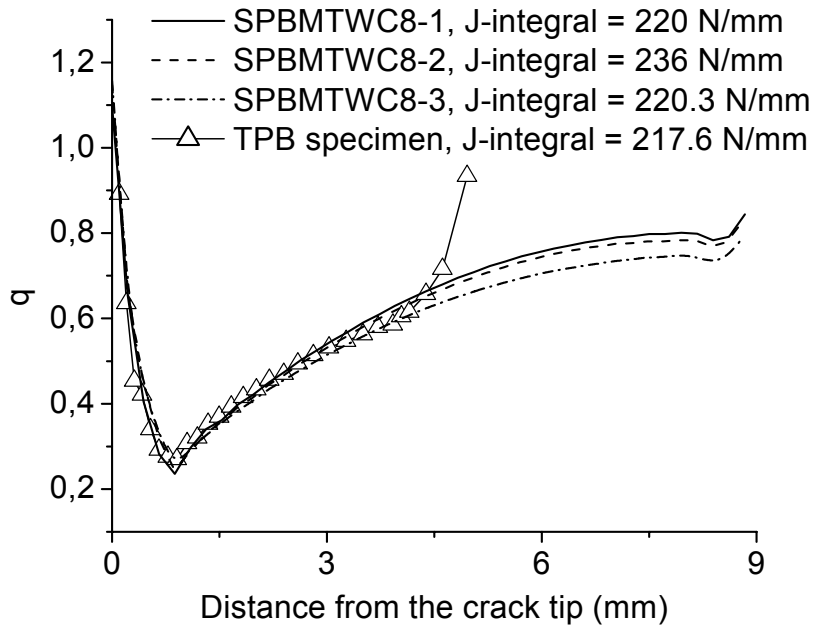


Bild Z-13 Vergleich der Mehrachsigkeit des Spannungszustandes, ausgedrückt in q , zwischen TPB Proben und Geradrohren mit Schlitz (ND 200) unter Biegebelastung

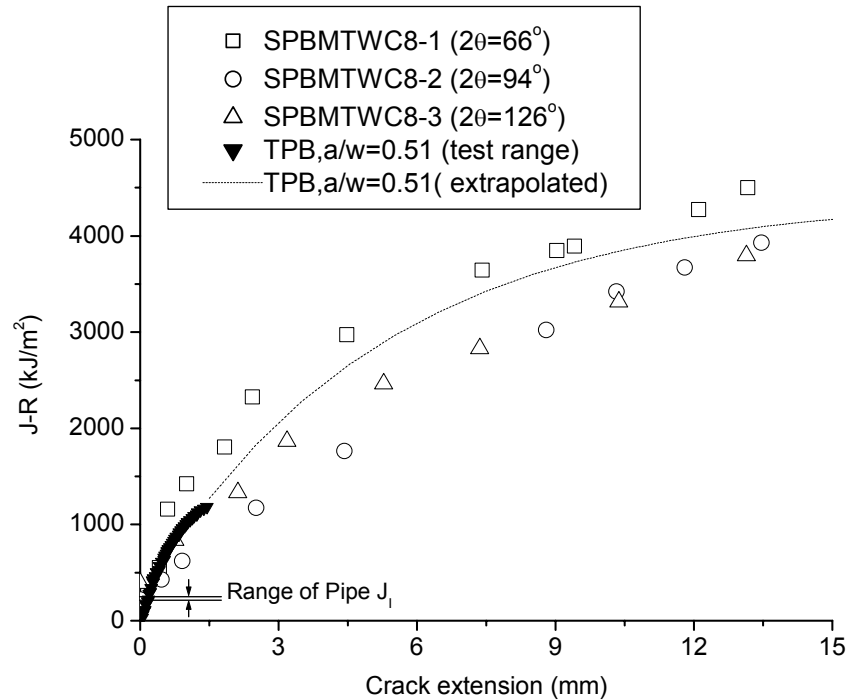


Bild Z-14 J-R Kurven ermittelt an TPB Proben und Geradrohren (ND 200) unter Biegebelastung

Schlussfolgerungen

Es konnte gezeigt werden, dass auf der Basis dieser neu entwickelten Abhängigkeiten und Ergebnisse die Verfahren zur Integritätsbewertung von Rohrleitungen und Rohrbogen verbessert werden konnte. Insbesondere konnten Kriterien dargestellt werden, die eine Übertragbarkeit von bruchmechanischen Werkstoffgesetzen, die an Kleinproben ermittelt werden, auf reale Bauteile zulassen.

1. INTRODUCTION

1.1 Problem Definition

Integrity assessment of piping components is very essential for safe and reliable operation of both conventional and nuclear power plants. It is especially important for nuclear power plants because the concept of leak-before-break (LBB) is now widely used to exclude the conventional postulation of rupture in high energy piping systems of nuclear power plants. LBB concept essentially demonstrates through fracture mechanics analysis that there is negligible chance of any catastrophic break of primary heat transport (PHT) pipes without giving prior indication of leakage. The mechanical evaluation of pipe failures has evolved over time. An initial purpose of such analysis was to determine the causes of large breaks occurring in oil and gas pipelines. The development of commercial nuclear power plants initiated the need for additional tools to assess the reliability and failure behavior of pressure vessel and piping components under different loading and environmental conditions. The results of these efforts have been transferred to other relevant industrial branches as well. The main effort in evaluating the mechanical and structural behavior of pressurized components started about 1950. Since that time, numerous investigations have been performed to assess the loading capacity and failure behavior of piping components. Investigations have also focused on determining failure loads and quantifying the margins of safety.

Safety principles and approaches for integrity assessment of piping components, especially for nuclear power plants vary somewhat from country to country. However, a generally accepted standard requires that the possibility of catastrophic failure from double-ended guillotine break (DEGB) must be completely excluded for pressure vessel and piping. The LBB assessment method is used for this purpose.

There are various issues in the integrity assessment of pipes and elbows that are unresolved or partially resolved and require experimental validation. The issues that are addressed in this work include the non-availability of closed-form collapse moment equation of elbows under combined internal pressure and bending moment, non-availability of general ' η_{pl} ' and ' γ ' functions to evaluate J-R

curves from experimental data, measurements of crack growth in fracture experiments, transferability of the specimen fracture properties to component level.

1.2 AIM OF THE PRESENT WORK :

Overall aim : To define improved fracture assessment methods in order to better quantify the safety and integrity assessment of piping components and thus allow an optimized and economical operation of piping system.

This overall aim is achieved by doing the following :

- Propose new closed-form collapse moment equations of defect-free elbows subjected to combined loading of in-plane closing/opening moment and internal pressure.
- Derivation of limit load based general expressions of ' η_{pl} ' and ' γ ' functions to evaluate J-R curve from experimentally measured data from pipes and elbows and use of these general expressions to propose new ' η_{pl} ' and ' γ ' functions for piping components with various crack configurations subjected to different loading conditions.
- Study the possibilities to improve the crack growth measurement by compliance technique.
- Establish the role of stress triaxiality near the crack tip to transfer the fracture properties of small specimen to component through fracture experiments on full scale piping components and small specimens.

2. LITERATURE REVIEW

2.1 LEAK-BEFORE-BREAK CONCEPT AND INTEGRITY ASSESSMENT OF PIPING COMPONENTS

The safety of nuclear reactors has always engaged the attention of the designers of such plants. The primary heat transport (PHT) system piping which enables cooling of the reactor core has been one of the important items where considerable research has been carried out. A failure in the piping could lead to a loss-of-coolant accident and may lead to the release of radioactive materials to the public domain. Hence one of the current active research areas is the improvement and enhancement of the methodology of integrity assessment of piping components with/without the presence of flaws.

One of the hypothetical design basis events traditionally considered in the design of PHT system piping of a pressurized heavy water reactor (PHWR) (also called CANDU reactor) or pressurized water reactor (PWR) is an instantaneous double-ended guillotine break (DEGB) of the largest heat transport pipe. This concept was originally initiated for sizing of the containment and emergency core cooling systems (ECCS). Regulatory philosophy for the design of piping systems, however, tended to shift the postulate of DEGB to a design basis for making provisions of protection against DEGB. A natural consequence of an accepted pipe break postulate would require provision of massive pipe whip restraints to minimize pipe deflection.

However, the US Nuclear Regulatory Commission (USNRC) staff issued a generic letter 84-01 [1] accepting that the DEGB of the PWR primary loop piping was unlikely to occur, provided it can be demonstrated by deterministic fracture mechanics analyses that postulated small through wall flaws in plant-specific piping would be detected by the plants leakage monitoring systems long before the flaws could grow to unstable sizes. A detailed discussion of limitations and acceptance criteria for LBB used by the NRC staff is provided in NUREG-1061, Vol.3 [2]. A new NRC Standard Review Plan (SRP) section, numbered 3.6.3 [3], and entitled 'Leak-Before-Break Evaluation Procedures', providing review

guidance for the implementation of the revised GDC-4 was published for public comment in 1987 [4]. Now, LBB concept is used in general to design almost all the PWRs in US.

The LBB concept aims at the application of fracture mechanics principles to demonstrate that piping is very unlikely to experience DEGB without giving prior indication of leakage. The LBB methodology as followed in USA [2] and Canada [5] consists of demonstrating three levels of safety against DEGB. These three levels may be viewed as defense in depth strategy. Level 1 safety assessment is performed by designing the piping as per ASME Sec.III [6] with a well defined factor of safety. It does not, however, consider the presence of any flaw other than what is permitted in the non-destructive examination (NDE). Level 2 safety assessment consists of postulating a part-through crack at the inside surface of piping components, that may go undetected during NDE and then demonstrate through fatigue (or any other growth mechanism that may be operative in service) crack growth study that it will not grow to critical size between two successive in-service inspection/repair interval or, possibly, during the entire life period of the reactor. Level 3 safety assessment consists of postulating a through wall crack that will ensure detectable leakage in the nuclear power plant (NPP) and then demonstrate that it will remain stable under the maximum credible loading condition that may be encountered during an accident e.g. safe shutdown earthquake (SSE).

IAEA Technical Documents [7,8] have summarized the views of various countries on applicability of LBB. In Canada, the LBB concept has been successfully used for the large diameter pipes in the primary heat transport circuit of the Darlington nuclear power plants (CANDU) to obviate the need for pipe whip restraints [5]. In France, the LBB concept is not used formally. Existing regulations are designed to ensure either that fracture will not occur (RPV) or that the rupture of a large diameter (500 mm) pipe can be handled (pipe whip restraint systems and ECCS). The former case is supported by periodic inspections. However, various fracture mechanics studies of piping components

are being carried out for application of LBB in French PWRs and Liquid Metal Fast Breeder Reactors [9]. In Germany, the general concept for break preclusion, similar but not identical to LBB, is used for nuclear piping systems. It consists of two elements, namely, basic safety and independent redundancies. The applicability of the concept was discussed and accepted by the German authorities [10-13]. In Japan, the regulatory body has completed the discussion on LBB guidelines to be applied to stainless steel pipe of the primary heat transport circuit in both PWRs and BWRs. This guideline has not been arranged as the open regulation. However, the regulatory body approved the application of this guideline to some PWR plants. The purpose is to allow removal of pipe whip restraints structure. There is no plan to apply LBB to BWRs at present, although regulatory guidelines will apply to both. References [14-16] describe some aspects of the status of LBB in Japan. In United Kingdom (UK), the LBB concept has been used in the case of Magnox reactors to justify plant life extension, particularly in respect of the RPVs [17-18]. For the Prototype Fast Reactor, LBB is used on a case-by-case basis as one of several safety arguments to justify continued operation of components where cracking is known to have occurred. The UK has played a prominent role in developing LBB methodology as part of the design envelope for the European Fast Reactor. Some other countries, for example, Spain [19] and Czechoslovakia [20] are also at various stages of formulation of guidelines for applying the LBB concept to design the Nuclear Power Plants. Similarly, India has also embarked upon the application of LBB concept to design the PHT system piping of 500 MWe Indian PHWRs that are under constructions [21,22].

2.2 LIMIT LOAD OF UN-CRACKED PIPES AND ELBOWS

The first level of integrity assessment of piping components is usually performed without postulation of any crack. During integrity assessment, it is very important to know the load bearing capacity of the structure for its safe and reliable design. The limit load of a component indicates its load bearing capacity.

Limit analysis calculates the maximum load that a given structure made of perfectly plastic material can sustain. Limit analysis does not consider the hardening of material.

In general, limit load is defined as the load at which the entire ligament becomes fully plastic and there is net section collapse of the structure. However, it is not so easy to precisely determine the load at which the entire ligament becomes plastic. Usually, it is determined from the load-deflection or load-strain curve. Particular care should be given to ensure that the strains or deflections, that are used, are indicative of the load carrying capacity of the structure. There are various definitions of limit load depending on the meaning of failure, which are illustrated in Fig. 2.1. Broadly, two categories are there, namely, collapse and instability.

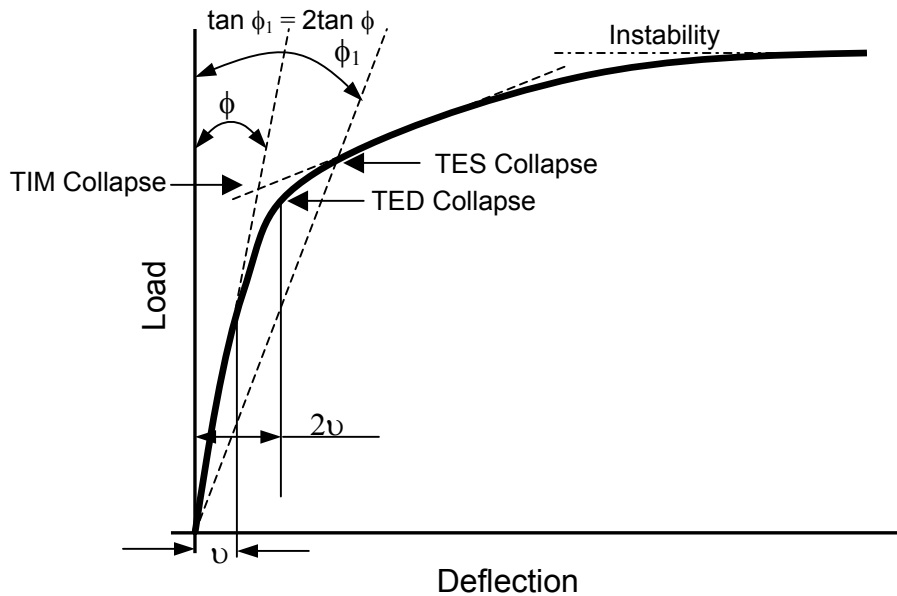


Fig.2.1 Various definitions of limit load

Instability is defined as the asymptotic load when deflection becomes unbounded and the structure becomes a mechanism or in case of displace-controlled loading, load starts falling. Mathematically, it is denoted by $dP/d\Delta = 0$, where, P is the load and Δ is the deflection. *Collapse* is defined on a conservative estimate. Mainly three definitions of collapse are there, namely, twice elastic

slope (TES), twice elastic deflection (TED) and tangent intersection method (TIM). In case of TES method, a straight line from origin with the linear elastic slope is drawn, which makes an angle of ' ϕ ' with the vertical axis of load. Subsequently, a second line is drawn with angle ' ϕ_1 ' with the vertical axis of load such that: $\tan \phi_1 = 2 \tan \phi$. The intersection of this second line with the load-deflection curve is called the TES collapse load. In case of TED method, deflection at the first departure from initial linearity is determined (v) and then a vertical line is drawn at twice this deflection ($2v$). The intersection between the second vertical line with the load-deflection curve is denoted as TED collapse load. In case of TIM method, a tangent is drawn in the plastic part of the load-deflection curve where load-deflection curve reaches a linear state. The intersection between the initial linear elastic line and the plastic tangent line is termed as the TIM collapse load. It is clear, all these definitions are arbitrary. However, TES method, in general, produces the most consistent and reproducible results and for this reason, is widely used and recommended by ASME also.

2.2.1 Limit Load of Un-cracked Pipe

The limit moment of a thick pipe ($\zeta = t/R_o > 0.1$) is given as [23,24] :

$$M_o = 4\sigma_f R_o^2 t \left(1 - \zeta + \frac{\zeta^2}{3} \right) \quad (2.1)$$

where, R_o is the outer radius of the pipe and σ_f is the flow stress of the pipe material. For thin pipe ($\zeta < 0.1$), the terms in parenthesis in eqn.(2.1) can be neglected.

The limit pressure of a pipe subjected to pure internal pressure is evaluated based on the hoop stress. The limit pressure is expressed as [25] :

$$P = \frac{\sigma_f t}{R} \quad (2.2)$$

The limit moment of a pipe subjected to combined bending moment and internal pressure (P) is given as [26,27] :

$$M_0 = (4\sigma_f R^2 t) \cdot \cos\left(\frac{\pi PR}{4t\sigma_f}\right) \quad (2.3)$$

Therefore, it is seen that the limit load expressions of un-cracked pipe subjected to pure moment, internal pressure and combined moment and pressure loading are all available in the literature.

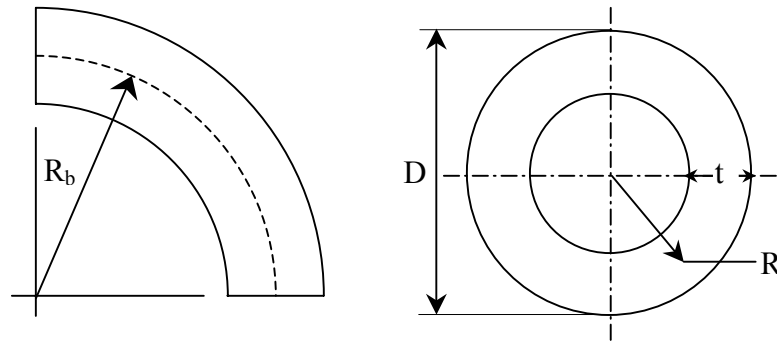
2.2.2 Limit Load of Un-cracked Elbow

Pipe bends or elbows are commonly used components in a piping system. They are very flexible compared to the straight pipes. Because of this increased flexibility, they are forced to accommodate large displacements arising from the differential thermal movements. However, care must be taken so that deformations of the bend remain predominantly elastic. Otherwise, the resistance to deformation may decrease rapidly leading to the failure of the system. It is, therefore, important to know its collapse load for the safe operation of the plant. Different studies had earlier been carried out to evaluate the plastic collapse loads of elbows. Marcal [28] was the first to present the results for elastic-plastic behavior of pipe bends with in-plane bending moment. Spence and Findlay [29] found approximate bounds on limit moments for in-plane bending by utilizing previously existing analyses in conjunction with the limit theorems of perfect plasticity. Spence and Findlay [29] expressed the lower bound in-plane limit moment of an elbow as :

$$\begin{aligned} M_L &= 0.8 h^{0.6} (D^2 t \sigma_y) \quad ; \quad \text{for } h < 1.45 \\ &= (D^2 t \sigma_y) \quad ; \quad \text{for } h > 1.45 \end{aligned} \quad (2.4)$$

$$h = tR_b/R^2 \quad (2.5)$$

where, h is the elbow factor or pipe bend characteristics, R_b is the mean bend radius of elbow, D is the outer diameter, R is the mean radius of elbow cross section and t is the wall thickness of elbow (see Fig.2.2).



Elbow Cross Section

Fig.2.2 Geometry of Elbow

Calladine [30] tried to find the lower-bound limit moment of a thin curved tube under pure bending moment by using the classical elastic shell analysis in conjunction with the limit theorems of plasticity. Calladine [30] expressed the lower bound in-plane collapse moment as :

$$M_L = 0.935 h^{2/3} (4R^2 t \sigma_y) \quad ; \quad \text{for } h < 0.5 \quad (2.6)$$

Both the above expressions are based on small displacement analysis and assume ideal plastic material behavior. Based on large displacement analysis Goodall [31] proposed the maximum load carrying capacity of the elbow subjected to closing bending moment as

$$M_L = \frac{1.04 h^{2/3} (D^2 t \sigma_y)}{(1 + \beta)} \quad (2.7)$$

$$\text{with, } \beta = \left(2 + \frac{(3h)^{2/3}}{3} \right) \left(\frac{4\sqrt{3(1-\nu^2)}}{\pi} \cdot \frac{\sigma_y}{E} \cdot \frac{R}{t} \right) \quad (2.8)$$

Griffiths [32] performed experimental study on both cracked and un-cracked elbows mainly to see the effect of cracks on limit loads. For un-cracked elbow, he suggested to multiply the Calladine formula (eqn.(2.6)) [30] by a factor of 1.33 to account for the stiffening effect of tangent pipes attached to the elbow. Touboul et al [33] proposed the following equations of collapse moments of

elbows based on the experimental study at Commissariat à l'Energie Atomique (CEA), France :

$$M_L = 0.715 h^{2/3} (4R^2 t \sigma_y) \quad (\text{closing mode}) \quad (2.9)$$

$$M_L = 0.722 h^{1/3} (4R^2 t \sigma_y) \quad (\text{opening mode}) \quad (2.10)$$

Drubay et al [34] proposed the closing mode collapse moment as :

$$M_L = 0.769 h^{2/3} (4R^2 t \sigma_y) \quad (2.11)$$

Fig.2.3 shows the variation of normalized collapse moment with elbow factor (h), predicted by the above equations for typical values of $R = 250$ mm, $t = 25$ mm, $\sigma_y = 300$ MPa, $E = 200$ GPa and $\nu = 0.3$. All the above equations are applicable only for the pure in-plane bending moment. The effect of internal pressure is not taken into account. Goodall [35] was the first to propose the closed-form equation of limit load of elbows under combined internal pressure and in-plane bending moment through the small displacement analysis. The equation proposed was

$$M_L = 1.04 h^{2/3} (1 - P_r R / 2t \sigma_y)^{1/3} (D^2 t \sigma_y) \quad (2.12)$$

From the above equation it is seen that internal pressure (P_r) reduces the limit moment. This is against the observations of Rodabaugh [36], Hilsenkopf et al [37], Touboul et al [33], Shalaby and Younan [38,39] and Chattopadhyay et al [40]. This shortcoming of the equation is because of the small displacement analysis by Goodall which could not capture the stiffening effect of internal pressure. Touboul et al [33] proposed an equation for instability moment (maximum moment in the moment-rotation curve) under combined internal pressure and bending moment as follows :

$$M_L = M_L (P_r = 0) \cdot \left[1 + \left(\frac{0.7}{h} \right) \left(\frac{P_r R}{t \sigma_y} \right) \right] \cdot \left[1.4 - 0.5 \frac{P_r R}{t \sigma_y} \right] \quad (2.13)$$

where $M_L (P_r = 0)$ indicates the instability moment with no internal pressure. This equation did not differentiate between the opening and closing mode of bending

moment whereas the effect of internal pressure on the limit moments are different for these two modes as observed by Shalaby and Younan [38,39]. Touboul et al, however, did not propose any equation for collapse moment under combined loading.

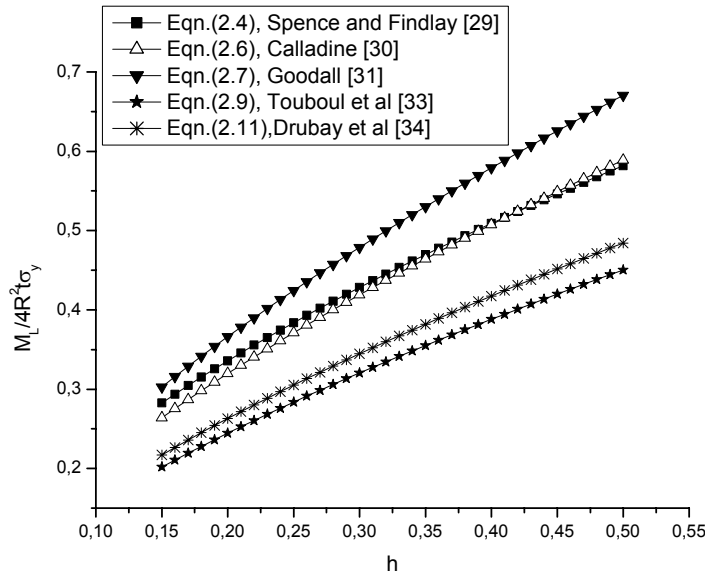


Fig.2.3 Variation of normalized collapse moment of un-cracked elbow with elbow factor

2.3 INTEGRITY ASSESSMENT OF PIPING COMPONENTS WITH CRACKS

After the first level of integrity assessment of un-cracked piping components without postulation of any crack, the second level of integrity assessment is usually carried out with postulation of cracks. Component with cracks should be treated with fracture mechanics procedure. If the piping material is brittle, linear elastic fracture mechanics (LEFM) principles are to be used. For ductile material, the elastic-plastic fracture mechanics (EPFM) principles are applicable. If the piping material is extremely ductile and tough, one need not adopt the fracture mechanics principles at all, limit load concept is sufficient for its integrity assessment. However, industrial piping material is normally ductile, where LEFM principles are not applicable; only EPFM and limit load theory are to be used. Additionally, there are other methods also, for example, R6 method [18], to assess the integrity of ductile piping. Here, the

basics of EPFM methodology with J-integral-Tearing Modulus (J-T) [41] concept and limit load methods are described briefly.

2.3.1 Elastic-Plastic Fracture Mechanics (EPFM) Methodology

2.3.1.1 Material Parameters

In the EPFM design criteria, the fracture resistance curve expressed as J-R curve goes as input material parameters. The J-R curve is expressed as material J-resistance (J_{mat}) versus crack growth (Δa) curve. Fig.2.4a shows a typical J-R curve for ductile materials. The J-resistance at the onset of crack initiation is known as J-initiation toughness. Various definitions of initiation are there in the literature. The ASTM [42] definition of initiation is based on 0.2 mm offset blunting line equation as shown in Fig.2.4a and is usually designated as J_{Ic} . Another definition is based on stretched zone width (SZW) and is usually designated as J_i (see Fig.2.4a) [42a]. Ductile material has rising J-R curve, which indicates that fracture resistance increases with crack growth. The J-R curve is considered as a material parameter provided it satisfies certain conditions in terms of the specimen geometry. Usually, Compact Tension (CT) or Side Edge Notched Bend (SENB) specimens (see Figs. 2.4b and 2.4c) are tested to generate the material J-R curve.

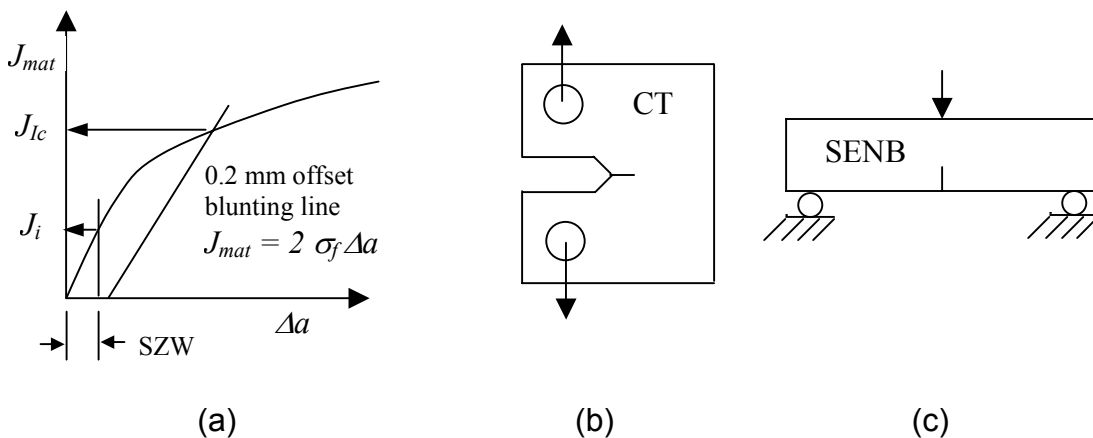


Fig. 2.4 (a) Typical J-R curve (b) CT specimen (c) SENB specimen

2.3.1.2 Design Criteria

A cracked structure made of ductile material, when subjected to external load, undergoes various phases of crack growth. Figure 2.5 illustrates these phases. Initially the crack tip remains very sharp. When it is loaded, the crack tip first blunts. During blunting phase, little amount of crack growth occurs. With the increase of load, crack growth starts at certain load, which is termed as 'crack initiation'. With further increase of load, the stable crack growth continues. Finally, at certain load, 'unstable ductile tearing' will start and crack will grow rapidly leading to instability. From design point of view, it is important to determine at what load 'crack initiation' and 'unstable ductile tearing' will start. These are discussed below.

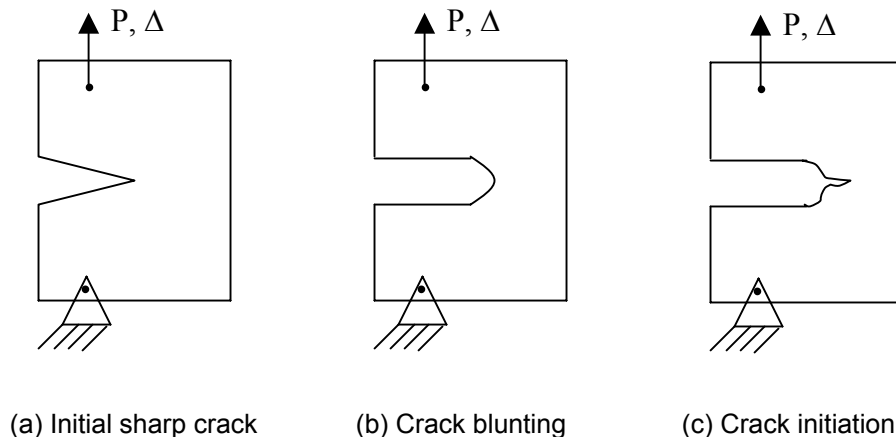


Fig.2.5 Various stages of crack initiation in ductile material

Crack initiation

To predict crack initiation for a particular structural geometry made of ductile material, the design criteria is as follows:

$$J_{app}(a, P) = J_{Ic} \text{ or } J_i \quad (2.14)$$

where, J_{app} is the applied *J-integral* which is function of applied load (P), crack length (a) and structural geometry; and J_{Ic} or J_i is assumed to be the *J*-initiation toughness, which is the material property as shown in Fig.2.4a. For a given load

on a particular structure of a specific material, one can obtain the critical crack length to cause crack initiation using Eq.(2.14). Alternatively, one can also obtain the critical load to cause crack initiation for a fixed crack length using Eq.(2.14).

Unstable ductile tearing : J-integral – Tearing Modulus Method

Once crack initiates in a ductile material, crack can propagate in a stable or unstable manner. It is often important to know the load at which unstable ductile tearing starts. For better utilization of increasing fracture resistance of ductile material with crack growth, one can design a structure based on the unstable ductile tearing load rather than the crack initiation load. Because, design based on crack initiation load for a ductile material may sometimes be too conservative. To obtain the crack instability load for a given initial crack length in a particular structure of ductile material, Paris et al [41] proposed the J-integral – Tearing Modulus method. In this approach, “applied” and “material” J-Integrals and Tearing Modulus are calculated and compared with each other in the manner shown in Figs.2.6 – 2.7 to determine the stability of the crack extension. Equilibrium requires that the applied J-Integral (the parameter describing the crack driving force) be equal to the material J-Integral (the material resistance to crack extension). Under this condition, the stability of crack extension is dependent on the magnitude of the applied Tearing Modulus compared to the material Tearing Modulus; crack extension will be stable if it is less than the material Tearing Modulus, and will be unstable if the reverse is true. It is to be noted that at applied J-Integral levels below material J_i , crack does not initiate.

$$J_{app} \geq J_{mat} : \text{necessary condition for crack instability.} \quad (2.15)$$

$$T_{app} \geq T_{mat} : \text{sufficient condition for crack instability.} \quad (2.16)$$

$$\text{with, } T_{app} = \frac{E}{\sigma_f^2} \cdot \frac{dJ_{app}}{da} \Big|_P \text{ assuming load controlled condition.} \quad (2.17)$$

$$\text{and } T_{mat} = \frac{E}{\sigma_f^2} \cdot \frac{dJ_{mat}}{da} \quad (2.18)$$

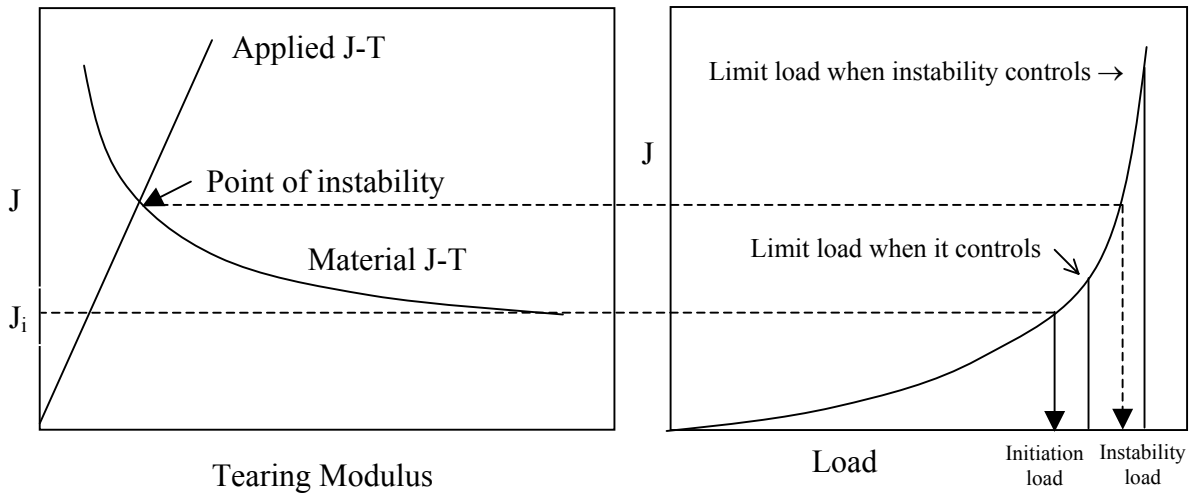


Fig. 2.6 Crack stability assessment diagram in J-T space

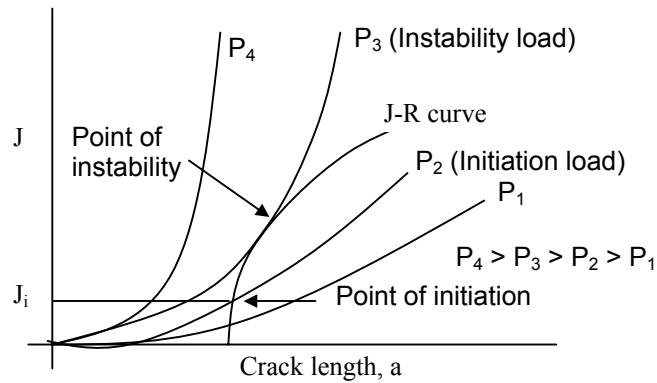


Fig. 2.7 Crack stability assessment diagram in J-a space

Point of instability in J-T diagram could be evaluated using R-curve approach as shown in Fig.2.7 where, instability condition is characterized by the tangency of applied J-a curve at a given load with material J-R curve [41]. However, a point to be noted here is that J-R curve is dependent on dimension and type of loading (geometry) and the above-mentioned procedure requires additional parameter e.g. triaxiality in the vicinity of crack tip. This is discussed in detail in section 2.3.3.

2.3.1.3 Competition between unstable ductile tearing and attainment of limit state

The unstable ductile tearing load, calculated using the J-T method is always to be compared with the limit load, because for ductile material, there is a competition between unstable ductile tearing and attainment of limit state. If the limit load is less than the instability load determined by J-T approach, limit load controls the design and is taken as the critical failure load. Various equations of limit load of cracked pipes and elbows are available in the literature. These are described in the next section. If no equation is available for a particular geometry, limit load may be determined by non-linear finite element analysis.

2.3.2 Limit Load Equations of Cracked Pipes and Elbows

2.3.2.1 Straight Pipe

Limit moment of through wall circumferentially cracked pipe subjected to bending moment is calculated as follows [23] :

$$M_L = 4R^2 t\sigma_f [\cos(\theta/2) - 0.5 \sin (\theta)] \quad (2.19)$$

where, R is the mean radius of the pipe cross section, t is the wall thickness, σ_f is the pipe material flow stress taken as the average of yield and ultimate stress and θ is the semi-crack angle. Kastner et al [43] have observed that the choice of flow stress has a great influence in the estimation of critical crack lengths (and hence the critical moments also), especially for large crack size. While using $\sigma_f = (\sigma_y + \sigma_u)/2.4$ for axially cracked pipe under internal pressure, Kastner et al got all the experimental results conservative with respect to the theoretical predictions. Moulin and Delliou [44] also suggest a reduction factor of '0.85' to the Eqn.(2.19) to take care of the crack propagation at maximum moment. Equation (2.19) is then modified as :

$$M_c = 0.85 \times 4R^2 t\sigma_f [\cos(\theta/2) - 0.5 \sin (\theta)] \quad (2.20)$$

This is equivalent to the definition of $\sigma_f = (\sigma_y + \sigma_u)/2.4$ instead of $\sigma_f = (\sigma_y + \sigma_u)/2$ in Eqn.(2.19). Equations are also available to account for the limited ductile tearing before the onset of collapse of through wall circumferentially cracked pipe subjected to bending moment. Various approaches, e.g. 'G factor' by Asada et al [15] , 'Z factor' [25] have been proposed. As per the 'G factor' approach, critical moment of a circumferentially cracked pipe is given as follows :

$$M_c = M_L / G \quad (2.21)$$

$$G = \{0.692 - 0.0115D_N\} + \{0.188 + 0.0104D_N\}\log_{10}(\theta) \quad (2.22)$$

$$6 \leq D_N \leq 30$$

where, D_N is the nominal pipe diameter in inch, θ is the semi-crack angle in degree and M_L is the plastic collapse moment as per Eqn.(2.19). The value of 'G' is more than '1.0' and takes care of the onset of ductile tearing prior to plastic collapse. As per the 'Z factor' approach, critical moment of a circumferentially cracked pipe is given as follows :

$$M_c = M_L / Z \quad (2.23)$$

$$Z = \left[\frac{\sigma_f}{2.4S_m}, 1.958 \frac{\sigma_f}{S_m} \frac{1 + 0.0152(D_N - 4)A}{\sigma_y^{0.46}} \right]_{\max} \quad (2.24)$$

Valid for, $27.1 \text{ ksi (187 MPa)} \leq \sigma_y \leq 40 \text{ ksi (276 MPa)}$ and $J_{Ic} \geq 1050 \text{ lb/in (184 kJ/m}^2\text{)}$

$$A = [0.125(R/t) - 0.25]^{0.25} \quad \text{for } 5 \leq R/t \leq 10$$

where, S_m is the ASME code specified allowable stress $[(2/3)\sigma_y, (1/3)\sigma_u]_{\min.}$ and σ_y is the yield stress in ksi.

It may be mentioned here that the term limit moment is generally used to collectively indicate either instability or collapse (see Fig.2.1). All these limit load equations of cracked pipe do not explicitly mention whether it indicates instability or collapse. However, with the use of flow stress as average of yield and ultimate

strength, it seems that these equations indicate the instability load, i.e. the maximum load in the load deflection curve.

2.3.2.2 Elbow

For an elbow with through wall circumferential crack under in-plane bending moment, the limit moment is given by Zahoor [45]:

$$M_L = M_o \left[1 - 0.2137 \left(\frac{a}{D_m} \right) - 0.0485 \left(\frac{a}{D_m} \right)^2 - 1.0559 \left(\frac{a}{D_m} \right)^3 \right] \quad (2.25)$$

$$M_o = 0.935 \sigma_f D_m^2 h^{2/3} \quad (2.26)$$

Applicability : $a/D_m \leq 0.8$, $h = 4R_b t/D_m^2 \leq 0.5$ and $D_m/t \geq 15$

The limit moment formula for long radius elbow ($R_b/D_m = 1.5$) with an axial through wall crack at crown is also given by Zahoor [45] as follows :

$$M_L = M_o \left[1 - 0.0824 \left(\frac{a}{D_m} \right) - 1.3755 \left(\frac{a}{D_m} \right)^2 + 0.9327 \left(\frac{a}{D_m} \right)^3 \right] \quad (2.27)$$

Applicability : $a/D_m \leq 0.9$, $h = 4R_b t/D_m^2 \leq 0.5$ and $D_m/t \geq 15$

where, 'a' is the half crack length, 'D_m' is the mean diameter of the elbow cross section, 'R_b' is the mean bend radius of elbow, 't' is the elbow wall thickness, $h = 4R_b t/D_m^2$ is the elbow factor and 'σ_f' is the material flow stress.

2.3.3 Transferability of Specimen Fracture Resistance Data to Components

Elastic-Plastic Fracture Mechanics analysis usually requires as basic input the material fracture resistance data, expressed in the form of J-Resistance (J-R) curve (see section 2.3.1 and Fig.2.4a). Material J-resistance tends to increase during fracture process of ductile material. Over the years, material J-R curve has been evaluated by conducting tests on high constraint geometries like compact-tension (CT) and three point bend (TPB) specimens as per ASTM E-

1820 [42]. J-R curve was assumed to be readily transferable from small laboratory specimen to full scale component. However, it is now well known that real life structures exhibit fracture resistance that is different from laboratory specimens. This is attributed to the difference in the state of stresses around the crack tips. In other words, it is realized that J-R curve does not depend on material only, it also depends on the stress triaxiality in the vicinity of crack. The transferability of the specimen J-R curve to component level is thus an important issue in fracture mechanics. There are various parameters to quantify the stress triaxiality ahead of crack tip, e.g. T -stress proposed by Williams [45a] and also Q parameter proposed by O'dowd and Shih [45b]. Extensive work [46-48] has been carried out in MPA, University of Stuttgart, Germany to address the issue of transferability. A new parameter (q) was introduced by Clausmeyer et al [46] to quantify the crack tip triaxiality. Due to the material mechanics background, ' q ' is preferred to other parameters and is used in this work. It is defined as follows.

$$q = \frac{\sigma_e}{\sqrt{3} \cdot \sigma_m} \quad (2.28)$$

$$\sigma_m = \frac{\sigma_1 + \sigma_2 + \sigma_3}{3} \quad (2.29)$$

$$\sigma_e = \frac{1}{\sqrt{2}} \left[(\sigma_1 - \sigma_2)^2 + (\sigma_2 - \sigma_3)^2 + (\sigma_3 - \sigma_1)^2 \right]^{1/2} \quad (2.30)$$

where, σ_e is Von-Mises effective stress, σ_m is hydrostatic stress and $\sigma_1, \sigma_2, \sigma_3$ are the principal stresses.

The small values of ' q ' represent high degree of stress triaxiality. This quotient can be determined from the finite element analysis of the specimen and the component. Comparing the ' q ' values of the specimen and the component helps in assessing whether fracture properties of the specimen are transferable to the component or not. The following conclusions can be drawn from [46-48] :

- a quantitative assessment with regard to crack initiation is possible by the comparison of the effective (physical) crack initiation value (J_i) with the calculated crack driving force (J -integral). (J_i) is determined from the stretched zone as measured in scanning electron microscope.

- Beyond the crack initiation, if the variation of 'q' across the ligament for the specimen and the component matches, then it is possible to transfer the specimen J-R curve to the components.
- There is a possibility of assessing the fracture behavior of the components qualitatively on the basis of variation of 'q' across the ligament beyond the crack initiation load. For the small values of 'q' in the ligament ($q \leq 0.3$) and $dq/dy \cong 0.0$, very little or no stable crack extension before fracture can be expected. Stable crack growth can be expected if $dq/dy > 0.0$.

2.4 DETERMINATION OF J-R CURVE FROM EXPERIMENTAL DATA: η_{pl} AND γ FUNCTIONS

As mentioned earlier in section 2.3.1 and 2.3.3, J-R curve is one of the very important inputs in elastic-plastic fracture analysis of cracked components. The evaluation of J-R curve from test data generally requires the experimental load vs. load-line-displacement and load vs. crack growth data. Rice et al [49] proposed splitting the total J-integral into elastic (J_e) and plastic (J_p) components:

$$J = J_e + J_p \quad (2.31)$$

$$J_e \text{ is evaluated as : } J_e = K^2 / E' \quad (2.32)$$

where, $E' = E$ for plane stress case and $E' = E / (1-\nu^2)$ for plane strain condition, K is the elastic stress intensity factor, E is the Young's modulus and ν is the Poisson's ratio.

Experimental evaluation of the J_p requires the ' η_{pl} ' function, proposed by Rice et al [49], to multiply the area under the load vs. plastic load-line-displacement curve. However, the J-integral, thus evaluated, requires modification if crack growth occurs. A ' γ ' term was proposed by Hutchinson and Paris [50] and later generalized by Ernst et al [51] and Ernst & Paris [52] to correct the J-integral to account for crack growth. The general expression to evaluate J_p from experimental data is as follows [24,53,54]:

$$J_p = \int_0^{\Delta_{pl}} \eta_{pl} P d\Delta_{pl} + \int_{a_0}^a \gamma J_p da \quad (2.33)$$

where, P is the total applied load, Δ_{pl} is the plastic load-line-displacement, ' a_0 ' is the initial crack length per crack tip, ' a ' is the current crack length per crack tip, η_{pl} and γ are two geometry dependent functions.

Equation (2.33) is solved in an iterative way. First, an approximate ' J_p ' is evaluated using the first term on the right hand side (RHS) of eqn.(2.33). Subsequently, this approximate ' J_p ' is corrected by the second term of the RHS of eqn.(2.33). Zahoor and Kanninen [54] suggested that if a sufficiently small increment of crack growth (Δa) is chosen, convergence is achieved in the first iteration. The above process of iteration can be expressed as [24] :

$$J_p = J_{p0} + \int_{a_0}^a \gamma J_{p0} da \quad (2.34)$$

$$J_{p0} = \int_0^{\Delta_{pl}} \eta_{pl} P d\Delta_{pl} \quad (2.35)$$

If the trapezoidal rule of numerical integration is invoked to solve eqns.(2.34) and (2.35), ' J_p ' can be expressed as follows :

$$J_{p_i} = [J_{p_{i-1}} + \eta_{pl_{i-1}} (U_{pl_i} - U_{pl_{i-1}})] [1 + \gamma_{i-1} (a_i - a_{i-1})] \quad (2.36)$$

with,

$$(U_{pl_i} - U_{pl_{i-1}}) = \left(\frac{P_{i-1} + P_i}{2} \right) (\Delta_{pl_i} - \Delta_{pl_{i-1}}) \quad (2.37)$$

where, U_{pl} is the area under the load vs. plastic load-point-displacement curve. The subscripts 'i' and 'i-1' indicate the current and previous load steps respectively.

The load, P and plastic load-line-displacement, Δ_{pl} are used here in a generic sense. For moment loading, applied load indicates the applied moment

(M) and plastic load-line-displacement indicates the plastic rotation (ϕ_{pl}) at the point where moment is applied.

Stress intensity factors for most geometries of interest under various loading conditions are available [24,44,55-57]. However, the ' η_{pl} ' and ' γ ' functions are available for limited geometry under certain specific loading conditions. ASTM E 1820-99 [42] gives an expression for the plastic J-integral, J_p of three point bend (TPB) specimen as:

$$J_{p_i} = \left[J_{p_{i-1}} + \left(\frac{2}{b_{i-1}} \right) \left(\frac{U_{p_i} - U_{p_{i-1}}}{B} \right) \right] \left[1 - \frac{a_i - a_{i-1}}{b_{i-1}} \right] \quad (2.38)$$

where, ' b ' is the remaining ligament and ' B ' is the specimen thickness without any side-groove. Comparing eqns.(2.36) and (2.38), the η_{pl} and γ functions for TPB specimen are :

$$\eta_{pl} = 2/bB \quad (2.39)$$

$$\gamma = -1/b \quad (2.40)$$

In case of through wall circumferentially cracked straight pipe under 4 point bending load, Zahoor & Kanninen [54] and Zahoor [24] express J_p as follows :

$$J_p = J_{p0} + \int_{\theta_0}^{\theta} \gamma J_{p0} . d\theta \quad (2.41)$$

J_{p0} is calculated from eqn.(2.35).

$$\eta_{pl} = \frac{0.5 [\sin(\theta/2) + \cos \theta]}{2Rt[\cos(\theta/2) - 0.5\sin \theta]} \quad (2.42)$$

$$\gamma = \frac{[0.5 \cos (\theta/2) - \sin \theta]}{[\sin(\theta/2) + \cos \theta]} \quad (2.43)$$

where, ' R ' is the mean pipe radius, ' t ' is the pipe wall thickness and ' θ ' is the semi-circumferential crack angle. Figure 2.8 shows the variation of η_{pl} and γ functions (eqs.(2.42) and (2.43)) with crack angle.

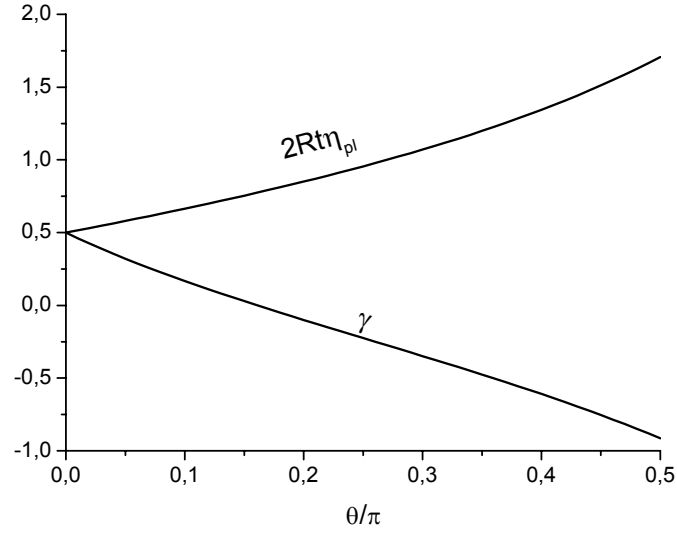


Fig.2.8 η_{pl} and γ functions for throughwall circumferentially cracked pipe under bending [54]

In the case of a through wall circumferentially cracked straight pipe under axial tension, Zahoor & Norris [58] and Zahoor [24] express J_p through eqns. (2.41) and (2.35) with ' η_{pl} ' and ' γ ' as follows :

$$\eta_{pl} = \frac{[1 + \cos \theta / \sin \psi]}{2Rt[2\psi - \theta]} \quad \text{where, } \psi = \cos^{-1}[0.5 \sin \theta] \quad (2.44)$$

$$\text{As per Zahoor and Norris [58], } \gamma = \frac{(0.5 \cos^2 \theta \cot \psi - \sin \theta \sin \psi)}{(1 + \cos \theta / \sin \psi) \sin^2 \psi} \quad (2.45)$$

In the case of a constant depth part-throughwall circumferentially cracked straight pipe under axial tension, Zahoor & Norris [58] and Zahoor [55] express J_p from eqns.(2.34) and (2.35) with ' η_{pl} ' and ' γ ' as follows:

$$\eta_{pl} = \frac{G_1}{2\pi R t \left(\frac{2\psi}{\pi} - \frac{x\theta}{\pi} \right)} \quad (2.46)$$

$$\gamma = \frac{\left(\frac{0.5}{t} \right) \left(\frac{\sin^2 \theta}{\theta} \right) \left(\frac{\cot \psi}{\sin^2 \psi} \right)}{G_1} \quad (2.47)$$

with, $G_1 = 1 + \frac{\sin \theta}{\theta \sin \psi}$, $\psi = \cos^{-1}[0.5 x \sin \theta]$ and $x = a/t$

where, 'a' is the crack depth and '2θ' is the crack angle.

In the case of a fully circumferential part-through cracked pipe under axial tension, Zahoor [55] gives the expression of the plastic J-integral without crack growth as :

$$J_p = \eta_{pl} \int_0^{\Delta_{pl}} P d\Delta_{pl} \quad (2.48)$$

$$\eta_{pl} = \frac{1}{2\pi R t \left[1 - x \frac{(2 - 2\zeta + x\zeta)}{(2 - \zeta)} \right]} \quad (2.49)$$

with, $x = a/t$ and $\zeta = t/R_o$ where, 'R_o' is the pipe outer radius.

Miura and Wilkowski [59,60] derived from dimensional analysis the 'η_{pl}' and 'γ' functions of pipes with through wall circumferential crack under combined bending and axial tension as follows :

$$J_p = \int_0^{\Delta_{pl}} \eta_{pl} P d\Delta_{pl} + \int_{\theta_o}^{\theta} \gamma J_p d\theta + \int_{s_o}^s \mu J_p ds \quad (2.50)$$

with,

$$\eta_{pl} = - \frac{(\partial h_p / \partial \theta)}{2R t h_p} \quad (2.51)$$

$$\gamma = \frac{(\partial^2 h_p / \partial \theta^2)}{(\partial h_p / \partial \theta)} \quad (2.52)$$

$$\mu = \frac{(\partial^2 h_p / \partial s \partial \theta)}{(\partial h_p / \partial \theta)} \quad (2.53)$$

$$h_p = \cos\left(\frac{\theta}{2} + \frac{\pi}{2} s\right) - 0.5 \sin \theta \quad (2.54)$$

$$s = \frac{T}{2\pi R t \sigma_f} \quad (2.55)$$

where, 'T' is the axial tension and 'σ_f' is the material flow stress. Eqn.(2.50) assumes that the plastic load-line-displacement due to axial tension is negligible.

In the case of constant axial tension, the third term in eqn.(2.50) vanishes and thus, the plastic J-integral, J_p is evaluated as :

$$J_p = \int_0^{\Delta_{pl}} \eta_{pl} P d\Delta_{pl} + \int_{\theta_0}^{\theta} \gamma J_p d\theta \quad (2.56)$$

with η_{pl} and γ as per eqns.(2.51) and (2.52).

2.5 MEASUREMENT OF CRACK GROWTH DURING FRACTURE EXPERIMENTS

Fracture resistance of a ductile material is usually expressed as J-R curve that quantifies the J-resistance with respect to crack growth. Generation of J-R curve through fracture experiments, therefore, requires measurement of crack growth at various stages of loading of the specimen. Earlier, multiple specimen technique was used to obtain J-R curve through fracture experiments. In this technique, crack growth used to be measured physically after breaking open the fracture surface and subsequent heat-tinting of each specimen. However, this technique was costly due to requirement of large number of specimens. Consequently, single specimen technique of evaluation of J-R curve has emerged where, crack growth is measured either by potential drop or partial unloading compliance technique [61,62] at various stages of loading without breaking the specimen. These techniques have made it possible to generate the complete material J-resistance curve by testing a single specimen.

The potential drop technique utilizes a voltage change to infer crack growth. If a constant current passes through the un-cracked ligament of a test specimen, the voltage must increase as the crack grows, because electrical resistance across the crack increases and the remaining ligament cross-section decreases. The disadvantages of this technique is that it requires additional instrumentation [63] and sometimes it becomes difficult to separate the voltage change due to crack growth and plastic energy near the crack tip of a ductile material [64].

The partial unloading compliance technique is the commonly used method to measure the crack growth in testing of fracture mechanics specimens such as compact tension (CT) and side edge notched bend (SENB) (also known as three point bend (TPB)) specimen. The crack length is computed at regular intervals during the test by partially unloading the specimen and measuring the compliance. As the crack grows, the specimen compliance changes (becomes less stiff). Figure 2.9 shows a typical load-displacement diagram with partial unloading at regular interval.

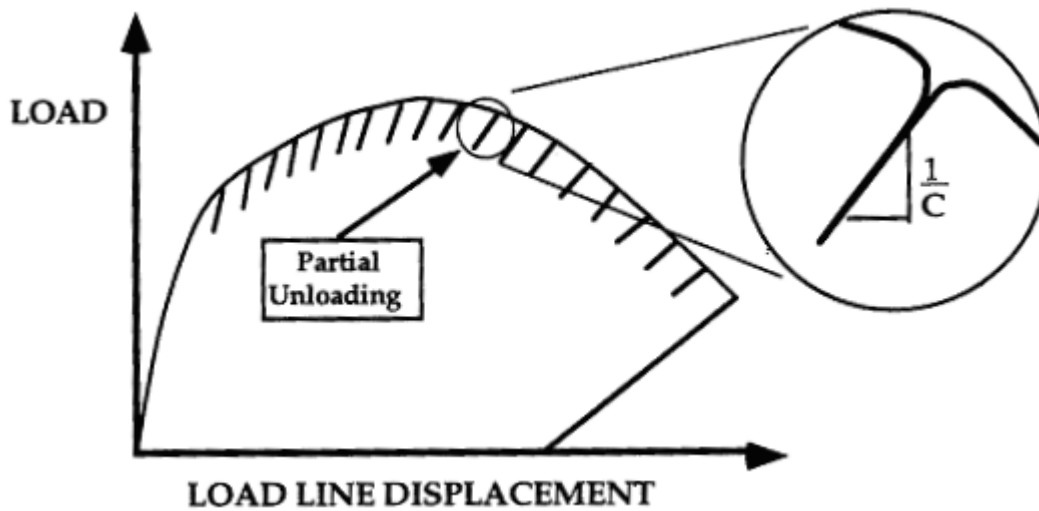


Fig.2.9 Typical load-displacement curve with partial unloading to measure crack growth by compliance technique

However, one pre-requisite of using this technique is to have a compliance function correlating the crack length and depth with the compliance. Correlations are available [42] for CT, TPB and some other type of specimens. The relation for CT specimen is as follows [42]:

$$a/w = 1.000196 - 4.06319u + 11.242u^2 - 106.043u^3 + 464.335u^4 - 650.677u^5 \quad (2.57)$$

$$u = \frac{1}{[B_e E' C]^{1/2} + 1} \quad (2.58)$$

$$B_e = B - \frac{(B - B_N)^2}{B} \quad (2.59)$$

where, C = crack opening elastic compliance ($\Delta CMOD/\Delta P$) on an unloading/reloading sequence, $E' = E$ for plane stress condition and $E' = E / (1 - \nu^2)$ for plane strain condition, B_N is the net thickness after side groove and B is the original thickness.

The compliance correlation for the TPBB specimen is as follows [42]:

$$a/w = 0.999748 - 3.9504u + 2.9821u^2 - 3.21408u^3 + 51.51564u^4 - 113.031u^5 \quad (2.60)$$

$$u = \frac{1}{\left[\frac{B_e W E' C}{S/4} \right]^{1/2} + 1} \quad (2.61)$$

where, S is the loading span and W is the width of the TPB specimen and other symbols have the same meaning as in eqns.(2.57-2.59)

However, for pipes, similar functions are not available in the literature. Therefore, investigations have been carried out in this work to study the variation of pipe compliance with crack geometry.

3. THEORETICAL INVESTIGATIONS

3.1 CLOSED-FORM COLLAPSE MOMENT EQUATIONS OF UN-CRACKED ELBOWS SUBJECTED TO COMBINED INTERNAL PRESSURE AND IN-PLANE BENDING MOMENT

3.1.1 Scope of the Work

As mentioned in section 2.2, limit load equations are available for un-cracked elbows under pure internal pressure and pure bending moment. However, in actual service conditions, an elbow is often subjected to combined internal pressure and bending moment. No limit load equations are available for such combined loading. In the present work, elastic-plastic finite element analysis has been carried out to evaluate collapse moments of un-cracked elbows subjected to combined internal pressure and in-plane bending moment. For various elbow factors and level of internal pressure, total 60 and 54 cases are analyzed for closing and opening mode of bending moment respectively. Based on these results, two closed-form equations are proposed to evaluate the collapse moments of elbows under combined internal pressure and in-plane closing and opening bending moment.

3.1.2 Finite Element Analysis

The finite element method is used to conduct the investigation of collapse loads of elbows of various sizes under combined internal pressure and bending moment. General purpose finite element program NISA [65] is used for this study. Non-linear finite element analysis has been carried out to determine the collapse moments of elbow for various geometric and loading combinations. Both geometric and material non-linearity are considered in the analysis. It has been seen in the course of this analysis that consideration of geometric non-linearity is very important for precise determination of elbow deflection under various combinations of the closing and opening bending moment and internal pressure. Moment *versus* end rotation curves are generated through finite element analysis where end rotation (ϕ) is defined as : $\phi = \tan^{-1}[(u_1-u_2)/2R]$, u_1 and u_2 are the axial displacements of two diametrically opposite points at mean

radial position, situated at the end plane of connecting straight pipe where moment is applied (see Fig.3.1). Collapse moments are obtained by twice elastic slope method from these curves. The following sections briefly describe the different aspects of the finite element analysis.

3.1.2.1 Geometry

Geometrically, a 90° elbow is characterized by two parameters, namely, R/t and elbow factor, $h=tR_b/R^2$ where R is the mean cross sectional radius, t is the wall thickness and R_b is the mean bend radius of the elbow. Table 3.1 shows the different combinations of these parameters taken in the study. The mean bend radius is always kept as three times the mean cross sectional radius in the present study indicating a long radius elbow. The R/t varies from 5 to 12.5 and elbow factor (h) varies from 0.24 to 0.6. These ranges have been decided keeping in view mainly the primary heat transport (PHT) piping of Pressurized Heavy Water Reactor (PHWR). In a typical case, the R/t and h values ranged from 5.6 to 6 and 0.54 to 0.58 respectively for 500 MWe Indian PHWR. In the present analyses, the elbow is connected with straight pipes of length equal to the six times the mean cross sectional radius. It is important to note that this straight pipe length allows free ovalisation propagation from mean elbow section. Figure 3.1 shows a typical elbow.

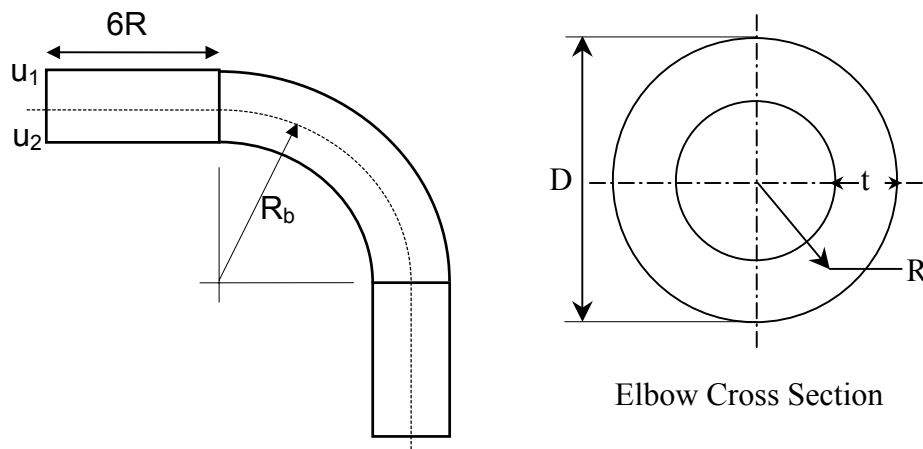


Fig.3.1 Geometry of a 90° elbow

Table 3.1 Geometry of the Elbows

R (mm)	t (mm)	R / t	R _b / R	h = tR _b /R ²
250	20	12.50	3	0.240
250	28	8.93	3	0.336
250	35	7.14	3	0.420
250	40	6.25	3	0.480
250	45	5.55	3	0.540
250	50	5.00	3	0.600

3.1.2.2 Material

The material is assumed isotropic. Strain hardening of the material is considered. Stress -strain response of a typical nuclear grade piping steel SA350 Gr LF2 at room temperature has been considered in the analysis. Table 3.2 shows the material properties used in the analysis. In the finite element analysis, material true stress - true strain behavior is used as input. Five points are considered to define the true stress - true strain response of the material. Von-Mises yield criteria and isotropic hardening are assumed in the elastic-plastic analysis.

Table 3.2 Material properties used in the analysis

Yield stress (MPa)	:	270				
UTS (MPa)	:	513				
Young's modulus (GPa)	:	203				
Poisson's ratio	:	0.3				
True stress (MPa)	:	300	370	450	520	605
True strain	:	4.76×10^{-3}	0.0174	0.042	0.079	0.167

3.1.2.3 Loading

The load in the elbows is split in two components : a constant internal pressure and varying in-plane bending moment monotonically increasing in definite steps. The maximum increase in moment in one load step was 102 kNm and minimum was 10.2 kNm. The pressure is applied in an initial step and subsequently held constant. The rationale behind keeping pressure constant is that internal pressure generally does not increase during service. Whereas,

bending moment may increase significantly in an accidental condition. Thus it is of interest to predict collapse moment of an elbow for a constant internal pressure. Internal pressure is normalized as, $p = (P_r R / t \sigma_y)$, where P_r is the applied internal pressure and σ_y is the material yield stress. The various normalized pressures considered in the analysis are $p = 0$ (i.e. pure bending moment), 0.1157, 0.2314, 0.3471, 0.463, 0.5785, 0.6943, 0.8099, 0.9257 and 1.0. Closed end condition is simulated by applying axial pressure of intensity 'PR/2t' at the end of the connecting straight pipe. There are two modes of in-plane bending moment : closing and opening. Kussmaul et al [66] reported a significant difference in the deflection behavior of elbow for these two modes of bending moment. Consequently, in the present study, both opening and closing bending moments are considered separately. Bending moment has been simulated as triangularly varying pressure applied on element face. However, within an element, face pressure has been kept constant. The face pressure value is obtained as 'M.c/I' where 'M' is the applied bending moment, 'I' is the area moment of inertia of the elbow cross section and 'c' is the vertical distance of the element face center from the neutral axis. The application of bending moment in this way avoids the unwanted plastic deformation at the point of load application. The axial component of pressure stress and the triangularly varying bending stress have been applied as follower pressure i.e. they act always perpendicular to the end plane even after deformation.

3.1.2.4 Definition of Collapse Moment

Collapse moment has been evaluated from the moment v/s end rotation curves by twice elastic slope method (see Fig.2.1). In this method, a tangent to the initial linear part of the moment-rotation curve is drawn. The angle (θ_1) that this tangent makes with the vertical axis of moment is evaluated as : $\tan (\theta_1) = (\phi_2 - \phi_1) / (M_2 - M_1)$ where ϕ_2 is the end rotation at moment $M_2 = 204$ kNm and ϕ_1 is the end rotation at moment $M_1 = 102$ kNm. Deformations remain predominantly elastic at the applied moment of 204 kNm in all the cases. Then another straight line is drawn at an angle (θ_2) with respect to the vertical axis such that $\tan (\theta_2) =$

$2 \tan (\theta_1)$. The intersection of the second line with the moment - end rotation curve is defined as the collapse moment. Moment v/s end rotation curves are generated through non-linear finite element analysis. Collapse moments are expressed in non-dimensional form defined as $m_L = M_L / 4R^2t\sigma_y$.

3.1.2.5 Finite Element Model

Twenty-noded solid elements with $3 \times 3 \times 3$ integration order are used to model the elbow. Because of symmetry, only one fourth of the elbow is modeled. There are total 195 elements and 1508 nodes. Fifteen elements along the circumference, thirteen elements along the elbow - straight pipe axis and one element across the thickness are taken to model the elbow. Figure 3.2 shows a typical finite element mesh. The same mesh pattern is used for all the cases. A mesh convergence study has been performed to check the adequacy of this mesh. A finer mesh consisting of 408 elements with 12 elements along the circumference, 17 elements along the axis and 2 elements across the thickness is generated and collapse moments are evaluated for a typical elbow of $h = 0.42$ for various normalized internal pressures (p). The normalized collapse moments (m_L) for $p = 0.0, 0.463, 0.9257$ and 1.0414 are respectively $0.6542, 0.7257, 0.5998$ and 0.5362 for coarse mesh and $0.6706, 0.7341, 0.5984$ and 0.5360 for fine mesh. The difference is only 2.4%, 1.1%, 0.23% and 0.04% respectively. This proves the adequacy of the present mesh. This is expected since moment-rotation curve is a gross structural behavior which does not strongly depend on mesh. A multi-point constraint is used at the end-plane of the straight pipe where the bending moment and axial stress due to pressure are applied. This keeps the plane cross section plane before and after deformation.

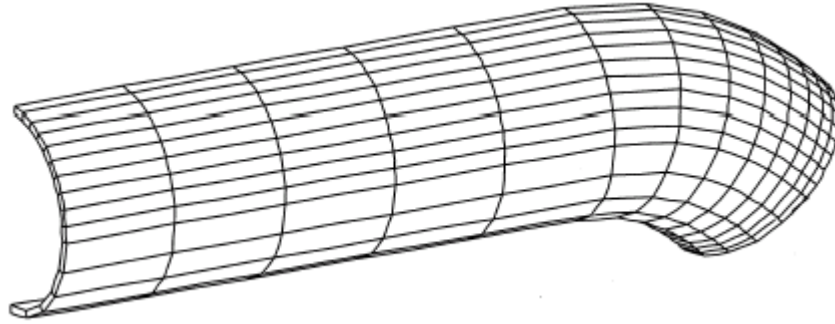


Fig.3.2 Typical finite element mesh of an elbow

3.1.3 Results and Discussion

Six elbows of various elbow factors have been analyzed. For each elbow, both closing and opening modes of bending moments are considered. In case of closing mode, ten and in case of opening mode, nine different normalized pressures ranging from $p = 0$ to 1.0 are considered in the analysis. Therefore, a total of 60 and 54 cases are analyzed for closing and opening moments, respectively. For each of these cases, moment v/s end rotation curves have been generated through non-linear finite element analysis. From these moment-end rotation curves, collapse moments are evaluated by twice elastic slope method as described earlier. In the presentation of results, collapse moment and internal pressure are expressed in normalized forms. The effect of internal pressure on various aspects of the elbow deformation is described below.

3.1.3.1 Moment v/s End Rotation Curves

It has been observed that moment v/s end rotation curves in case of pure closing bending without any internal pressure becomes almost flat after applied moment exceeds certain limit indicating the instability of the elbow. However, the same elbow when subjected to opening mode of bending moment, shows the rising nature of moment v/s end rotation curves. Figure 3.3 shows a typical comparison. It may be observed from Fig.3.3 that the elastic response of the elbow subjected to closing and opening mode of bending is almost the same

indicating that geometric non-linearity is not significant in the elastic response. The difference is mainly in the plastic response. The effect of internal pressure

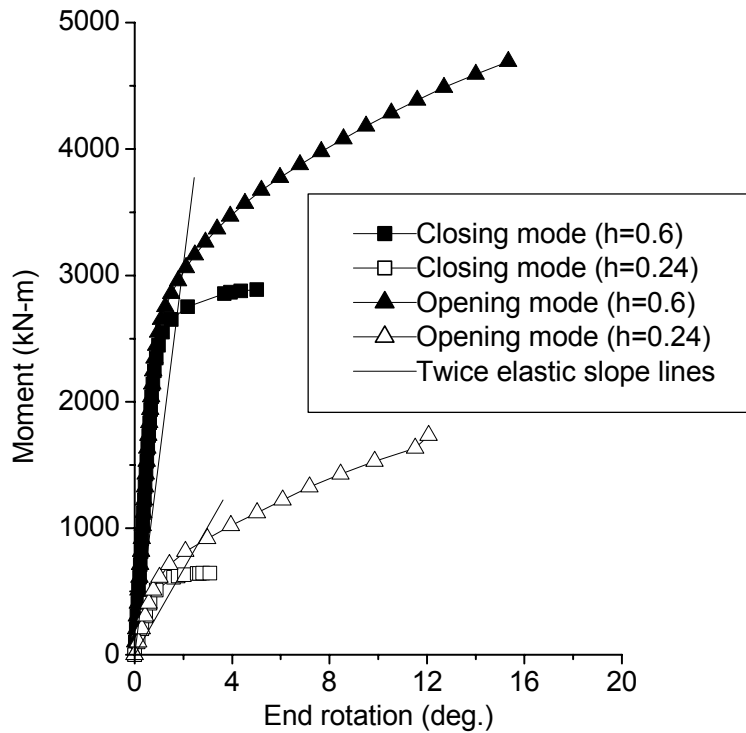


Fig.3.3 Comparison of moment – end rotation curves between pure closing and opening mode of bending moment

on the moment-end rotation curve and collapse moment is studied. It has been seen that internal pressure stiffens the elbow compared to when it is subjected to pure bending moment. The stiffening effect is more significant for thinner elbow subjected to closing mode of bending moment. Figures 3.4 and 3.5 show the stiffening effect of internal pressure on the moment - end rotation curve for two elbows having elbow factor of 0.24 and 0.6 respectively in closing mode of bending moment. Although analysis has been done for ten different normalized pressures, only four are shown in the figures for clarity. Figures 3.4 and 3.5 also show the twice elastic slope lines. It may be seen from Figs. 3.4 and 3.5 that the beneficial effect of internal pressure on collapse moment is more pronounced in case of thin elbow ($h=0.24$) as compared to thick elbow ($h=0.6$). A similar trend is observed in the opening mode of in-plane bending moment also.

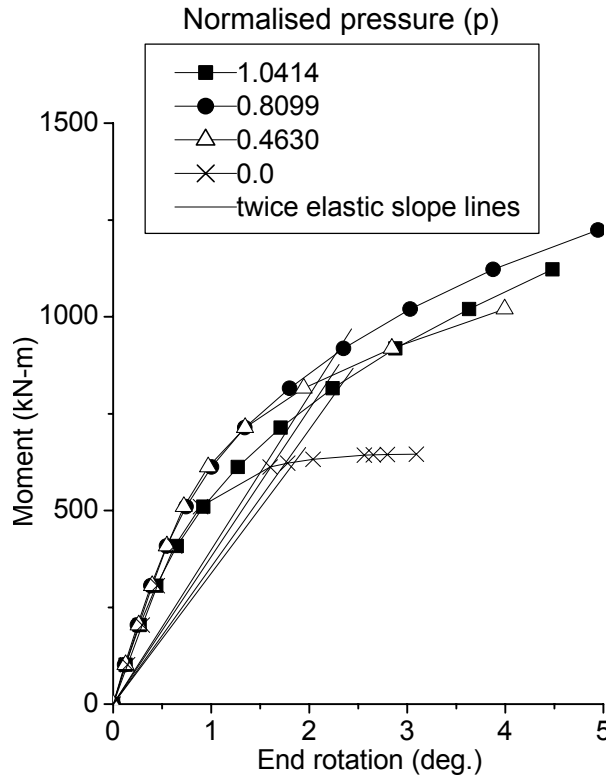


Fig.3.4 Closing moment vs. end rotation curves for elbow of $h = 0.24$ subjected to different internal pressures

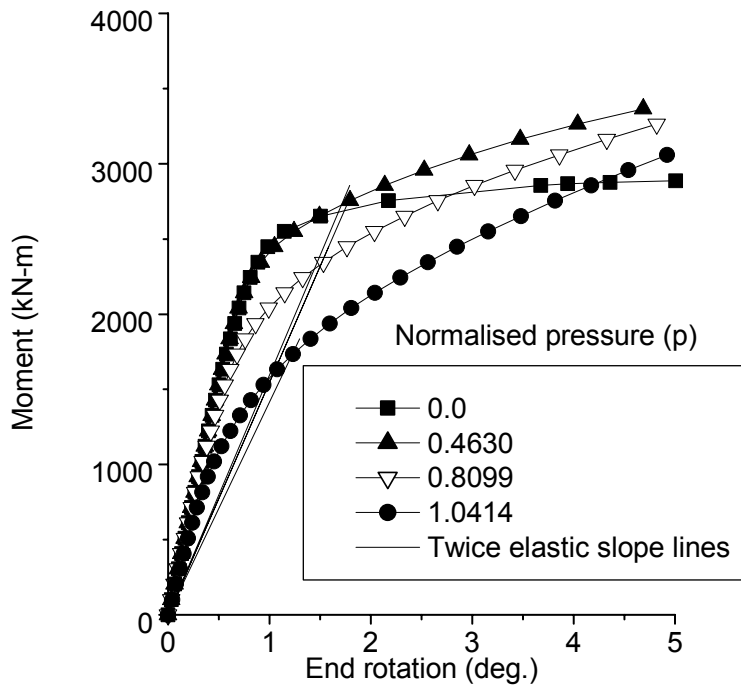


Fig.3.5 Closing moment vs. end rotation curves for elbow of $h = 0.6$ subjected to different internal pressures

3.1.3.2 Variation of Collapse Moment with Internal Pressure

Figures 3.6 and 3.7 show the effect of normalized internal pressure on the normalized collapse moments of the elbows subjected to closing and opening mode of bending respectively. In both the cases, it is observed that collapse moment increases gradually with application of internal pressure. It reaches a peak and then starts falling with further increase in internal pressure. This is in agreement with the observations of Shalaby and Younan [38,39]. The ovalisation of the elbow cross section plays an important role in its collapse behavior. The application of uniform internal pressure opposes the ovalisation of the elbow cross section, thus delaying the collapse phenomenon. Ovalisation is more prominent in case of thin walled elbow. That is why internal pressure enhances the limit moments significantly in thin walled elbow. However, if the internal pressure is increased beyond a limit, the hoop stress due to internal pressure nullifies the beneficial effect on the limit moments and finally the limit moment starts reducing with increase in internal pressure. The effect of normalized

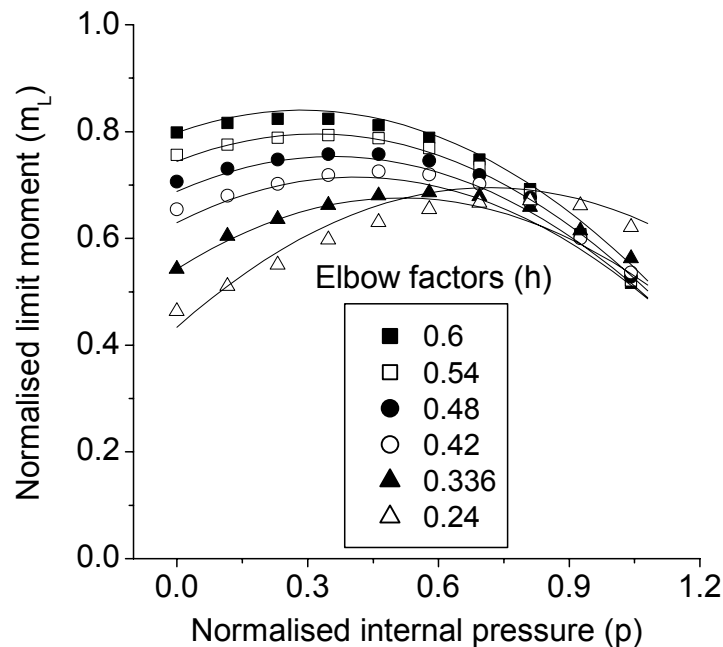


Fig.3.6 Normalized closing limit moments for various normalized internal pressures and elbow factors (symbols show the FE results and solid lines show predictions of closed-form eqn.(3.1))

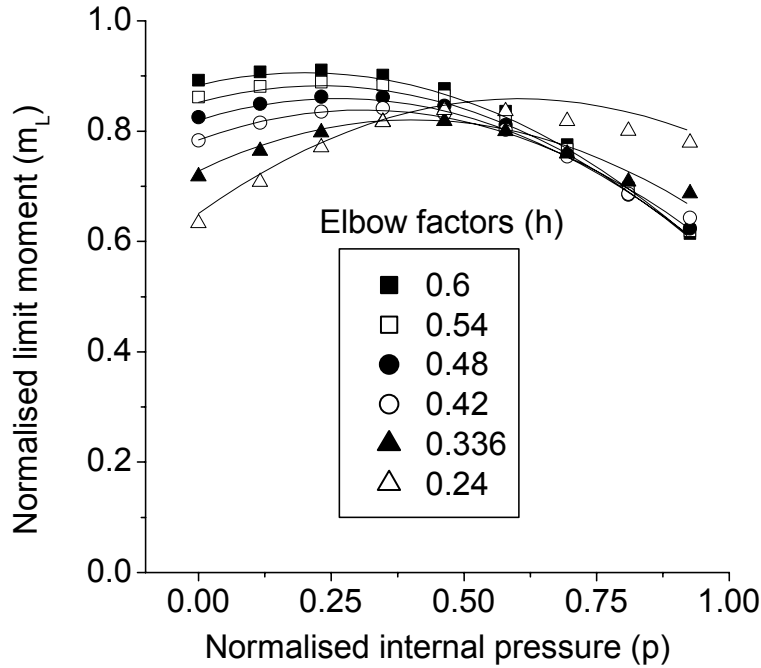


Fig.3.7 Normalized opening limit moments for various normalized internal pressures and elbow factors (symbols show the FE results and solid lines show predictions of closed-form eqn.(3.2))

internal pressure on the normalized collapse moment in closing and opening mode is essentially the same. However, in case of opening mode, the fall of normalized collapse moment starts at lower value of normalized internal pressure. The end rotation at collapse moment has been less than 2.5° in all the cases. Maximum equivalent plastic strains at closing collapse moments have been noted in some cases to ascertain the degree of strain hardening at collapse and shown in Table 3.3.

Table 3.3 Plastic strains observed for few cases at $p = 1.0$

Elbow factor (h)	Bending moment (kNm)	Plastic strain (%)
0.24	838	2.52
0.42	1267	3.68
0.6	1743	5.65

3.1.3.3 Variation of Collapse Moment with Elbow factor

The variation of normalized collapse moment with elbow factor (h) for different normalized internal pressures is studied. It has been observed that at lower values of pressure, normalized collapse moment increases with elbow factor. However, at higher pressure, normalized collapse moments remains almost constant or decrease slightly with respect to elbow factor. This indicates less significant role of ovalisation at high pressure. Figure 3.8 shows the nature of variation of normalized collapse moment with elbow factor for closing mode of bending moment. Almost same nature is observed for opening mode also.

3.1.3.4 Deformed Shape of Elbow Cross Section

It is seen from Fig.3.3 that an elbow under opening mode of bending moment is stiffer than in closing mode. It is also seen from Figs.3.4 – 3.7 that internal pressure stiffens the elbow up to a certain extent. These behaviours of moment v/s rotation curves and collapse moments can be explained through the ovalisation of elbow cross section. Figure 3.9 shows the deformed shape of the elbow cross section at the middle of its axis length in closing bending moment of 612 kNm for normalized pressures, $p = 0$ and 0.4628. The ovalisation of the cross section is seen from the Fig. 3.9. The diameter across the intrados - extrados contracts while the diameter across the crown expands. This reduces the cross-sectional moment of inertia. It may also be seen from Fig.3.9 that internal pressure reduces the ovalisation and thereby stiffens the elbow.

Figure 3.10 shows the deformed shape of elbow cross section at the middle of its axis length for various values opening bending moment. It may be seen that the diameter across the intrados-extrados expands during ovalisation. This increases the cross-sectional moment of inertia and hence stiffens the elbow. This explains the rising nature of moment-end rotation curve of an elbow subjected to opening bending moment compared to a curve with almost zero slope when subjected to closing mode (Fig.3.3).

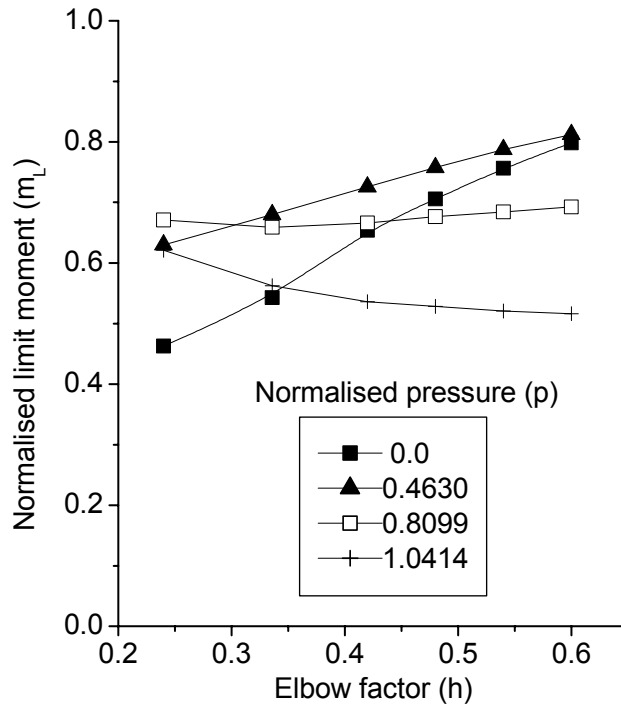


Fig.3.8 Variation of normalized limit moment with elbow factor for different degrees of internal pressure for closing case

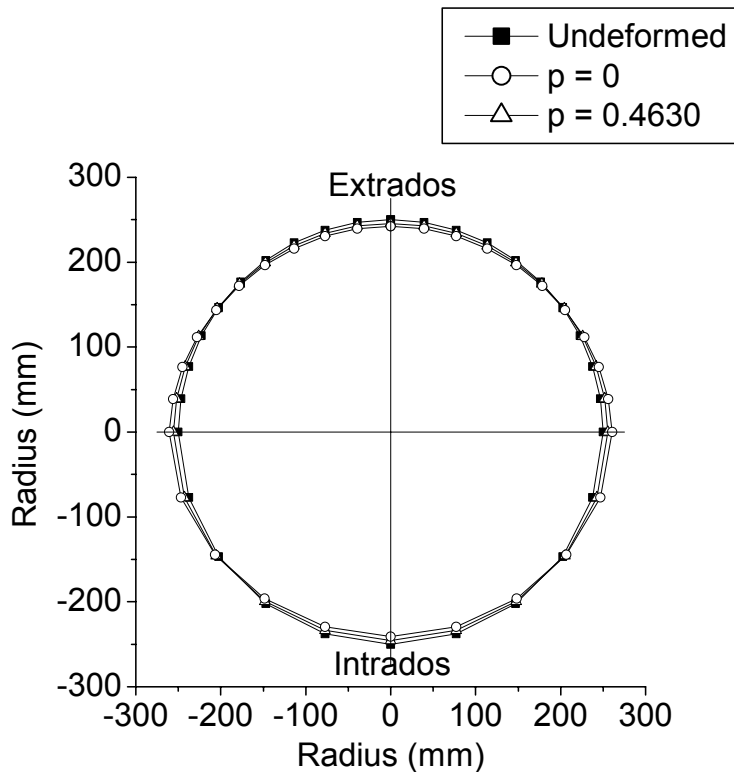


Fig.3.9 Deformed shape of elbow cross sections at various levels of internal pressure for closing moment of 612 kNm and elbow factor of 0.24

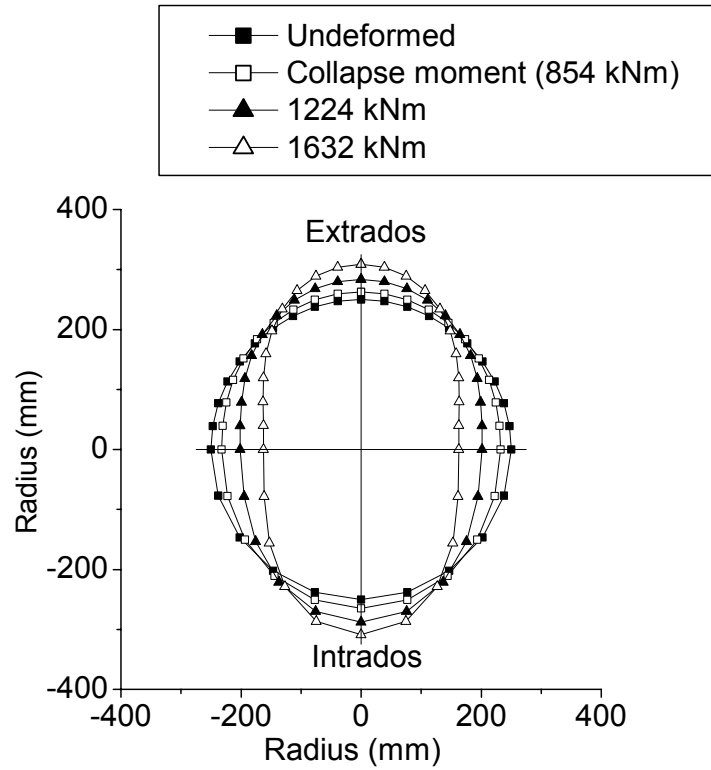


Fig.3.10 Deformed shape of elbow cross sections at various opening bending moments (internal pressure = 0, elbow factor = 0.24)

3.1.3.5 Proposed Closed-Form Equations

Based on the above results of the normalized limit moments for various sizes of elbow subjected to different levels of constant internal pressure and closing / opening in-plane bending moment, two closed-form equations are proposed to evaluate the collapse moment:

$$m_L = 1.122 h^{2/3} + 0.175 \frac{p}{h} - 0.508 p^2 \quad (\text{for closing case}) \quad (3.1)$$

$$m_L = 1.047 h^{1/3} + 0.124 \frac{p}{h^{1.2}} - 0.568 p^2 \quad (\text{for opening case}) \quad (3.2)$$

Applicability : $0.24 \leq h \leq 0.6$ and $0.0 \leq p \leq 1.0$

The root mean square error (RMSE) is 2.831% and 1.572% for closing and opening cases respectively where error and RMSE are defined as follows :

$$\text{Error } (E_i) = \left[\frac{(m_L)_{FEM} - (m_L)_{pr}}{(m_L)_{FEM}} \right]_i \quad (3.3)$$

$$\text{RMSE} = \left[\sum_{i=1}^n \frac{E_i^2}{n} \right]^{1/2} \quad (3.4)$$

where, $(m_L)_{FEM}$ is the normalized limit moment from finite element analysis and $(m_L)_{pr}$ is the normalized limit moment predicted through equations (3.1) and (3.2). Figures 3.6 and 3.7 show the comparison of fitted and finite element data. The fit seems to be all right except for $h = 0.24$, where the maximum error (E_i) is 6.4% and -4.3% for closing and opening cases respectively. This may be within the acceptable limits.

3.1.3.6 Comparison of Closed-Form Equation Predictions with Available Results

It is useful to compare the present results with the results already available in the literature. The comparisons for un-pressurized and pressurized cases are done separately. For un-pressurized cases, the prediction of closing collapse moment as per Eqn.(3.1) is compared with Spence & Findlay (Eqns.2.4 & 2.5), Calladine (Eqn.2.6), Goodall (Eqns.2.7 & 2.8), Touboul et al (Eqn.2.9) and Griffiths (see Chapter 2.2.2). Table 3.4 shows the comparison of normalized closing collapse moment (m_L) for $h = 0.24$ and 0.42 . It is seen that the present results are higher than those of Spence & Findlay [29], Calladine [30] and Touboul et al [33]. This is due to two reasons - stiffening effect of connecting straight pipes and consideration of strain hardening in the present analysis. This is comparable with the results of Griffiths [32] who observes that 90° bend specimens without defects give consistently higher values of collapse moments than those predicted by Calladine [30] and this is predominantly due to the constraining effect of the tangent pipes, an effect that becomes significant for $R_b/R < 3$. Griffiths [32] suggests a factor of '1.33' to multiply the Calladine equation (Eqn.2.6) to match his elbow test data for $R_b/R = 2$. From the present

Eqn.(3.1), the factor becomes 1.2 which is less than 1.33. This is understandable because the present analysis is for $R_b/R = 3$ and the stiffening effect reduces with increasing R_b/R .

Table 3.4 Comparison of closing m_L for $p = 0.0$

h	Spence & Findlay	Calladine	Touboul et al	Griffiths (1.33 × Calladine)	Present
0.24	0.368	0.361	0.276	0.480	0.433
0.42	0.544	0.524	0.4	0.697	0.629

For pressurized cases, the present results predicted by Eqns.(3.1) and (3.2) are compared with those predicted by Eqn.(2.13) of Touboul et al [33] and digitized data from the graphs of Shalaby and Younan [38,39]. The comparison is done in the form of $M_L(p) / M_L(p = 0)$ v/s normalized internal pressure (p). Figure 3.11 shows the comparison for a typical elbow factor, $h = 0.4132$. It may be noted that as per the present definition of elbow factor, $h = tR_b/R^2$, the elbow factor of 0.4417 in Shalaby and Younan [38,39] becomes 0.4132. It is seen from Fig. 3.11 that the effect of internal pressure on limit moment as per Touboul et al [33] is much more pronounced than that as per the present Eqns. (3.1) and (3.2). This is expected since Eqn.(2.13) of Touboul et al [33] is for instability moment and the present equations (3.1) and (3.2) are for collapse moments and Touboul et al [33] observes that the pressure effect is larger upon instability than upon collapse moments. The pressure effect on collapse moments as per the present equations (3.1) and (3.2) is consistently higher than those as per Shalaby and Younan [38,39]. This is probably due to consideration of material strain hardening in the present analysis as compared to the assumption of elastic-perfectly plastic material response by Shalaby and Younan. From the above discussion, it is concluded that the present results are consistent with the available test data and analytical results.

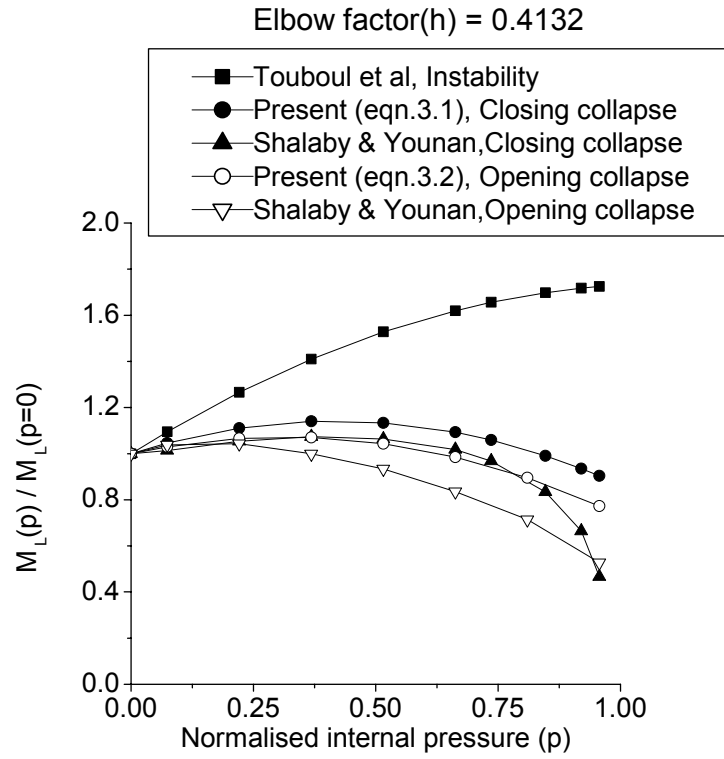


Fig.3.11 Effect of internal pressure on limit moments – a comparison

3.2 DERIVATION OF LIMIT LOAD BASED GENERAL EXPRESSIONS OF ‘ η_{pl} ’ AND ‘ γ ’ FUNCTIONS AND EVALUATING NEW ‘ η_{pl} ’ AND ‘ γ ’ FUNCTIONS FOR PIPES AND ELBOWS

3.2.1 Scope of the Work

Fracture resistance characteristics of the material is evaluated from J-R curve from test data of load-deflection and load-crack growth behavior of specimens or components through eqns. (2.31-2.33). Experimental evaluation of plastic part of J-integral through eqn.(2.33) requires ‘ η_{pl} ’ and ‘ γ ’ functions. It is clear from the forgoing discussion in section 2.4 that ‘ η_{pl} ’ and ‘ γ ’ functions are available for very limited number of geometries under specified loading conditions. No general expressions are available. Roos et al [67] proposed a limit load based general expression of ‘ η_{pl} ’. However, its application was shown only for a few laboratory specimens. No general expression is available in the literature for ‘ γ ’ functions. This puts considerable constraint on evaluation of the *J-R* curve from experimental data of many specimens and components and on the study of transferability of the specimen *J-R* curve to the component. In this study of transferability, it is required to compare the *J-R* curve of the specimen with that of the component. In the present work, general expressions for ‘ η_{pl} ’ and ‘ γ ’ functions in terms of derivatives of the limit load are proposed. The derivation assumes that the load can be represented as the product of two independent functions of crack length and plastic load-point deformation. A pre-requisite of getting the ‘ η_{pl} ’ and ‘ γ ’ functions for a particular geometric configuration and loading condition from the proposed expression is to have the limit load [18,19,26,27,28] of the structure as a function of crack length. To validate this general expression, existing ‘ η_{pl} ’ and ‘ γ ’ functions for various geometries and loading conditions are derived. The general expression is then used to derive the ‘ η_{pl} ’ and ‘ γ ’ functions for geometries and loading conditions for which no solutions are available in the open literature. These geometries include the constant depth part-through flawed pipe under combined bending and axial tension, a semi-

elliptical flawed pipe under axial tension and combined bending and axial tension, a throughwall axially and circumferentially cracked elbow (both short radius and long radius) under in-plane bending moment. Finally, these newly proposed ' η_{pl} ' and ' γ ' functions have been applied to generate J-R curve from fracture experiments of 200mm nominal bore (NB) diameter elbows with throughwall circumferential cracks at the intrados/extrados under in-plane opening/closing moment. The subsequent sections will describe the derivation of limit load based general expressions of ' η_{pl} ' and ' γ ' functions, validation of these general expressions through derivation of existing ' η_{pl} ' and ' γ ' functions and derivation of new ' η_{pl} ' and ' γ ' functions for various piping components with various crack configurations and loading conditions. Section 4.2 will describe the experimental application of these ' η_{pl} ' and ' γ ' functions of elbows.

3.2.2 Derivation of Limit Load Based General Expression of ' η_{pl} ' and ' γ ' Functions

Ernst et al [52,53] have shown that ' η_{pl} ' will always exist if and only if a separation of variables can be found for the expression of the load (P) in terms of crack length (a) and plastic load-line-displacement (Δ_{pl}). This can be verified by plotting ' P ' vs. ' Δ_{pl} ' for various constant ' a ' values. If any two curves for two constant values of ' a ' maintain a constant difference of ' P ' for a range of ' Δ_{pl} ', then separation exists for that range. This can be checked experimentally and/or numerically by generating the ' P ' vs. ' Δ_{pl} ' plots of identical geometrical configurations with identical materials differing only in their crack length. It has been checked experimentally by Sharobeam et al [68] for compact and single edge notched bend specimens and numerically by Chattopadhyay et al [22,69,70] for pipes and elbows that it is indeed true except for very low values of plastic displacement. Ernst et al [53] observe that ' η_{pl} ' approach will give sufficiently accurate results even if the above condition is slightly violated. It is, therefore, assumed here that load (P) can be expressed as a product of two independent functions, ' F ' and ' G ', of plastic load line displacement (Δ_{pl}) and crack length (a) respectively :

$$P = F(\Delta_{pl}). G(a) \quad (3.5)$$

Accordingly, the plastic component of the J-integral is a function of plastic load-line displacement and crack size,

$$J_p = J_p(\Delta_{pl}, a) \quad (3.6)$$

and therefore the differentiation results in,

$$dJ_p = \left. \frac{\partial J_p}{\partial \Delta_{pl}} \right|_a d\Delta_{pl} + \left. \frac{\partial J_p}{\partial a} \right|_{\Delta_{pl}} da \quad (3.7)$$

$$\text{Substituting, } J_p = - \frac{\partial U_{pl}}{\partial A} \quad (3.8)$$

where, ' U_{pl} ' is the plastic part of distortion energy and is represented by the area under the load (P) vs. plastic load-line-displacement (Δ_{pl}) curve and 'A' is the crack area. In conditions of ideal plastic material behavior and constant plastic load-line-displacement (Δ_{pl}),

$$U_{pl} = F_L \cdot \Delta_{pl} \quad (3.9)$$

where, F_L is the plastic limit load.

Substituting eqn.(3.9) in eqn.(3.8),

$$J_p = - \Delta_{pl} \cdot (\partial F_L / \partial A) \quad (3.10)$$

Substituting eqn.(3.10) in eqn.(3.7),

$$dJ_p = \left. \frac{\partial}{\partial \Delta_{pl}} \left(- \Delta_{pl} \cdot \frac{\partial F_L}{\partial A} \right) \right|_a d\Delta_{pl} + \left. \frac{\partial}{\partial a} \left(- \Delta_{pl} \cdot \frac{\partial F_L}{\partial A} \right) \right|_{\Delta_{pl}} da \quad (3.11)$$

$$= (dJ_p)_1 + (dJ_p)_2 \quad (3.12)$$

$$(dJ_p)_1 = \left. \frac{\partial}{\partial \Delta_{pl}} \left(- \Delta_{pl} \cdot \frac{\partial F_L}{\partial A} \right) \right|_a d\Delta_{pl} = - \frac{\partial F_L}{\partial A} d\Delta_{pl} \quad (3.13)$$

where, $\frac{\partial}{\partial \Delta_{pl}} \left(\frac{\partial F_L}{\partial A} \right) = 0$ due to assumed $\Delta_{pl} = \text{constant}$.

$$(dJ_p)_2 = \left. \frac{\partial}{\partial a} \left(-\Delta_{pl} \frac{\partial \mathcal{F}_L}{\partial A} \right) \right|_{\Delta_{pl}} da = \left[-\Delta_{pl} \frac{\partial}{\partial a} \left(\frac{\partial \mathcal{F}_L}{\partial A} \right) \right] da \quad (3.14)$$

Using eqn.(3.10),

$$(dJ_p)_2 = \left[\frac{J_p}{\frac{\partial \mathcal{F}_L}{\partial A}} \cdot \left(\frac{\partial^2 \mathcal{F}_L}{\partial a^2} \right) \cdot \frac{\partial a}{\partial A} \right] da \quad (3.15)$$

Therefore, from eqns.(3.12),(3.13) and (3.15),

$$dJ_p = -\frac{\partial \mathcal{F}_L}{\partial A} \cdot d\Delta_{pl} + \left[\left(\frac{\partial^2 \mathcal{F}_L}{\partial a^2} \right) \cdot \frac{J_p}{\frac{\partial \mathcal{F}_L}{\partial A}} \right] da \quad (3.16)$$

Integrating eqn.(3.16) and substituting eqn.(3.9),

$$J_p = -\frac{\partial \mathcal{F}_L}{\partial A} \cdot \frac{U_{pl}}{F_L} + \int_{a_0}^a \frac{\partial^2 \mathcal{F}_L / \partial a^2}{\partial \mathcal{F}_L / \partial a} \cdot J_p \cdot da \quad (3.17)$$

For elastic-plastic material,

$$U_{pl} = \int_0^{\Delta_{pl}} P \cdot d\Delta_{pl} \quad (3.18)$$

Therefore,

$$J_p = \int_0^{\Delta_{pl}} \left(-\frac{\partial \mathcal{F}_L}{\partial A} \cdot \frac{1}{F_L} \right) P d\Delta_{pl} + \int_{a_0}^a \frac{\partial^2 \mathcal{F}_L / \partial a^2}{\partial \mathcal{F}_L / \partial a} \cdot J_p \cdot da \quad (3.19)$$

Comparing eqns. (3.19) and (2.33), η_{pl} is defined as,

$$\eta_{pl} = -\frac{\partial \mathcal{F}_L}{\partial A} \cdot \frac{1}{F_L} \quad (3.20)$$

and γ as,

$$\gamma = \frac{\partial^2 F_L / \partial a^2}{\partial F_L / \partial a} \quad (3.21)$$

3.2.3 Validation of Proposed General Expression : Derivation of Available ' η_{pl} ' and ' γ ' Functions

In the following sections, ' η_{pl} ' and ' γ ' functions of various geometries under various loading conditions which are available in the open literature are derived using the limit load based general eqns.(3.20) and (3.21). This is to validate the eqns.(3.20) and (3.21).

3.2.3.1 TPB Specimen

The limit load expression of three point bend (TPB) specimen (Fig.3.12) is as follows [70] :

$$F_L = 0.728 \cdot \sigma_y \cdot (W - a)^2 \cdot \frac{2B}{S} \quad (3.22)$$

$$\text{Crack Area, } A = Ba \quad (3.23)$$

Substituting eqns.(3.22) and (3.23) in eqns. (3.20) and (3.21) leads directly to the results in eqns. (2.39) and (2.40).

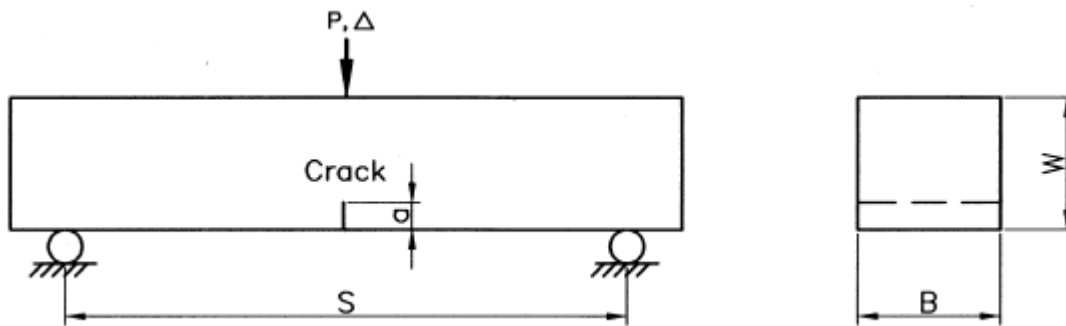


Fig.3.12 TPB specimen

3.2.3.2 Pipe with Throughwall Circumferential Crack Under 4 Point Bending

The limit load of a pipe with throughwall circumferential crack under 4 point bending load (Fig.3.13) is [23] :

$$F_L = P_L = \frac{16R^2 t \sigma_f}{Z - L} h(\theta) \quad (3.24)$$

$$h(\theta) = [\cos(\theta/2) - 0.5 \sin(\theta)] \quad (3.25)$$

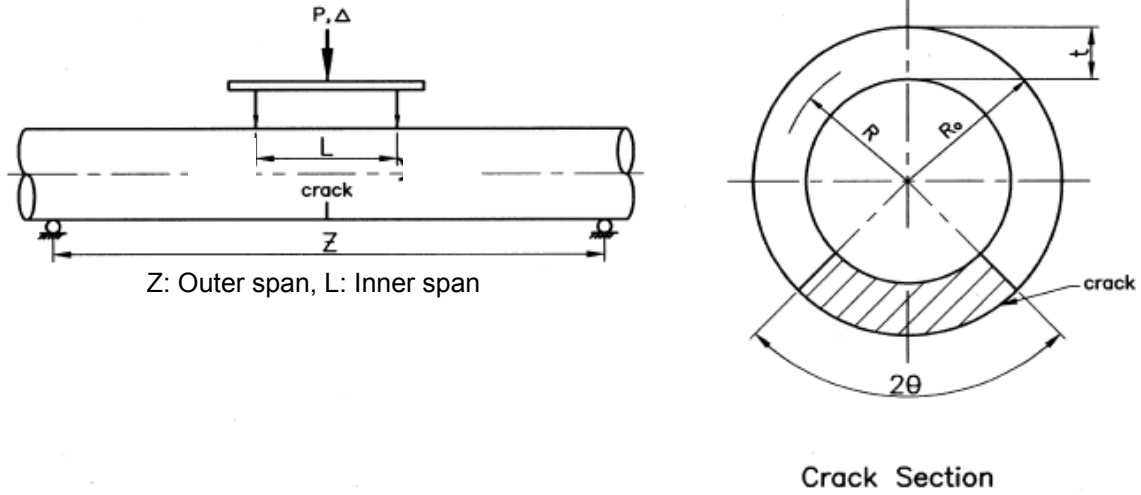


Fig.3.13 Pipe with throughwall circumferential crack under four point bending load

$$\text{The crack area, } A = 2Rt\theta \quad (3.26)$$

$$\text{The crack length, } 2a = 2R\theta \quad (3.27)$$

Therefore, substituting eqns.(3.24 – 3.27) in eqns.(3.20) and (3.21),

$$\eta_{pl} = -\frac{1}{2Rt} \cdot \frac{h'(\theta)}{h(\theta)} \quad (3.28)$$

$$\gamma = \frac{1}{R} \cdot \frac{h''(\theta)}{h'(\theta)} \quad (3.29)$$

$$\text{where, } h'(\theta) = \frac{dh}{d\theta} \quad \text{and} \quad h''(\theta) = \frac{d^2h}{d\theta^2}$$

Therefore, from eqns. (2.33) and (3.27 – 3.29) and noting that 'da = Rdθ',

$$J_p = -\frac{1}{2Rt} \cdot \int_0^{\Delta_{pl}} \frac{h'(\theta)}{h(\theta)} \cdot Pd\Delta_{pl} + \int_{\theta_0}^{\theta} \frac{h''(\theta)}{h'(\theta)} \cdot J_p \cdot d\theta \quad (3.30)$$

which is same as given by Zahoor and Kanninen [54].

3.2.3.3 Pipe with Throughwall Circumferentially Crack Under Axial Tension

The limit load of a pipe with throughwall circumferential crack under axial tension (Fig.3.14) is as follows [24,58] :

$$F_L = P_L = \frac{P_o(2\psi - \theta)}{\pi} \quad (3.31)$$

where,

$$P_o = 2\pi Rt\sigma_f \quad (3.32)$$

$$\psi = \cos^{-1}(0.5 \sin \theta) \quad (3.33)$$

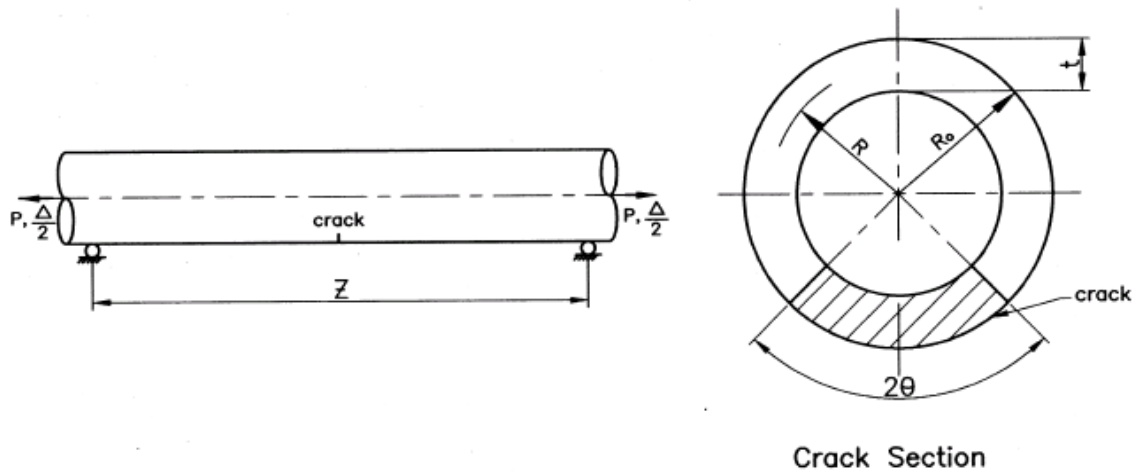


Fig.3.14 Pipe with throughwall circumferential crack under axial tension

In the cracked cross section, eqns.(3.26) and (3.27) hold true in this geometry also.

From eqn.(3.33),

$$\frac{\partial \psi}{\partial \theta} = -\frac{0.5 \cos \theta}{\sin \psi} \quad (3.34)$$

Using eqns.(3.26) and (3.31) in eqn.(3.20),

$$\eta_{pl} = -\frac{1}{2Rt(2\psi - \theta)} \left(2 \frac{\partial \psi}{\partial \theta} - 1 \right) \quad (3.35)$$

Substituting eqn.(3.33) in eqn.(3.35) leads directly to the results of eqn.(2.44).

$$\frac{\partial F_L}{\partial a} = \frac{1}{R} \cdot \frac{\partial F_L}{\partial \theta} = - \left(1 + \frac{\cos \theta}{\sin \psi} \right) \cdot \left(\frac{P_o}{\pi R} \right) \quad (3.36)$$

Differentiating eqn.(3.36) further,

$$\frac{\partial^2 F_L}{\partial a^2} = - \frac{P_o}{\pi R^2} \cdot \left[\frac{0.5 \cos^2 \theta \cot \psi - \sin \psi \sin \theta}{\sin^2 \psi} \right] \quad (3.37)$$

Substituting eqns.(3.36) and (3.37) in eqn.(3.21),

$$\gamma = \frac{1}{R} \cdot \left(\frac{0.5 \cos^2 \theta \cot \psi - \sin \psi \sin \theta}{G_1 \sin^2 \psi} \right) \quad (3.38)$$

The ' γ ' expression in eqn.(2.45) is applicable when ' J_p ' is calculated from eqn.(2.41) i.e. ' $d\theta$ ' is used in place of ' da ' in the second term on the right hand side of eqn.(2.33). However, the ' γ ' expression in eqn.(3.38) is applicable when ' J_p ' is calculated from eqn.(2.33). Using eqn.(3.27), it is apparent that ' γ ' expressions as per eqns.(3.38) and (2.45) are same if consistent equation is used to evaluate ' J_p '.

3.2.3.4 Pipe with Constant Depth Part-Throughwall Circumferential Crack Under Axial Tension

The limit load of a pipe with constant depth part-throughwall circumferential crack under axial tension (Fig.3.15) is as follows [24,58] :

$$F_L = P_o \left[\frac{2\psi}{\pi} - \left(\frac{x\theta}{\pi} \right) \cdot \left(\frac{2 - 2\zeta + x\zeta}{2 - \zeta} \right) \right] \quad (3.39)$$

where,

P_o is as defined in eqn.(3.32)

$$\psi = \cos^{-1}(A_1 \sin \theta) \quad (3.40)$$

$$A_1 = \left[\frac{x}{2} \right] \cdot \left[\frac{(1 - \zeta)(2 - 2\zeta + x\zeta) + (1 - \zeta + x\zeta)^2}{1 + (2 - \zeta)(1 - \zeta)} \right] \quad (3.41)$$

$$x = \frac{a}{t} \quad (3.42)$$

$$\zeta = \frac{t}{R_o} \quad (3.43)$$

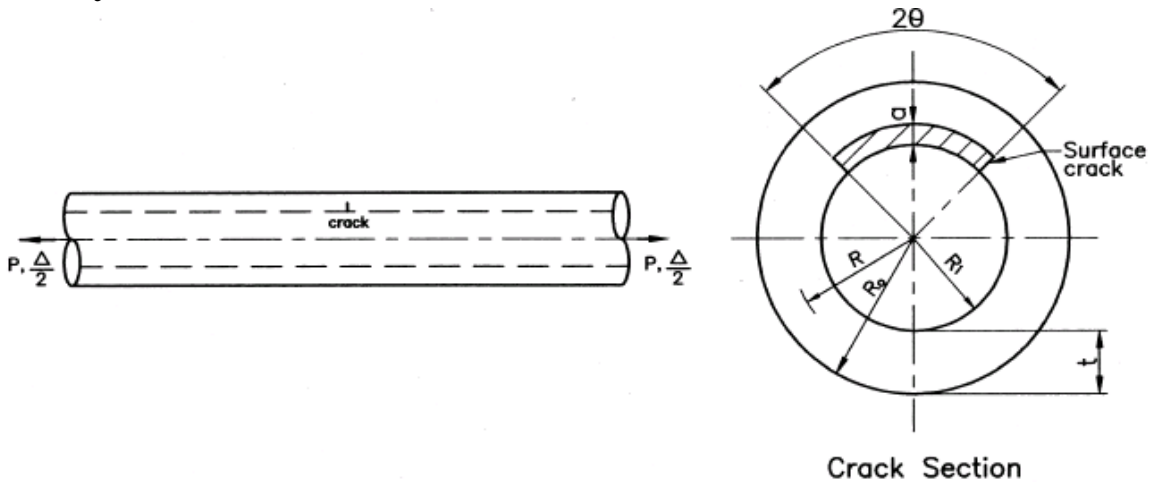


Fig.3.15 Pipe with constant depth part-through circumferential crack under axial tension

To simplify the ' η_{pl} ' and ' γ ' functions, it is assumed that, $\zeta \approx 0.0$, which is generally true for technically used thin piping components.

Then, eqns.(3.39) reduces to,

$$F_L = P_o \left[\frac{2\psi}{\pi} - \frac{x\theta}{\pi} \right] \quad (3.44)$$

and (3.41) reduces to

$$A_1 = \frac{x}{2} \quad (3.45)$$

If it is assumed that the crack grows only in the radial direction but not in the circumferential direction (i.e. $d\theta = 0$),

$$\partial A = 2R_i \theta \partial a \quad (3.46)$$

Differentiating eqn.(3.44),

$$\frac{\partial F_L}{\partial a} = \frac{-P_o}{\pi t} \left(\frac{\sin \theta}{\sin \psi} + \theta \right) \quad (3.47)$$

Differentiating eqn.(3.47) further and noting that $d\theta = 0$,

$$\frac{\partial^2 F_L}{\partial a^2} = \frac{-P_o}{\pi t} \left[\left(\frac{0.5}{t} \right) \left(\frac{\cot \psi}{\sin^2 \psi} \right) \sin^2 \theta \right] \quad (3.48)$$

Substituting eqns.(3.44), (3.46 – 3.48) in eqns.(3.20) and (3.21),

$$\eta_{pl} = \frac{\left(1 + \frac{\sin \theta}{\theta \sin \psi} \right)}{2\pi R_i t \cdot \left(\frac{2\psi}{\pi} - \frac{x\theta}{\pi} \right)} \quad (3.49)$$

$$\gamma = \frac{\left(\frac{0.5}{t} \right) \left(\frac{\sin^2 \theta}{\theta} \right) \left(\frac{\cot \psi}{\sin^2 \psi} \right)}{\left(1 + \frac{\sin \theta}{\theta \sin \psi} \right)} \quad (3.50)$$

which are same as eqns.(2.46) and (2.47) except that the inner radius of pipe, ' R_i ' is used in eqn.(3.49) instead of mean pipe radius, ' R ' in eqn.(2.46). If ' R ' is used in eqn.(3.46) instead of ' R_i ', eqn. (3.49) reduces exactly to eqn.(2.46). However, it is more appropriate to use ' R_i ' in eqn.(3.46) than ' R '.

3.2.4 Evaluation of New ' η_{pl} ' and ' γ ' Functions for Various Geometry and Loading Conditions

In this section, new ' η_{pl} ' and ' γ ' functions for various geometry and loading conditions for which no solutions are available in the open literature are derived using the limit load based general equations (3.20) and (3.21).

3.2.4.1 Throughwall Circumferentially Cracked Thick Pipe Under Combined Bending and Tension

Although, for this geometry and loading conditions (Fig.3.16), the ' η_{pl} ' and ' γ ' functions have been recently given by Miura and Wilkowski [59,60], these do not, however, incorporate terms applicable for thick pipes ($R/t < 10$). In the

present case, ' η_{pl} ' and ' γ ' functions are proposed which incorporate these terms. The limit moment of a throughwall circumferentially cracked pipe under combined bending and tension is [23,24]:

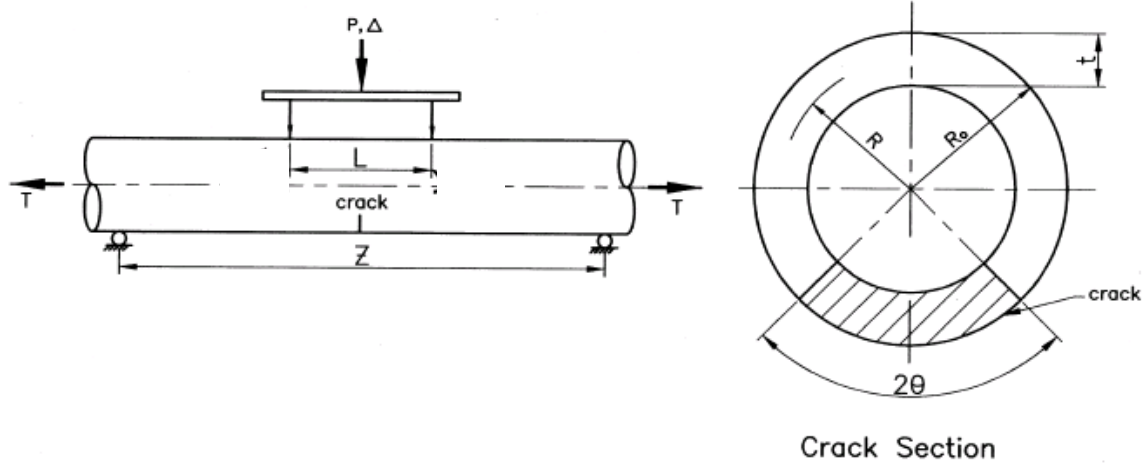


Fig.3.16 Pipe with throughwall circumferential crack under combined bending and axial tension

$$M_L = M_o \cdot (\cos \alpha' - 0.5 \sin \theta) \quad (3.51)$$

Applicability : $R/t < 10$ and $s = \frac{T}{2\pi R t \sigma_f} < 0.25$

where,

$$M_o = 4\sigma_f R_o^2 t \left(1 - \zeta + \frac{\zeta^2}{3} \right) \quad (3.52)$$

$$\alpha' = 0.5\theta F_1 + \frac{T}{4\sigma_f R_o t (1 - \zeta)} \quad (3.53)$$

$$F_1 = \left[\frac{1 - \zeta}{1 - 0.5\zeta} \right] \left[1 + \frac{0.5\zeta}{1 - \zeta} \right] \quad (3.54)$$

T = Axial tension and σ_f = flow stress of pipe material

ζ is as defined in eqn.(3.43).

Differentiating eqn. (3.51) with the assumption of constant axial tension,

$$\frac{\partial F_L}{\partial \theta} = -0.5M_o (F_1 \sin \alpha' + \cos \theta) \quad (3.55)$$

$$\frac{\partial^2 F_L}{\partial \theta^2} = -0.5M_o(0.5F_1^2 \cos \alpha' - \sin \theta) \quad (3.56)$$

Noting that eqn.(3.26) holds here and using eqns.(3.51) and (3.55) in eqn.(3.20),

$$\eta_{pl} = \frac{0.5 [F_1 \sin \alpha' + \cos \theta]}{2Rt[\cos \alpha' - 0.5 \sin \theta]} \quad (3.57)$$

Similarly, noting that eqn.(3.27) holds here and using eqns. (3.55) and (3.54) in eqn.(3.21),

$$\gamma = \frac{1}{R} \left(\frac{0.5F_1^2 \cos \alpha' - \sin \theta}{F_1 \sin \alpha' + \cos \theta} \right) \quad (3.58)$$

If eqn.(2.41) is used to define ' J_p ' instead of eqn.(2.33) i.e. if ' $d\theta$ ' is used in the second term of the right hand side of eqn.(2.33) instead of ' da ', the expression of ' γ ' becomes :

$$\gamma = \left(\frac{0.5F_1^2 \cos \alpha' - \sin \theta}{F_1 \sin \alpha' + \cos \theta} \right) \quad (3.59)$$

For thin pipes, $\zeta \approx 0.0$; therefore, $F_1 \approx 1.0$.

In that case, the ' η_{pl} ' and ' γ ' functions of eqns. (3.57) and (3.59) reduces to eqns. (2.51) and (2.52). If axial force, $T = 0$ and $F_1 \approx 1.0$, the ' η_{pl} ' and ' γ ' functions of eqns.(3.57) and (3.59) reduce to eqns. (2.42) and (2.43) which are for a throughwall circumferentially cracked pipe under pure bending moment. Figures 3.17 and 3.18 compare the present ' η_{pl} ' and ' γ ' values with those given by Miura and Wilkowski [59] for combined loading. It can be seen from Fig.3.17 that the present ' η_{pl} ' values are larger than those given by Miura and Wilkowski [59] for $s > 0$, where, s is as defined in eqn.(2.55). The difference increases with increasing crack angle. At $s = 0$, both are almost identical. It is seen from Fig.3.18 that the present ' γ ' functions are almost the same as those given by Miura and Wilkowski [59] for all values of ' s '.

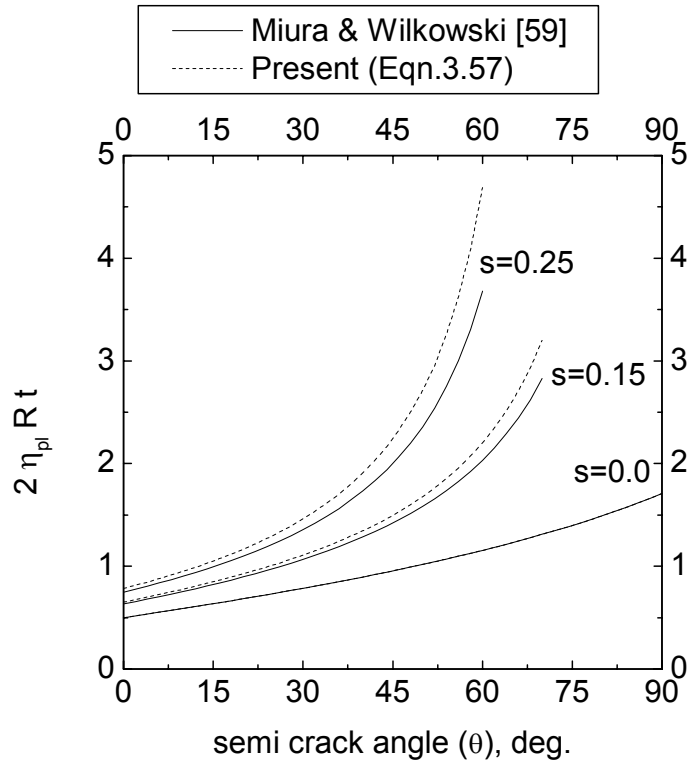


Fig.3.17 Comparison of ' η_{pl} ' for thick ($R/t=5$) pipe with throughwall circumferential crack under combined bending and axial tension for various values of axial tension

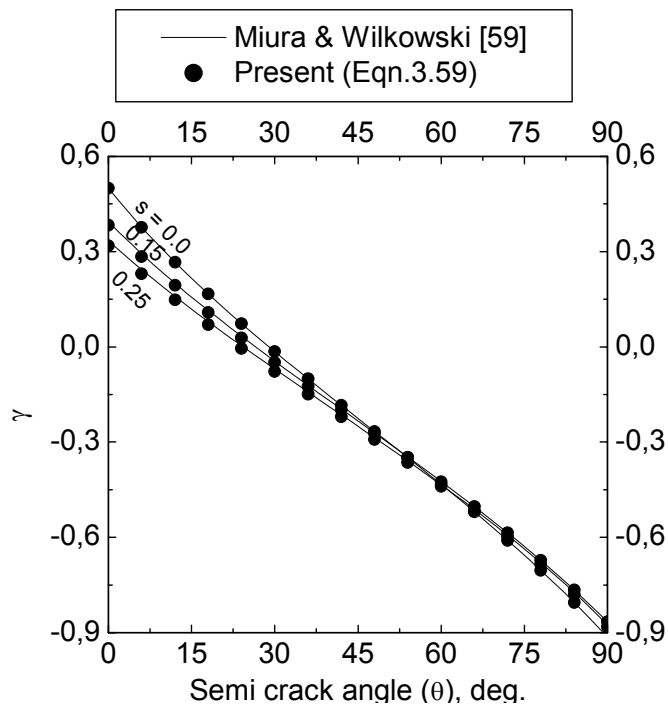


Fig.3.18 Comparison of ' γ ' for thick ($R/t=5$) pipe with throughwall circumferential crack under combined bending and axial tension for various values of axial tension

It may be noted that if the limit moment expression of throughwall circumferentially cracked pipe under combined axial tension and bending does not consider the thickness correction terms i.e. if eqn.(3.51) is modified as used by Miura and Wilkowski [59] :

$$M_L = M_o \left[\cos\left(\frac{\theta}{2} + \frac{\pi}{2} s\right) - 0.5 \sin \theta \right]$$

the 'η_{pl}' and 'γ' functions derived through eqns.(3.20) and (3.21) will be exactly the same as in eqns. (2.51) and (2.52) derived by Miura and Wilkowski [59,60].

3.2.4.2 Pipe with Constant Depth Part-Throughwall Circumferential Crack Under Combined Bending Moment and Axial Tension

The limit moment of a pipe with a constant depth part-throughwall circumferential crack under combined bending moment and axial tension (Fig.3.19) is [55,72] :

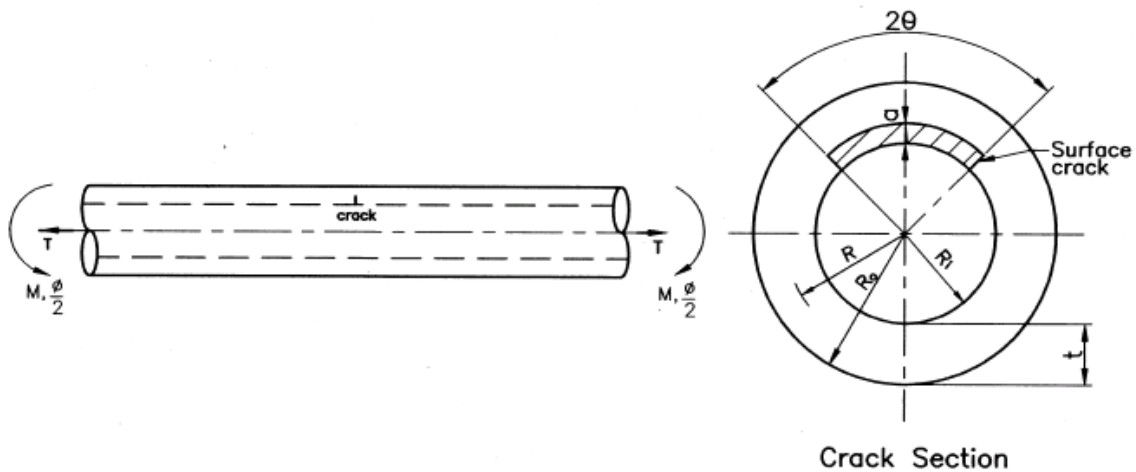


Fig.3.19 Pipe with constant depth part-through circumferential crack under combined bending and axial tension

$$M_L = 2\sigma_f R^2 t \left[2 \sin \beta - \left(\frac{a}{t}\right) \sin \theta \right] \quad (3.60)$$

where,

$$\beta = 0.5\pi \left[1 - \left(\frac{\theta}{\pi} \right) \cdot \left(\frac{a}{t} \right) - s \right] \quad (3.61)$$

's' is as defined in eqn.(2.55).

The following assumptions are made :

$$\theta + \beta < \pi \quad \text{and} \quad s < 0.25$$

It is also assumed that axial load and ' θ ' is constant during crack growth, i.e. $\partial\theta = 0$. Therefore, differentiating eqn.(3.60) with respect to crack depth ' a ',

$$\frac{\partial F_L}{\partial a} = -2\sigma_f R^2 (\theta \cos \beta + \sin \theta) \quad (3.62)$$

Differentiating eqn.(3.62) further with respect to crack depth ' a ',

$$\frac{\partial^2 F_L}{\partial a^2} = -\frac{\sigma_f R^2 \theta^2}{t} \sin \beta \quad (3.63)$$

Substituting eqns.(3.46), (3.60), (3.62) and (3.63) in eqns.(3.20) and (3.21),

$$\eta_{pl} = \frac{1}{2R_i t} \cdot \frac{\left(\cos \beta + \frac{\sin \theta}{\theta} \right)}{\left(2 \sin \beta - \frac{a}{t} \cdot \sin \theta \right)} \quad (3.64)$$

$$\gamma = \frac{1}{2t} \cdot \frac{\sin \beta}{\left(\frac{\cos \beta}{\theta} + \frac{\sin \theta}{\theta^2} \right)} \quad (3.65)$$

If it is assumed that the plastic load-line-displacements due to axial tension is negligible, ' J_p ' can be evaluated using eqns. (2.34) and (2.35) with the ' η_{pl} ' and ' γ ' functions from eqns.(3.64) and (3.65). It is again emphasized here that load, ' P ' and plastic load-line-displacement, ' Δ_{pl} ' in eqn.(2.35) are used in generic sense i.e. in case of moment load, ' P ' indicates moment and ' Δ_{pl} ' indicates plastic load-point-rotation. Figures 3.20 and 3.21 show the variation of ' η_{pl} ' and ' γ ' with respect to crack depth (a/t), normalized axial tension (s) and semi-crack angle (θ).

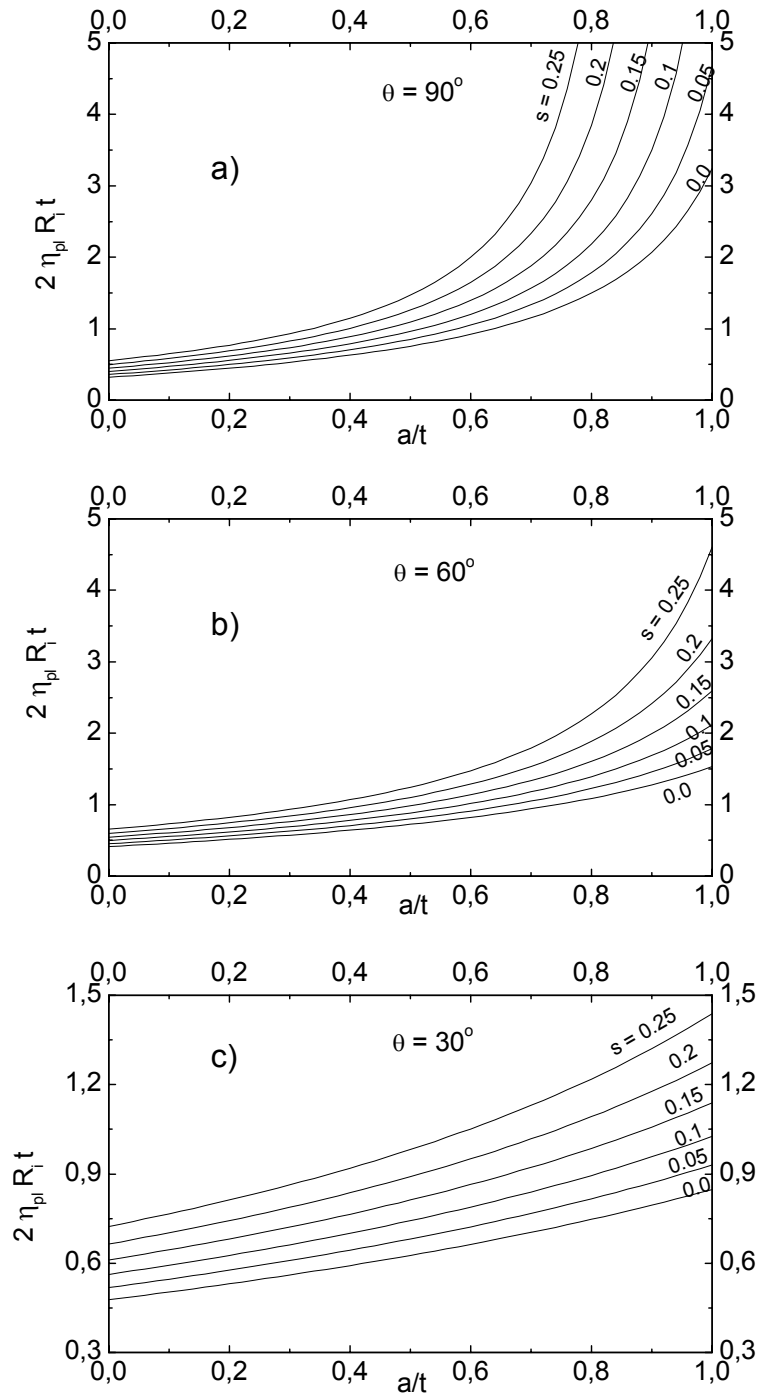


Fig.3.20 Variation of ' η_{pl} ' for pipe with constant depth part-through circumferential crack under combined bending and axial tension : (a) $\theta = 90^\circ$, (b) $\theta = 60^\circ$, (c) $\theta = 30^\circ$

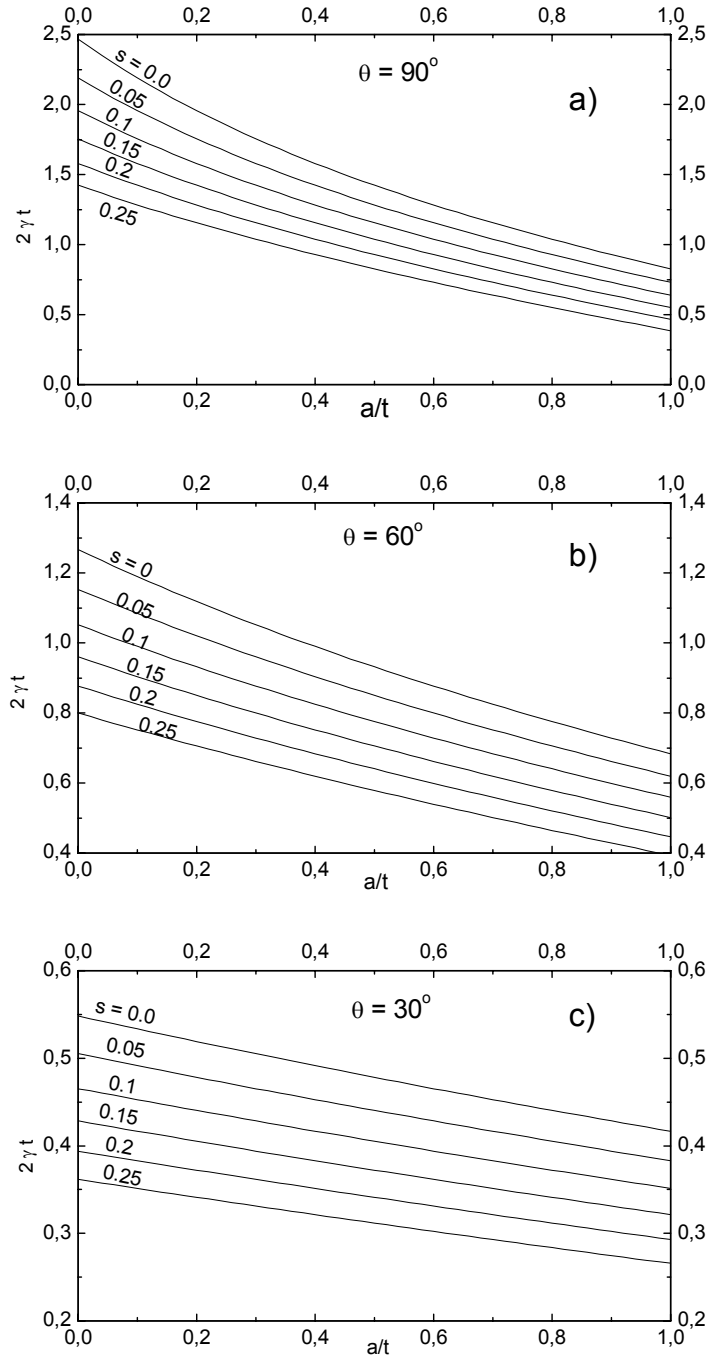


Fig.3.21 Variation of ' γ ' for pipe with constant depth part-through circumferential crack under combined bending and axial tension : (a) $\theta = 90^\circ$, (b) $\theta = 60^\circ$, (c) $\theta = 30^\circ$

3.2.4.3 Pipe with Semi-elliptical Part-Throughwall Circumferential Crack Under Axial Tension

The limit load formula of a pipe with a semi-elliptical part-throughwall circumferential crack under axial tension (Fig.3.22) is the same as that for a pipe with a constant depth part-throughwall circumferential crack under axial tension expressed through eqns. (3.39 – 3.43) and in simplified form through eqns. (3.44 – 3.45). The derivation of ‘ η_{pl} ’ and ‘ γ ’ functions is almost the same as that for a pipe with a constant depth part-throughwall circumferential crack under axial tension (derived in section 3.2.3.4) except for the calculation of crack area. In the case of a semi-elliptical part-throughwall circumferential crack, the crack area,

$$A = \frac{\pi R_i \theta a}{2} \quad \text{and hence,} \quad \partial A = \frac{\pi R_i \theta}{2} \cdot \partial a \quad (3.66)$$

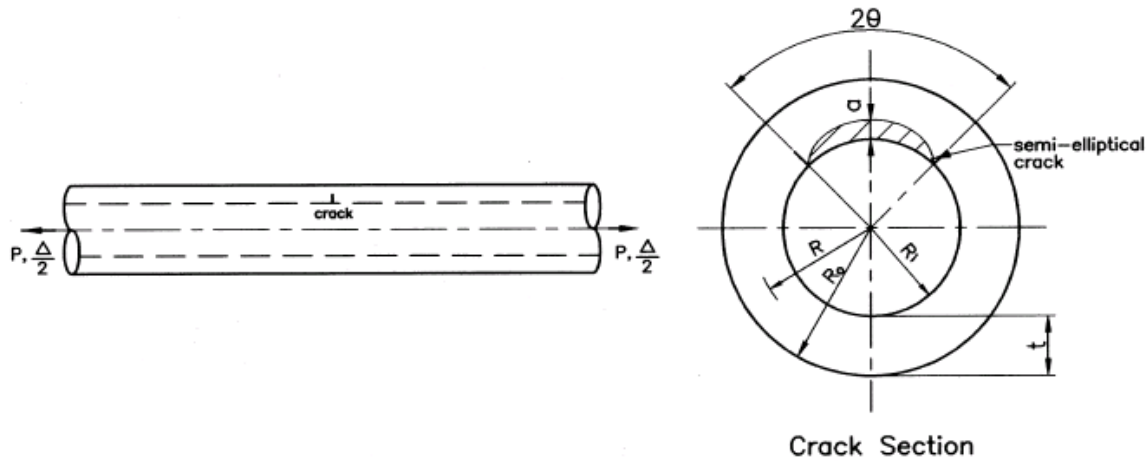


Fig.3.22 Pipe with semi-elliptical part-through circumferential crack under axial tension

Therefore, ‘ η_{pl} ’ is expressed by slightly modifying eqn.(3.49),

$$\eta_{pl} = \left(\frac{2}{\pi^2 R_i t} \right) \frac{\left(1 + \frac{\sin \theta}{\theta \sin \psi} \right)}{\left(\frac{2\psi}{\pi} - \frac{x\theta}{\pi} \right)} \quad (3.67)$$

The expression for the ‘ γ ’ function is the same as that for a constant depth part-throughwall circumferential crack and expressed through eqn.(3.50).

3.2.4.4 Pipe with Semi-elliptical Part-Throughwall Circumferential Crack Under Combined Bending Moment and Axial Tension

The limit load of a pipe with a semi-elliptical part-throughwall circumferential crack under combined axial tension and bending moment (Fig.3.23) is exactly the same as that for a pipe with a constant depth part-throughwall circumferential crack under the same loading condition, eqns. (3.60 – 3.61). The derivation of ‘ η_{pl} ’ and ‘ γ ’ functions is almost the same as for a pipe with a constant depth part-throughwall circumferential crack under combined bending moment and axial tension (derived in section 3.2.4.2) apart from the calculation of crack area. In the case of a semi-elliptical part-throughwall circumferential crack, the crack area and its derivative are expressed by eqn.(3.66). Therefore, ‘ η_{pl} ’ is expressed by slightly modifying eqn.(3.64),

$$\eta_{pl} = \frac{2}{\pi R_i t} \cdot \frac{\left(\cos \beta + \frac{\sin \theta}{\theta} \right)}{\left(2 \sin \beta - \frac{a}{t} \cdot \sin \theta \right)} \quad (3.68)$$

The expression for the ‘ γ ’ function is the same as that in the case of a constant depth part-throughwall circumferential crack under the same loading condition and expressed through eqn.(3.65).

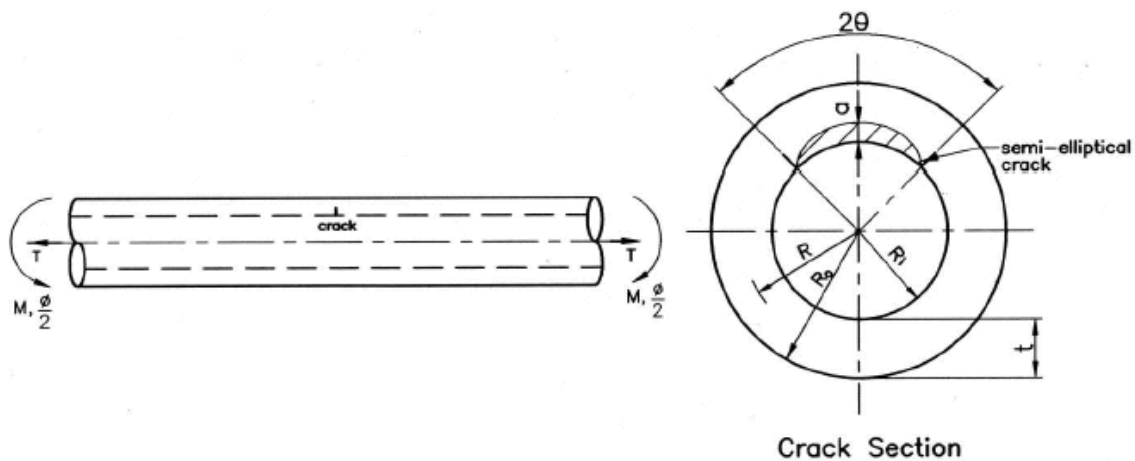


Fig.3.23 Pipe with semi-elliptical part-through circumferential crack under combined bending and axial tension

3.2.4.5 Pipe with Full Circumferential Part-Throughwall Crack Under Axial Tension

The limit load of a pipe with a fully circumferential part-throughwall crack under axial tension (Fig.3.24) is [71] :

$$F_L = \frac{2\pi}{\sqrt{3}} \cdot \sigma_f \cdot [R_o^2 - (R_i + a)^2] \quad (3.69)$$

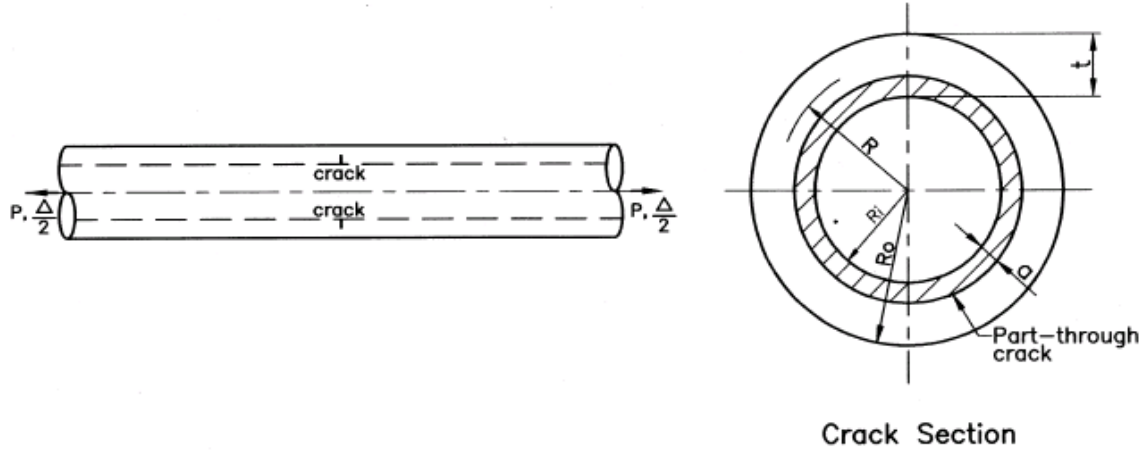


Fig.3.24 Pipe with full circumferential part-through crack under axial tension

Zahoor [55] gives the expression of ' η_{pl} ' for a non-growing crack for this geometry and loading condition as :

$$\eta_{pl} = \frac{1}{\left[2\pi R t \left\{ 1 - \frac{x(2 - 2\zeta + x\zeta)}{(2 - \zeta)} \right\} \right]} \quad (3.70)$$

x and ζ are as defined in eqns.(3.42) and (3.43) respectively.

However, no expression for the ' γ ' function is given by Zahoor [55].

The crack area could be expressed as , $A = 2\pi R_i a$ (3.71)

Substituting eqns.(3.69) and (3.71) in eqns.(3.20) and (3.21),

$$\eta_{pl} = \frac{1}{2\pi R t} \cdot \frac{\left(1 + \frac{a}{R_i} \right)}{\left(1 + \frac{a}{2R} \right) \left(1 - \frac{a}{t} \right)} \quad (3.72)$$

and

$$\gamma = \frac{1}{t \left(\frac{R_i}{t} + \frac{a}{t} \right)} \quad (3.73)$$

It may be shown that the ' η_{pl} ' function by eqns.(3.70) and (3.72) are the same for thin pipes ($\zeta \approx 0$) and for small crack depths ($a \ll R_i$).

Substituting $\frac{a}{R_i} \approx 0$ and $\frac{a}{2R} \approx 0$ in eqn.(3.72),

$$\eta_{pl} = \frac{1}{2\pi R t} \cdot \frac{1}{\left(1 - \frac{a}{t} \right)} \quad (3.74)$$

The same expression for the ' η_{pl} ' function is obtained from eqn.(3.70) when $\zeta \approx 0$ is assumed. Figure 3.25 compares the present ' η_{pl} ' values with those given by Zahoor [55]. It may be seen that these values differ for thick pipes ($R/t=5$) and the difference increases with crack depth ' a/t '. However, for thin pipes ($R/t=20$), the difference is negligible. Figure 3.26 shows the variation of ' γ ' with respect to crack depth ' a/t ' for various R/t . It may be seen that ' γ ' depends weakly on crack depth.

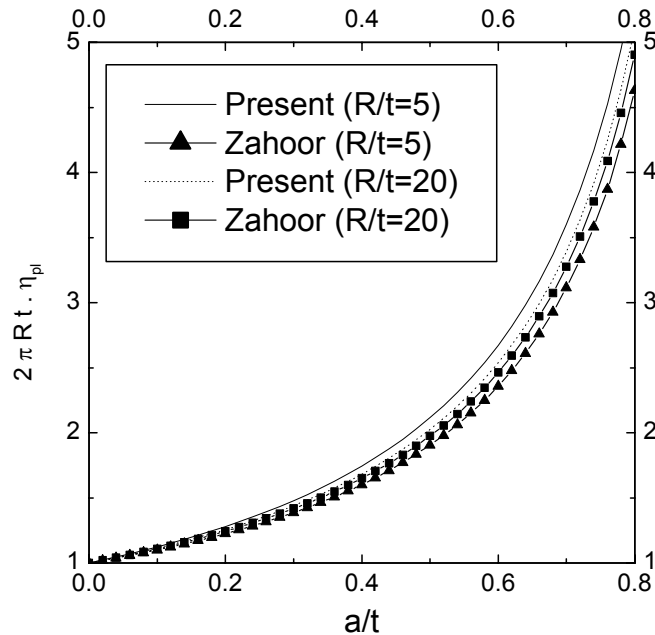


Fig.3.25 Comparison of ' η_{pl} ' for pipe with a full circumferential part-through crack under axial tension

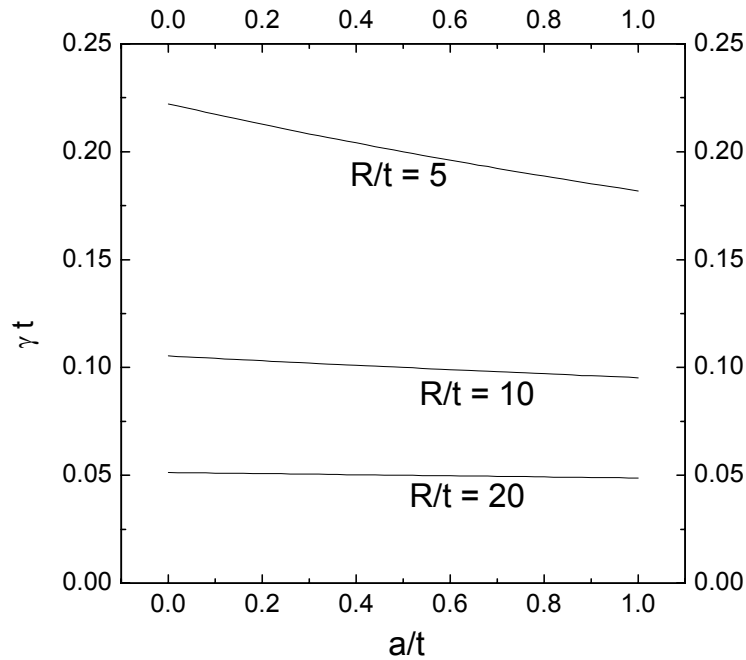


Fig.3.26 Variation of 'γ' for pipe with a full circumferential part-through crack under axial tension

3.2.4.6 Elbow with Throughwall Circumferential Crack Under In-plane Bending Moment

Figure 3.27 shows the geometry of the elbow with throughwall circumferential crack under in-plane opening bending moment.

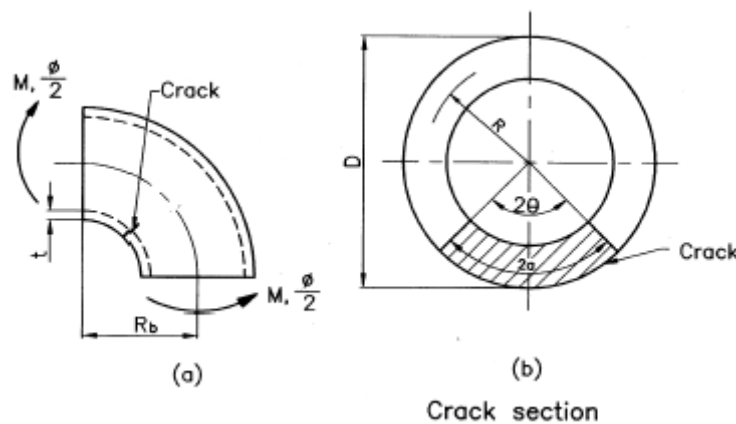


Fig.3.27 Elbow with throughwall circumferential crack under in-plane bending moment

The limit moment for this configuration is given by Zahoor [45] :

$$M_L = M_o \left[1 - 0.2137 \left(\frac{a}{D_m} \right) - 0.0485 \left(\frac{a}{D_m} \right)^2 - 1.0559 \left(\frac{a}{D_m} \right)^3 \right] \quad (3.75)$$

$$\text{with, } M_o = 0.935 \sigma_f D_m^2 t h^{2/3} \quad (3.76)$$

Applicability : $a/D_m \leq 0.8$, $h = 4R_b t/D_m^2 \leq 0.5$ and $D_m/t \geq 15$

where, 'a' is the half crack length, 'D_m' is the mean diameter of the elbow cross section, 'R_b' is the mean bend radius of elbow, 't' is the elbow wall thickness, $h = 4R_b t/D_m^2$ is the elbow factor and 'σ_f' is the material flow stress.

Denoting 'θ' as the semi-circumferential-crack angle and putting 'a = (D_m/2).θ' in eqn.(3.75),

$$M_L = M_o \cdot e(\theta) \quad (3.77)$$

where,

$$e(\theta) = \left[1 - 0.10685\theta - 0.012125\theta^2 - 0.1319875\theta^3 \right] \quad (3.78)$$

Following the same procedure as in section 3.2.3.2 for throughwall circumferentially cracked pipe under bending load,

$$\eta_{pl} = -\frac{1}{2Rt} \cdot \frac{e'(\theta)}{e(\theta)} \quad (3.79)$$

$$\gamma = \frac{1}{R} \cdot \frac{e''(\theta)}{e'(\theta)} \quad (3.80)$$

where,

$$e'(\theta) = \frac{de}{d\theta} \quad \text{and} \quad e''(\theta) = \frac{d^2e}{d\theta^2}$$

Substituting eqn.(3.78) in eqns. (3.79 – 3.80)

$$\eta_{pl} = \frac{1}{2Rt} \cdot \frac{(0.10685 + 0.02425\theta + 0.3959625\theta^2)}{(1 - 0.10685\theta - 0.012125\theta^2 - 0.1319875\theta^3)} \quad (3.81)$$

$$\gamma = \frac{1}{R} \cdot \frac{(0.02425 + 0.791925\theta)}{(0.10685 + 0.02425\theta + 0.3959625\theta^2)} \quad (3.82)$$

If eqn.(2.41) is used to define ' J_p ' instead of eqn.(2.33) i.e. if ' $d\theta$ ' is used in the second term of the right hand side of eqn.(2.34) instead of ' da ', the expression of ' γ ' becomes :

$$\gamma = \frac{(0.02425 + 0.791925\theta)}{(0.10685 + 0.02425\theta + 0.3959625\theta^2)} \quad (3.83)$$

Figure 3.28 shows the variation of ' η_{pl} ' and ' γ ' as a function of crack angle. It should be noted that for moment loading of an elbow as shown in Fig.3.27(a), eqn.(2.35) is modified as:

$$J_{po} = \int_0^{\phi_{pl}} \eta_{pl} \cdot M \cdot d\phi_{pl} \quad (3.84)$$

where, ' ϕ_{pl} ' is the plastic load point rotation and ' M ' is the applied moment.

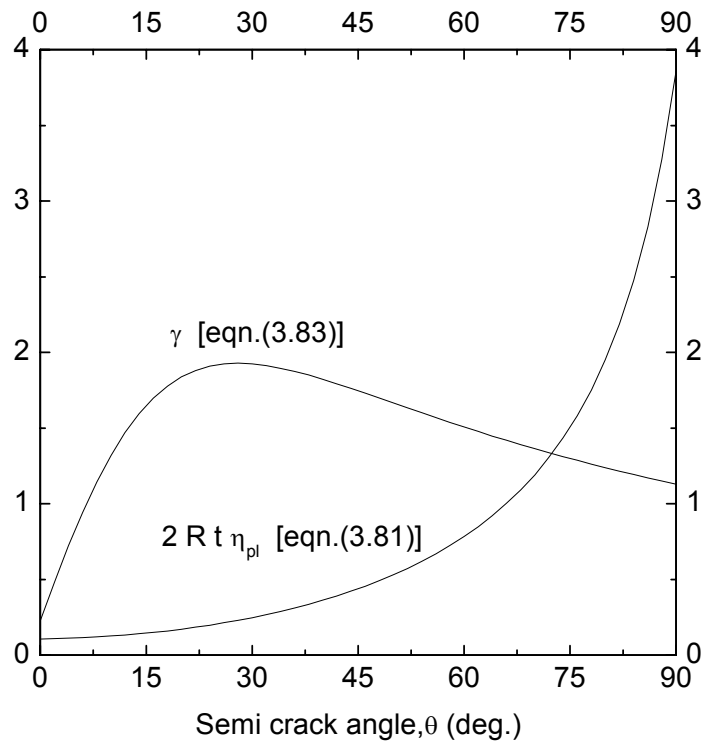


Fig.3.28 Variation of ' η_{pl} ' and ' γ ' for elbow with throughwall circumferential crack under in-plane bending moment

3.2.4.7 Elbow with Throughwall Axial Crack Under In-plane Bending Moment

Figure 3.29 shows the geometry of the elbow with a throughwall axial crack under in-plane bending moment. The crack can be at three locations, namely, extrados, crown and intrados (Fig.3.29). Depending on the bend radius, elbows are classified in two categories : long radius elbow ($R_b/D_m \geq 1.5$) and short radius elbow ($R_b/D_m \leq 1.0$), where, R_b indicates the mean bend radius of the elbow at the crown. The limit moments for these various configurations have been given by Zahoor [45]. Using eqns.(3.20) and (3.21), ' η_{pl} ' and ' γ ' functions have been derived for these various configurations.

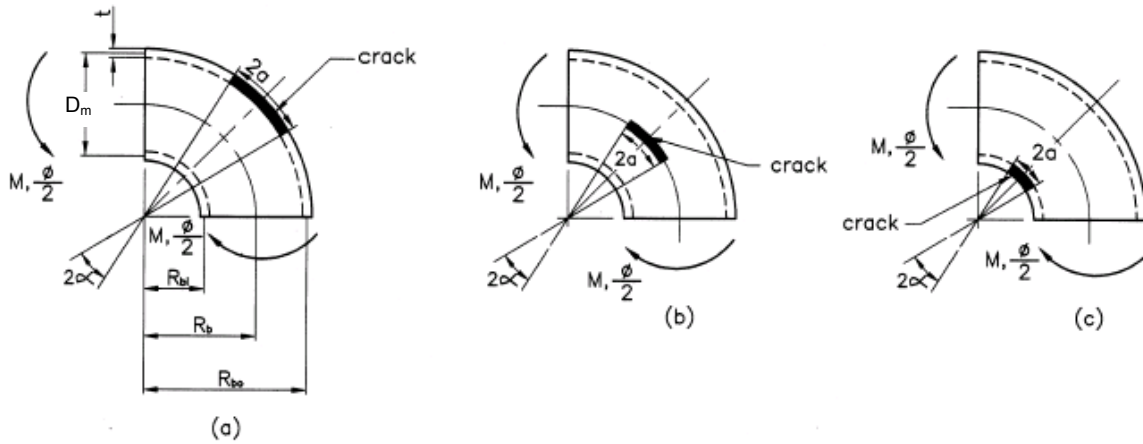


Fig.3.29 Elbow with throughwall axial crack at (a) extrados, (b) crown and (c) intrados under in-plane bending moments

3.2.4.7.1 Long Radius Elbow ($R_b/D_m = 1.5$)

For Extrados Crack

Figure 3.29(a) shows the crack configuration. The limit moment is [45]:

$$M_L = M_o \left[1 - 0.2056 \left(\frac{a}{D_m} \right) - 0.3455 \left(\frac{a}{D_m} \right)^2 + 0.1719 \left(\frac{a}{D_m} \right)^3 \right] \quad (3.85)$$

with M_o as defined in eqn.(3.76).

Applicability : $a/D_m \leq 0.9$, $4R_b t/D_m^2 \leq 0.5$ and $D_m/t \geq 15$

For this crack configuration, the following relation can be written :

$$2a = \left(R_b + \frac{D_m}{2} \right) \cdot 2\alpha \quad (3.86)$$

where, ' α ' is the semi-axial crack angle in radian.

Substituting $\frac{R_b}{D_m} = 1.5$ in eqn.(3.86) results in,

$$\frac{a}{D_m} = 2\alpha \quad (3.87)$$

Substituting eqn.(3.87) in eqn.(3.85),

$$M_L = M_o \cdot e(\alpha) \quad (3.88)$$

with M_o as defined in eqn.(3.76).

where,

$$e(\alpha) = (1 - 0.4112\alpha - 1.382\alpha^2 + 1.3752\alpha^3) \quad (3.89)$$

$$\text{Crack area, } A = 2R_{bo}t\alpha \quad (3.90)$$

where, R_{bo} is the elbow bend radius at extrados.

Substituting eqns.(3.88 – 3.90) in eqn.(3.20),

$$\eta_{pl} = -\frac{1}{2R_{bo}t} \cdot \frac{e'(\alpha)}{e(\alpha)} \quad (3.91)$$

$$\text{where, } e'(\alpha) = \frac{de}{d\alpha}$$

Eqn.(3.86) can be written in modified form as follows :

$$a = R_{bo}\alpha \quad (\text{since } R_{bo} = R_b + D_m/2, \text{ see Fig.3.29a}) \quad (3.92)$$

Substituting eqns.(3.88) and (3.92) in eqn.(3.21),

$$\gamma = \frac{1}{R_{bo}} \cdot \frac{e''(\alpha)}{e'(\alpha)} \quad (3.93)$$

$$\text{where, } e''(\alpha) = \frac{d^2e}{d\alpha^2}$$

Substituting eqn.(3.89) in eqns. (3.91) and (3.93),

$$\eta_{pl} = \frac{1}{2R_{bo}t} \cdot \frac{(0.4112 + 2.764\alpha - 4.1256\alpha^2)}{(1 - 0.4112\alpha - 1.382\alpha^2 + 1.3752\alpha^3)} \quad (3.94)$$

$$\gamma = \frac{1}{R_{bo}} \cdot \frac{(2.764 - 8.2512\alpha)}{(0.4112 + 2.764\alpha - 4.1256\alpha^2)} \quad (3.95)$$

By slightly modifying eqn.(2.41), if ' J_p ' is expressed as follows :

$$J_p = J_{po} + \int_{\alpha_o}^{\alpha} \gamma \cdot J_{po} \cdot d\alpha \quad (3.96)$$

the expression of ' γ ' as per eqn.(3.95) gets modified as follows :

$$\gamma = \frac{(2.764 - 8.2512\alpha)}{(0.4112 + 2.764\alpha - 4.1256\alpha^2)} \quad (3.97)$$

where, α_o and α are initial and current half axial crack angle respectively.

For Crown Crack

Figure 3.29(b) shows the crack configuration. The limit moment is [45] :

$$M_L = M_o \left[1 - 0.0824 \left(\frac{a}{D_m} \right) - 1.3755 \left(\frac{a}{D_m} \right)^2 + 0.9327 \left(\frac{a}{D_m} \right)^3 \right] \quad (3.98)$$

with M_o as defined in eqn.(3.76).

Substituting the relation ' $a = R_b\alpha$ ' and noting that $\frac{R_b}{D_m} = 1.5$, the limit moment is expressed through eqn.(3.88) with

$$e(\alpha) = (1 - 0.1236\alpha - 3.094875\alpha^2 + 3.1478625\alpha^3) \quad (3.99)$$

Following the same steps as in case of extrados crack, and expressing ' J_p ' through eqn.(3.96),

$$\eta_{pl} = \frac{1}{2R_b t} \cdot \frac{(0.1236 + 6.18975\alpha - 9.4435875\alpha^2)}{(1 - 0.1236\alpha - 3.094875\alpha^2 + 3.1478625\alpha^3)} \quad (3.100)$$

$$\gamma = \frac{(6.18975 - 18.887175\alpha)}{(0.1236 + 6.18975\alpha - 9.4435875\alpha^2)} \quad (3.101)$$

For Intrados Crack

Figure 3.29(c) shows the crack configuration. The limit moment is [45] :

$$M_L = M_o \left[1 - 0.0206 \left(\frac{a}{D_m} \right) - 2.4405 \left(\frac{a}{D_m} \right)^2 + 2.2591 \left(\frac{a}{D_m} \right)^3 - 0.4816 \left(\frac{a}{D_m} \right)^4 \right] \quad (3.102)$$

with M_o as defined in eqn.(3.76).

Using the relation, $2a = \left(R_b - \frac{D_m}{2} \right) \cdot 2\alpha$ and noting that $\frac{R_b}{D_m} = 1.5$, it can be

written: $\frac{a}{D_m} = \alpha$

Substituting this relation in eqn.(3.102), the limit moment can be expressed through eqn.(3.88) with

$$e(\alpha) = (1 - 0.0206\alpha - 2.4405\alpha^2 + 2.2591\alpha^3 - 0.4816\alpha^4) \quad (3.103)$$

Following the same steps as in case of extrados crack, and expressing ' J_p ' through eqn.(3.96),

$$\eta_{pl} = \frac{1}{2R_{bt}} \cdot \frac{(0.0206 + 4.881\alpha - 6.7773\alpha^2 + 1.9264\alpha^3)}{(1 - 0.0206\alpha - 2.4405\alpha^2 + 2.2591\alpha^3 - 0.4816\alpha^4)} \quad (3.104)$$

$$\gamma = \frac{(4.881 - 13.5546\alpha + 5.7792\alpha^2)}{(0.0206 + 4.881\alpha - 6.7773\alpha^2 + 1.9264\alpha^3)} \quad (3.105)$$

Figures 3.30 and 3.31 show the variation of ' η_{pl} ' and ' γ ' of a long radius elbow as a function of crack angle and position.

3.2.4.7.2 Short Radius Elbow ($R_b/D_m = 1.0$)

For Extrados Crack

Figure 3.29(a) shows the crack configuration. The limit moment is [45] :

$$M_L = M_o \left[1 - 0.15 \left(\frac{a}{D_m} \right) \right] \tag{3.106}$$

with M_o as defined in eqn.(3.76).

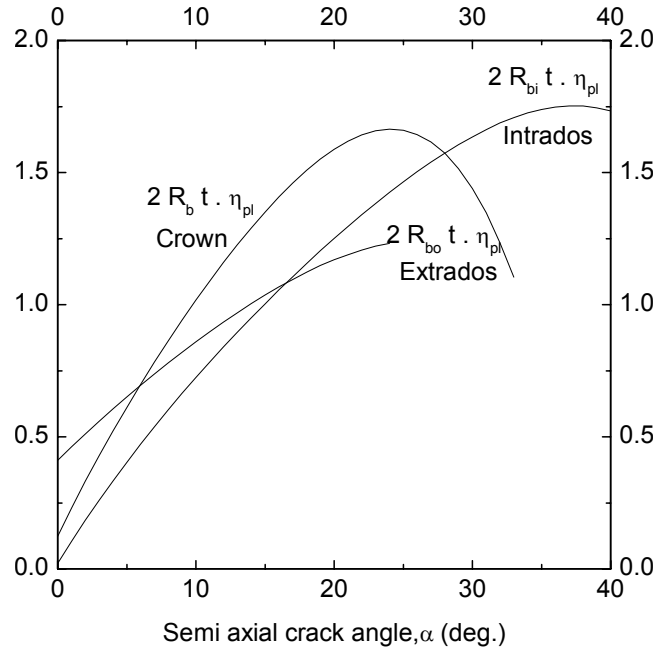


Fig.3.30 Variation of ' η_{pl} ' for long radius elbow with throughwall axial crack at various locations under in-plane bending moment

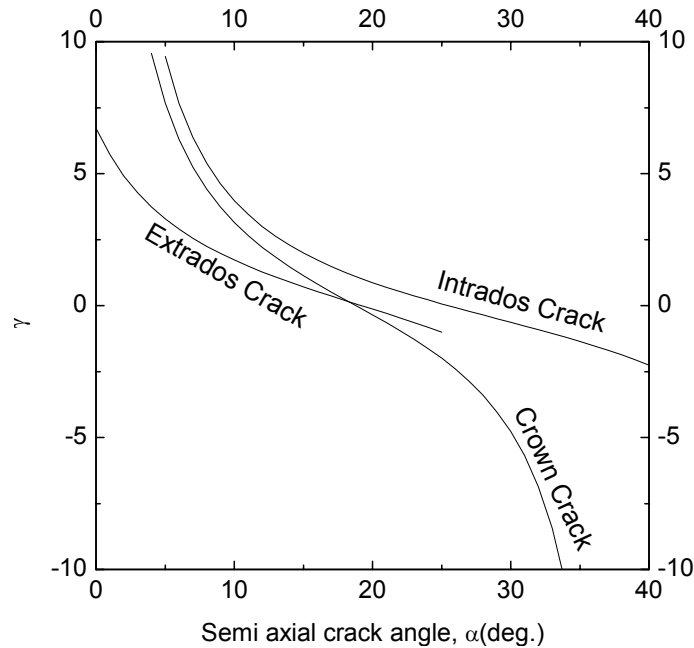


Fig.3.31 Variation of ' γ ' of long radius elbow with throughwall axial crack at various locations under in-plane bending moment

Eqn.(3.86) holds true for this crack configuration also and substituting $\frac{R_b}{D_m} = 1.0$

in eqn.(3.86), $\frac{a}{D_m} = 1.5\alpha$

Therefore, eqn.(3.106) can be written as :

$$M_L = M_o [1 - 0.225\alpha] \quad (3.107)$$

with M_o as defined in eqn.(3.76).

Following the same steps as in case of long radius elbow with extrados crack, and expressing ' J_p ' through eqn.(3.96),

$$\eta_{pl} = \frac{1}{2R_{bo}t} \cdot \frac{0.225}{(1 - 0.225\alpha)} \quad (3.108)$$

$$\gamma = 0 \quad (3.109)$$

For Crown Crack

Figure 3.29(b) shows the crack configuration. The limit moment [45] is the same as in eqn.(3.106). Following the same steps as in the previous section for extrados crack,

$$\eta_{pl} = \frac{1}{2R_b t} \cdot \frac{0.15}{(1 - 0.15\alpha)} \quad (3.110)$$

and ' γ ' is the same as expressed in eqn.(3.109).

For Intrados Crack

Figure 3.29(c) shows the crack configuration. The limit moment [45] is the same as in eqn.(3.106). Following the same steps as in case of extrados crack,

$$\eta_{pl} = \frac{1}{2R_{bi}t} \cdot \frac{0.075}{(1 - 0.075\alpha)} \quad (3.111)$$

and ' γ ' is again the same as expressed in eqn.(3.109).

Figure 3.32 shows the variation of of ' η_{pl} ' of a short radius elbow as a function of crack angle and position.

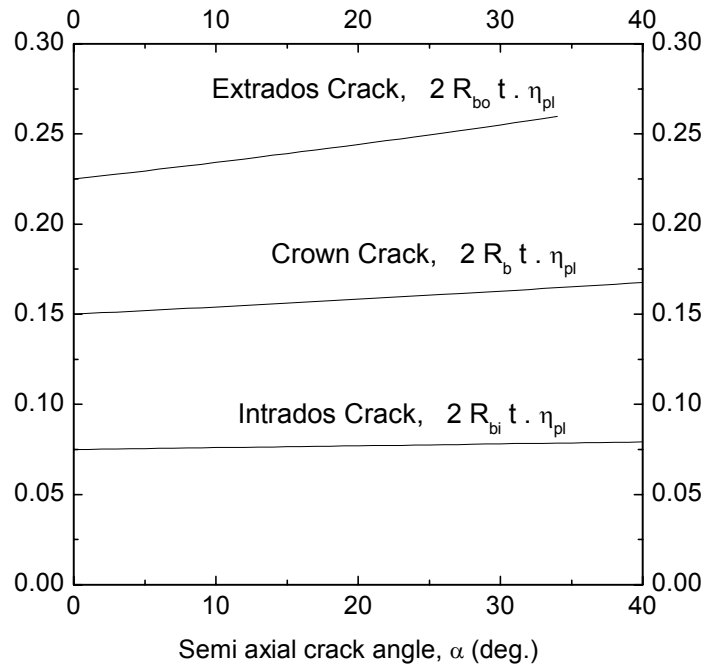


Fig.3.32 Variation of ' η_{pl} ' for short radius elbow with throughwall axial crack at various locations under in-plane bending moment

3.3 STUDYING THE POSSIBILITIES TO IMPROVE THE CRACK GROWTH MEASUREMENT BY COMPLIANCE TECHNIQUE

3.3.1 Scope of the Work

As mentioned in section 2.5, unloading compliance technique is one of the convenient methods to measure crack growth during fracture experiments. However, one correlation expressing crack size as a function of unloading compliance is the pre-requisite of this technique. Such correlations are available [42] for commonly used laboratory specimens, for example, compact tension (CT), three point bend (TPB) specimens etc. Conventionally, compliance correlation is derived by generating compliance *versus* crack length data by performing small displacement linear elastic finite element analysis. However, it does not account for the large deformation that may take place during the loading of the specimen. The unloading compliance may be influenced by the increasing stiffness of the specimen because of change in basic geometry. In that case, the compliance function not only depends on crack length but also on the current load level. It is, therefore, of interest to study the effect of load level on the unloading compliance. This requires carrying out non-linear finite element analysis to generate compliance data at different load levels. In the present work, elastic-plastic finite element analysis is carried out on three point bend (TPB) specimens and throughwall circumferentially cracked pipes under four point bending load. In case of TPB specimens, unloading compliance correlation is available [42]. However, this correlation does not consider the effect of deformation on the compliance. The objective of this study is, therefore to investigate whether deformation of the TPB specimen changes the unloading compliances or not and whether this change, if any, warrants any modifications in the existing compliance correlation.

However, no such correlation is available for throughwall circumferentially cracked straight pipe under four point bending load which is often used in fracture studies of piping components. Because of ovalisation of pipe cross

section during deformation, compliance not only depends on current crack length, but also on current load. In the present work, elastic-plastic finite element analysis has been carried out on pipes having various diameter, thickness and circumferential throughwall crack sizes. The objective is to study how initial elastic compliance is affected by deformation of the basic pipe cross section.

3.3.2 Methodology

3.3.2.1 TPB Specimen

Each TPB specimen (Fig.3.12) is loaded beyond limit load (P_0) with periodic unloading. The limit load is computed using the following equation:

$$P_o = \frac{1.456b^2\sigma_f}{S} \quad (3.112)$$

where, ' b ' is the remaining ligament in crack section, ' σ_f ' is the material flow stress and ' S ' is the loading span.

The load vs crack opening displacement has been generated for the entire load range with periodic unloading at 40, 50, 60, 70, 80, 85, 90, 95, 100, 110, 120, 130, 140, 150, 160 and 170% of limit load. The amount of unloading is 15% of limit load. Stiffness is evaluated from the slope of the load – CMOD curve by least square linear curve fitting of the unloading path. Compliance is evaluated by taking reciprocal of the stiffness at different stages of unloading including initial elastic portion. Compliance is defined as follows :

$$C = \frac{CMOD}{P} \quad (3.113)$$

where, $CMOD$ is the crack mouth opening displacement and ' P ' is the total load.

Compliance of a specimen depends on its geometry. It is required to compute normalized compliance in such a way that it is a function of crack length only. The following formula is used to calculate normalized compliance (λ) [42]:

$$\lambda = \frac{1}{1 + \left(\frac{3.95S}{CE'BW} \right)^{0.5}} \quad (3.114)$$

$$E' = \frac{E}{1 - \nu^2}$$

where, 'C' is as defined in eqn.(3.113), 'E' is the young's modulus and 'ν' is the Poisson's ratio of material and other symbols are explained in Fig.3.12.

For TPB specimens, closed-form solution exists [42] between the crack length and initial elastic compliance. The equation is as follows:

$$a/w = \lambda (-1.03 + 6\lambda - 6.37\lambda^2 + 2.73\lambda^3 - 0.312\lambda^4) \quad (3.115)$$

The present results have been validated against the above equation. Further, non-linear analysis has been performed to study how large deformation affects the above relation.

3.3.2.2 *Straight pipe*

Straight pipe with throughwall circumferential crack under four point bending load (Fig. 3.13) is considered for analysis. Each pipe is loaded beyond the theoretical plastic collapse load with periodic unloading. Theoretical plastic collapse load is calculated using the following equation:

$$P_L = \frac{16R^2t\sigma_f}{Z-L} \left[\cos\left(\frac{\theta}{2}\right) - 0.5\sin(\theta) \right] \quad (3.116)$$

where, R is the mean radius of the pipe cross section, t is the pipe wall thickness, θ is the semi-circumferential crack angle, σ_f is the material flow stress defined as the average of yield and ultimate strength, Z and L are the outer and inner span of the four point bending load respectively.

The load vs. crack mouth opening displacement (CMOD) has been generated for the entire load range with periodic unloading at

40,80,120,140,160,170,180,190 and 200% of theoretical collapse load. The amount of unloading is 15% of collapse load. Stiffness is evaluated from the slope of the load-CMOD curve by least square linear curve fitting of the unloading path. Compliance is evaluated by taking reciprocal of this stiffness evaluated at different stages of loading including the initial elastic portion. Compliance is defined as follows:

$$C = \text{CMOD}/M ; \quad M = P (Z - L)/4 \quad (3.117)$$

where, 'M' is the moment at the cracked cross section of the pipe, CMOD is the total crack mouth opening displacement, 'P' is the total applied load and 'C' is the compliance. Compliance has been normalized as follows:

$$\lambda = CEI/\pi R^2 \quad (3.118)$$

where, ' λ ' is the normalized compliance, 'E' is the Young's modulus of the pipe material, 'I' is the area moment of inertia of the pipe cross section and 'R' is the mean pipe radius. Applied moment is also normalized with respect to the theoretical collapse moment as follows :

$$m = M/M_L ; \quad M_L = P_L (Z - L)/4 \quad (3.119)$$

where, m is the normalized applied moment and M_L is the theoretical collapse moment of pipe containing a throughwall circumferential crack. The rationale of normalizing the compliance and load level is to make the equations applicable for any pipe geometry. Thus, normalized compliances (λ) have been generated for various values of normalized load levels (m) and crack angles (θ/π).

3.3.3 Finite Element Analysis

Finite element method is used to perform the forgoing work. General purpose finite element program NISA [65] is used for this study. Non-linear finite element analysis has been carried out to generate compliance data for all TPB specimens and throughwall circumferentially cracked straight pipes. Both geometric and material non-linearity are considered in this analysis.

3.3.3.1 TPB Specimens

Geometry

TPB specimens with different a/w ratios (0.1,0.2,0.3,0.4,0.5,0.6,0.7,0.8 and 0.9) are considered in this analysis. Specimens have width of 25 and unity thickness. The absolute value of specimen thickness does not play role, because compliance is normalized with respect to thickness. The load span is taken as four times of width i.e. 100 mm. The geometry of the specimen used in the present study is shown in the Fig. 3.12.

Material properties

Material properties used in finite element analysis are shown in Table 3.5 below :

Table 3.5 Material data used for analysis of TPB specimen

Young's modulus	: 203 GPa				
Poisson's ratio	: 0.3				
Yield stress	: 288 MPa				
Flow stress	: 354 MPa				
UTS	: 420 MPa				
True Stress (MPa)	: 344.12	393.37	450.33	488.54	512.86
True Strain	: 0.02529	0.05828	0.10272	0.15204	0.19786

Finite element model

Eight noded plane strain 2D elements are used to model the specimens. Because of symmetry, only one half of the specimen is modeled. Each node is considered to have two degrees of freedom. There are 300 elements and 971 nodes in the model. Symmetry boundary conditions are applied on the nodes lying in the crack plane. The roller support at one end of the specimen is simulated by constraining a particular node in vertical direction. Concentrated load is applied on a particular node in the crack plane.

3.3.3.2 Straight pipes

Geometry

Straight pipes of 200 and 400 mm nominal bore (NB) diameter are considered in the present study. The rationale of choosing these sizes is that fracture experiments are being carried out on these pipe dimensions. Initially two straight pipes: one of 200 mm NB and $R/t = 6.75$ and another of 400 mm NB and $R/t = 5.87$ are considered in this analysis, where, R and t are the pipe mean radius and wall thickness respectively. Since R/t ratios of these pipes are not much different, it is decided to consider four more straight pipes of 200 mm NB with R/t ratio varying from 9 to 20 to study the effect of R/t on compliance values. Thus total six straight pipes with different R/t ratios are considered in this study. Table 3.6 shows the various combinations of outer diameter and thickness considered in this analysis. The inner and outer span of the four point bending load for 200 mm NB pipe are 1480 and 4000 mm respectively and those for the 400 mm NB pipes are 1480 and 6000 mm respectively. Six throughwall circumferential crack angles, namely, 30° , 60° , 90° , 120° , 150° and 180° are considered for each size of pipe.

Table 3.6 Geometric details of straight pipes considered in this analysis

Outer diameter(mm)	Thickness (mm)	R/t
406	32.00	5.87
219	15.10	6.75
219	11.53	9.00
219	10.40	10.00
219	7.07	15.00
219	5.34	20.00

Material Properties

The pipe material is SA333 Gr 6. Stress-strain response of the material as obtained from the tensile tests of samples fabricated from these pipes conducted at room temperature are used in the analysis (see Chapter 4.1). The yield and ultimate strength of 400 mm NB pipe material are 312 & 459 MPa respectively and those for the 200 mm NB pipe material are 288 & 420 MPa respectively. Figure 3.33 shows the material stress-strain response used in the analysis for 400 mm NB pipes. Similar type of stress-strain response has also been obtained for 200 mm NB pipe material. The experimental true stress - true strain data is slightly modified near the yield point while giving material input data for finite element analysis. The small modification in the material stress-strain response helps in the finite element convergence process without much change of the basic material properties. Von-mises criterion and isotropic work hardening model are used in the elastic-plastic analysis. Five points are employed to define the stress-strain data of the material in a piece-wise linear fashion.

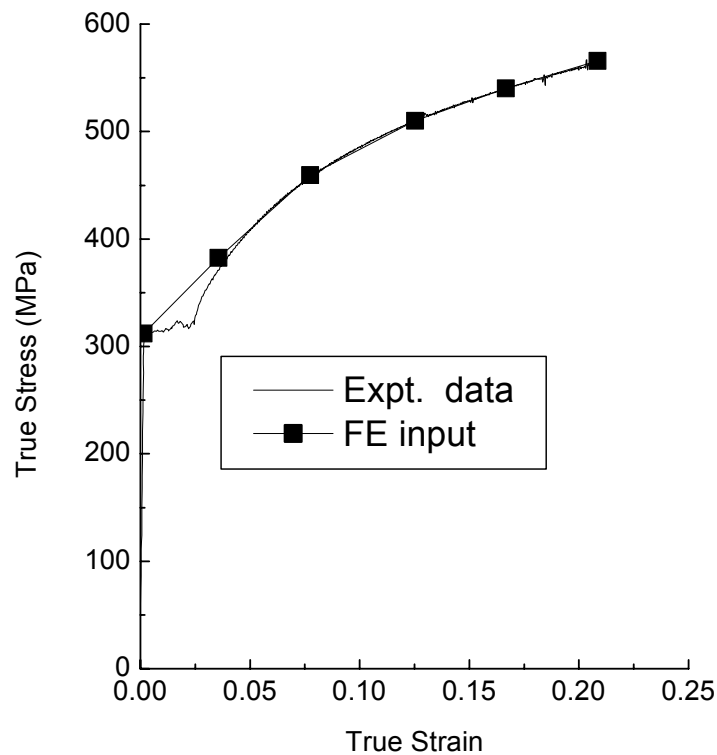


Fig.3.33 True stress – true strain curve for finite element analysis of straight pipes

Finite Element Model

Twenty-noded solid elements with $3 \times 3 \times 3$ integration order are used to model the straight pipes. Because of symmetry, only one fourth of the pipe is modeled. There are total 288 elements and 3170 nodes with one element across the thickness of the pipe. Spider web type mesh is used near the crack tip. A small hole of diameter of 0.5% of the crack length is introduced at the tip of the crack for better convergence in non-linear finite element analysis without affecting the results. Fig. 3.34 shows a typical FE mesh of straight pipe. Here, load-crack mouth opening displacement (CMOD) data is used to obtain the compliance function and since load - CMOD data is gross structural behavior, it is not much finite element mesh dependent. Concentrated load has been applied at a particular node.

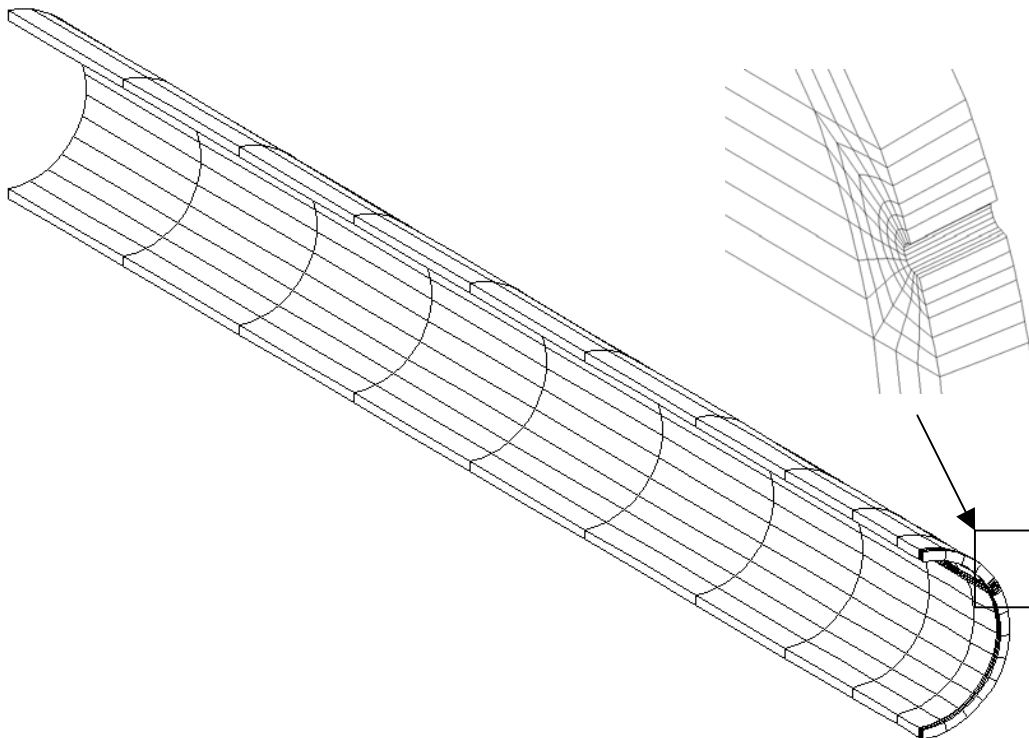


Fig. 3.34 Typical Finite Element Mesh of Straight Pipe

3.3.4 Results and Discussion

3.3.4.1 TPB Specimens

Figure 3.35 shows the load vs. CMOD curves for all the specimens. Compliance values are shown in Table 3.7 for various a/w and m , where 'm' is the normalized load expressed as the ratio of current load and limit load (P/P_0). All specimens are not loaded to the same load level in times of limit load because of convergence problem. Except for one specimen with a/w ratio 0.1, all other are loaded beyond limit load. The maximum load level i.e. 170% of limit load is reached for the specimen with $a/w = 0.9$. Compliance values at different load levels are varying for each specimen. Although this variation is not significant, however it is maximum for the specimens with low a/w ratios compared to other specimens with higher a/w ratios. This is due to the fact that geometrical changes are more pronounced in specimens with low a/w ratio having higher limit load than other specimens with higher a/w ratio. Fig. 3.36 shows the relationship between specimen a/w ratio and normalized initial elastic compliance. It is observed that normalized initial elastic compliance is varying almost linearly with a/w ratio. Finally a/w for each specimen is calculated using equation (3.115) from normalized initial elastic compliance to compare with actual a/w ratio and it is found that they are closely matching. Table 3.8 shows the actual a/w ratio and computed a/w ratio. From the above discussion it is clear that the existing compliance correlation for TPB specimens based on linear elastic analysis does not require any modification to take care of geometric deformation at various load levels.

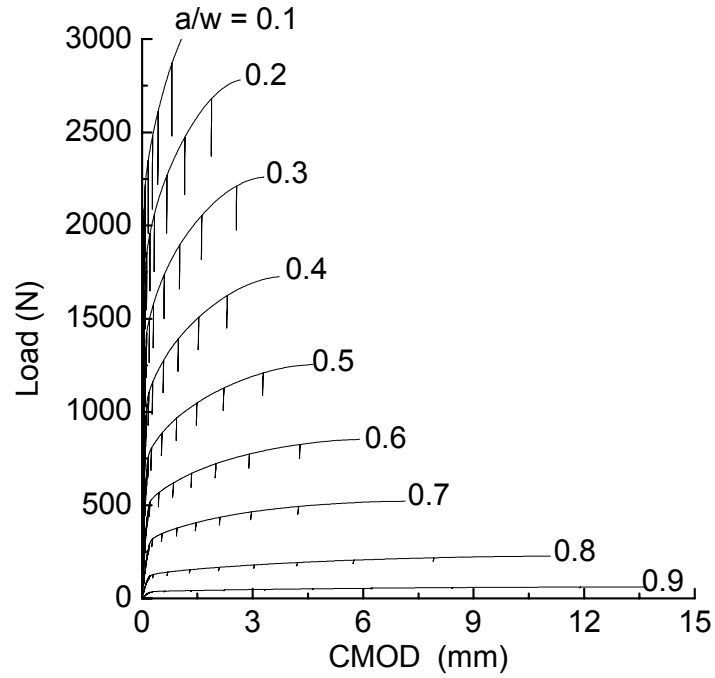


Fig.3.35 Load vs. CMOD curves for TPB specimens with various a/w ratios

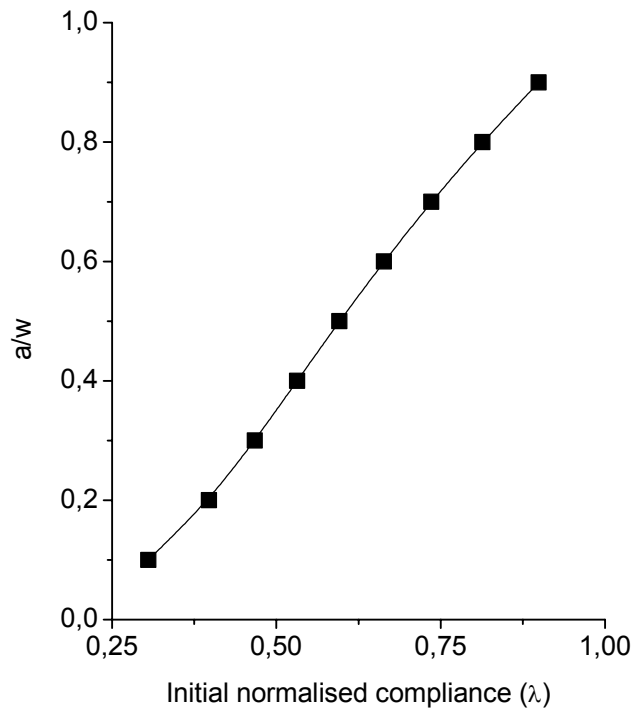


Fig.3.36 Crack size vs. initial normalized compliances of TPB specimen

Table 3.8 Comparison of a/w ratios using compliance method for TPB specimens

Actual a/w	Initial elastic Compliance (C)	Normalized Compliance, λ (eqn.(3.114))	Calculated a/w from eqn. (3.115)
0.1	0.13694E-04	0.30540	0.08653
0.2	0.30871E-04	0.39766	0.20380
0.3	0.54477E-04	0.46723	0.30200
0.4	0.91225E-04	0.53159	0.39584
0.5	0.15434E-03	0.59615	0.49005
0.6	0.27560E-03	0.66359	0.58644
0.7	0.54864E-03	0.73567	0.68570
0.8	0.13531E-02	0.81381	0.78820
0.9	0.56445E-02	0.89926	0.89528

3.3.4.2 Straight pipes

Figure 3.37 shows the moment vs. CMOD curves for 400 mm NB pipe and all other pipes show similar trend. All straight pipes are not loaded up to the same load level because of non-convergence. However all straight pipes are loaded up to or above the theoretical collapse load. The maximum load level reached is two times of theoretical collapse load especially for pipes with lower R/t ratios and higher crack angles (2θ). Table 3.9 shows the normalized compliances for 200 and 400 mm NB pipes with various sizes of cracks at various load levels. It can be seen that unloading compliance decreases with increase in load even for the same crack length. In other words, the pipe stiffens because of ovalisation of the circular cross section during deformation. The pattern of deformation is such that it increases area moment of inertia of pipe cross section, which is proportional to the fourth power of pipe diameter. It can also be seen that normalized compliances, λ (see eqn.(3.118)) for 200 and 400 mm NB pipes of almost same R/t ratios are almost identical at same normalized load level (m) (eqn.(3.119)) and normalized crack size (θ/π). However these values varies for pipes with different R/t ratio. It is clear from above that the deformation level of pipes significantly affects the compliance values. Therefore, any compliance correlation of pipe must include load/deformation as one of the parameters.

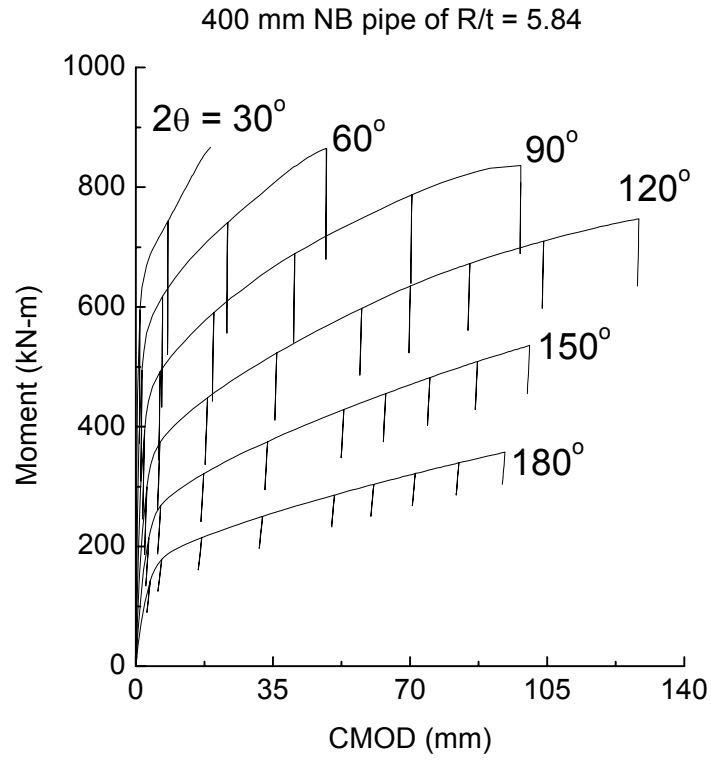


Fig.3.37 Moment vs. CMOD curves for 400 mm NB pipe with various crack sizes

Table 3.9 Normalized Compliances, λ (eqn.(3.118)) for 200 and 400 mm NB pipes

R/t = 5.84 (400 mm NB pipe)						
	λ					
	$2\theta=30^\circ$	60°	90°	120°	150°	180°
m=0.0	0.3717	0.9287	1.8407	3.3587	5.9570	10.6645
0.8	0.4141	0.9147	1.8142	3.3035	5.8415	10.4355
1.0	0.3186	0.8593	1.7553	3.2296	5.7285	10.2430
1.2	*	0.7341	1.5971	3.0230	5.4295	9.7450
1.4	*	0.5560	1.4273	2.7924	5.1130	9.1600
1.6	*	*	1.2227	2.5503	4.7380	8.6160
1.7	*	*	0.9781	2.4293	4.5655	8.3710
1.8	*	*	*	2.2970	4.4018	8.1125
1.9	*	*	*	2.1446	4.2373	7.8655
2.0	*	*	*	1.9338	4.0685	7.6290

R/t = 6.75 (200 mm NB pipe)						
	λ					
	$2\theta=30^\circ$	60°	90°	120°	150°	180°
m=0.0	0.3601	0.9203	1.8555	3.4326	6.1425	11.0430
0.8	0.3541	0.9083	1.8307	3.3761	6.0181	10.7920
1.0	0.3175	0.8597	1.7774	3.3054	5.9040	10.5930
1.2	0.2511	0.7412	1.6237	3.1045	5.6120	10.1015
1.4	*	0.5869	1.4462	2.8614	5.2645	9.4815
1.6	*	*	1.2224	2.5973	4.8740	8.8960
1.7	*	*	1.0279	2.4583	4.6898	8.6050
1.8	*	*	*	2.3115	4.5058	8.3290
1.9	*	*	*	2.1399	4.3253	8.0645
2.0	*	*	*	1.8662	4.1393	7.8085

R/t = 9 (200 mm NB pipe)						
	λ					
	$2\theta=30^\circ$	60°	90°	120°	150°	180°
m=0.0	.43252	1.16740	2.36579	4.34230	7.67116	13.59184
0.8	.42260	1.14414	2.31382	4.22281	7.41954	13.10955
1.0	.36512	1.06358	2.22704	4.10874	7.21853	12.74597
1.2	.26534	.88984	2.00919	3.81663	6.80989	12.00330
1.4	*	*	1.72901	3.47222	6.29755	11.17866
1.6	*	*	*	3.07340	5.79629	10.36726
1.7	*	*	*	2.86393	5.53213	9.98413
1.8	*	*	*	2.61483	5.28712	9.61632
1.9	*	*	*	*	5.03532	9.26826
2.0	*	*	*	*	4.76735	8.93294

Table 3.9 contd..

R/t = 10 (200 mm NB pipe)						
	λ					
	$2\theta=30^\circ$	60°	90°	120°	150°	180°
m=0.0	.43899	1.19686	2.45170	4.52517	8.00786	14.16807
0.8	.42743	1.17154	2.39153	4.38445	7.70890	13.62930
1.0	.36456	1.08473	2.29844	4.26102	7.48521	13.22961
1.2	.24949	0.90195	2.06630	3.94669	7.04477	12.44622
1.4	*	*	1.75680	3.57375	6.50177	11.55248
1.6	*	*	*	3.13793	5.96566	10.68945
1.7	*	*	*	2.90487	5.70141	10.29406
1.8	*	*	*	2.59727	5.42744	9.91008
1.9	*	*	*	*	5.14628	9.54510
2.0	*	*	*	*	4.85370	9.18139

R/t = 15 (200 mm NB pipe)						
	λ					
	$2\theta=30^\circ$	60°	90°	120°	150°	180°
m=0.0	.45309	1.34372	2.85454	5.35640	9.48535	16.67323
0.8	.43833	1.30294	2.74819	5.09411	8.92711	15.58498
1.0	.36543	1.19702	2.62816	4.92532	8.60554	14.95235
1.2	*	*	*	4.52414	8.03532	13.89104
1.4	*	*	*	4.03740	7.42025	12.77615
1.6	*	*	*	3.40704	6.72867	11.74784
1.7	*	*	*	*	6.37625	11.33936
1.8	*	*	*	*	5.95818	10.91263
1.9	*	*	*	*	*	10.46356

R/t = 20 (200 mm NB pipe)						
	λ					
	$2\theta=30^\circ$	60°	90°	120°	150°	180°
m=0.0	.46929	1.47908	3.22230	6.08844	10.75080	18.68080
0.8	.45058	1.41880	3.05264	5.68628	9.90097	17.22753
1.0	.36769	1.30022	2.91264	5.47533	9.49553	16.46781
1.2	*	*	2.52440	5.00297	8.82544	15.23833
1.4	*	*	*	4.40767	8.11259	13.99478
1.6	*	*	*	*	*	12.89377
1.7	*	*	*	*	*	12.41831
1.8	*	*	*	*	*	11.98114
1.9	*	*	*	*	*	11.44143

4. EXPERIMENTAL INVESTIGATIONS

4.1 EXPERIMENTS ON SMALL SPECIMENS

4.1.1 Scope of the Work

Tensile and fracture mechanics properties of materials are required as basic input in the integrity assessment of any component. Therefore, for analysis of the fracture experiments of piping components, tensile and fracture properties are evaluated by testing small tensile and three point bend (TPB) specimens respectively. One of the objectives of these tests on small specimens is also to address the issue of transferability of fracture properties from small specimens to full-scale components. To study this issue of transferability, one has to compare the fracture resistance (quantified by J-R curve) of small laboratory specimens and real components. The material of these piping components is carbon steel of grade SA333Gr 6. All the tests are carried out at room temperature. The chemical composition of this material is given in the following Table 4.1.

Table 4.1 Chemical composition of piping material SA333Gr6

Element	C	Mn	Si	P	S	Ni	Cr	Al	Cu	V
Wt. %	0.12	0.97	0.28	0.01	0.02	0.08	0.13	0.031	0.08	0.002

4.1.2 Geometry of the Specimens

Tests are carried out as per ASTM E8M-89b [73] on tensile samples machined from 200 mm and 400 mm nominal bore (NB) diameter pipes to generate the tensile properties. These pipes have been tested as a part of comprehensive *Component Integrity Test Program*. To remove the scatter due to different heat of materials, small samples have been machined from the actual full-scale pipes tested. J-R tests have been carried out on three point bend (TPB) specimens (Fig.3.12) of three different thicknesses, B = 8, 12.5 and 25 mm. The TPB specimens having thickness of 8 mm are machined from 200 mm NB pipes and the rest are machined from 400 mm NB pipes. For each thickness, specimens of varying crack length ($a/w = 0.2 - 0.51$) are tested. These samples

are non-standard with respect to ASTM E 1820 [42]. The objective of this study is to incorporate a wide range of crack tip triaxiality. Prior to conducting the J-R tests, each specimen are fatigue pre-cracked. Fatigue cracks were grown under software control using decreasing or constant ΔK envelopes, at a R-ratio of 0.1 and frequency of 20 Hz as per the procedure laid down in ASTM standard E 647. Prior to J-R tests and after fatigue pre-cracking, the TPB specimens are side-grooved to the extent of 20% of the thickness. The single specimen technique has been employed for determination of the J-R curve of the pre-cracked TPB specimens as per ASTM E 1820 [42]. For TPB specimens having $a/w > 0.282$, $\eta = 2$ is used to calculate J-integral from load deflection data. For shallow cracked TPB specimens ($a/w < 0.282$), Sumpter's [74] correlation of ' η ' factor is used.

4.1.3 Tensile Properties

There are two sizes of piping components which are subjected to fracture tests. Although all these pipe materials are of the same grade (ASTM Grade SA333Gr6), there are 2 categories based on heat of the material. Category 1 consists of materials from 200 mm NB pipes and category 2 consists of materials from 400 mm NB pipes. Table 4.2 shows the tensile properties of 2 categories of material. Figures 4.1 and 4.2 show the stress-strain curves obtained from category 1 and 2 material.

Table 4.2 Tensile properties of carbon steel (SA333Gr6) pipe materials

Source	Yield Stress (MPa)	UTS (MPa)	% Elongation	% Reduction in area at fracture	Young's modulus (GPa)	Poisson's ratio
200 mm NB pipe	288	420	36	77.23	203	0.3
400 mm NB pipe	312	459	41	77.1	203	0.3

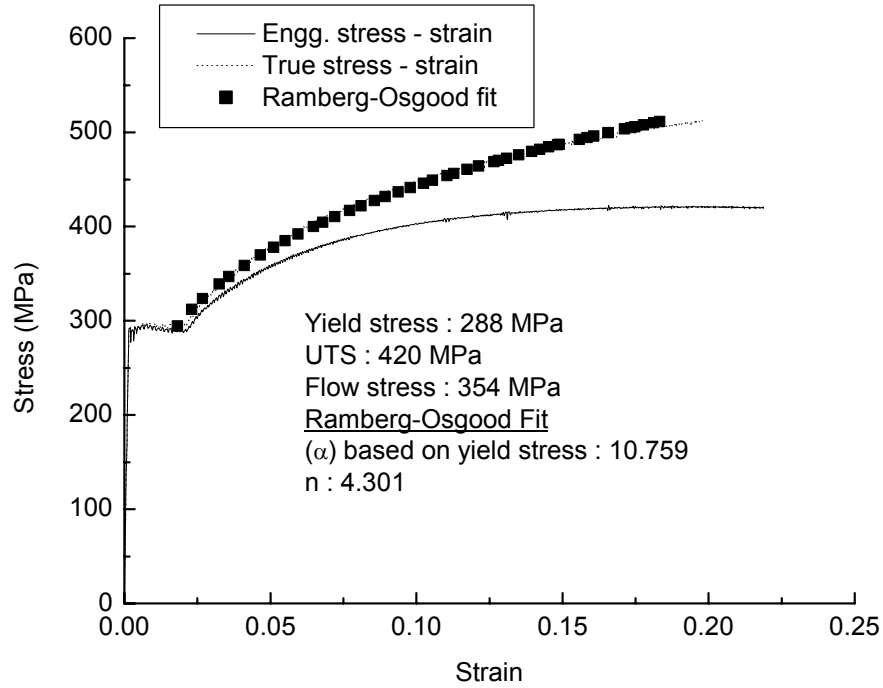


Fig.4.1 Stress-strain diagram obtained from 200 mm NB pipe material

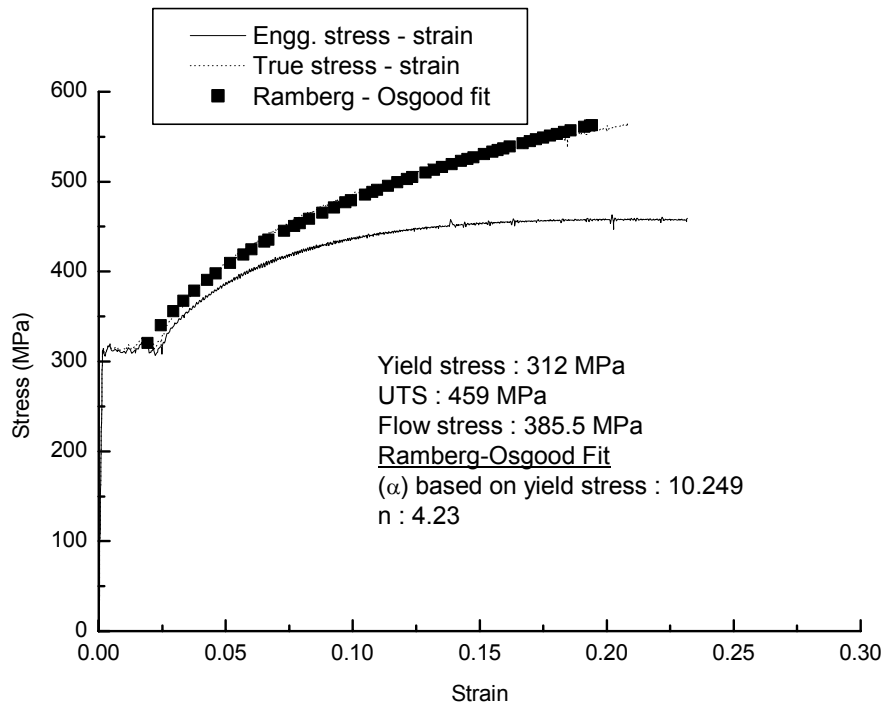


Fig.4.2 Stress-strain diagram obtained from 400 mm NB pipe material

4.1.4 Fracture Properties

In case of TPB specimens, 'a/w' has been varied from 0.2 to 0.51 by controlling the degree of fatigue pre-crack to have a wide range of crack tip triaxiality. However, no significant effect of 'a/w' on the specimen J-R curve has been observed. This may be due to very high toughness of the material. Consequently, two representative J-R curves have been used in the fracture analysis of pipes. For 200 mm NB pipe material, the J-R curve of TPB specimen having thickness, B=8 mm and a/w = 0.51 is considered. For 400 mm NB pipe material, the J-R curve of TPB specimen having thickness, B=25 mm and a/w = 0.2 is considered. Figures 4.3 and 4.4 show the power law and second order polynomial fit of the TPB specimen J-R curves. It may be seen that polynomial fit matches better the trend of experimentally obtained TPB specimen J-R curve. The initiation toughness (J_I) based on stretched zone width (SZW) for this material has been evaluated as 220 N/mm. The initiation toughness (J_{Ic}) based on ASTM blunting line equation with 0.2 mm offset (see Fig.2.4a) could not be determined in this case, as the ASTM blunting line equation based on material flow stress was not suitable for so highly ductile material of the pipes.

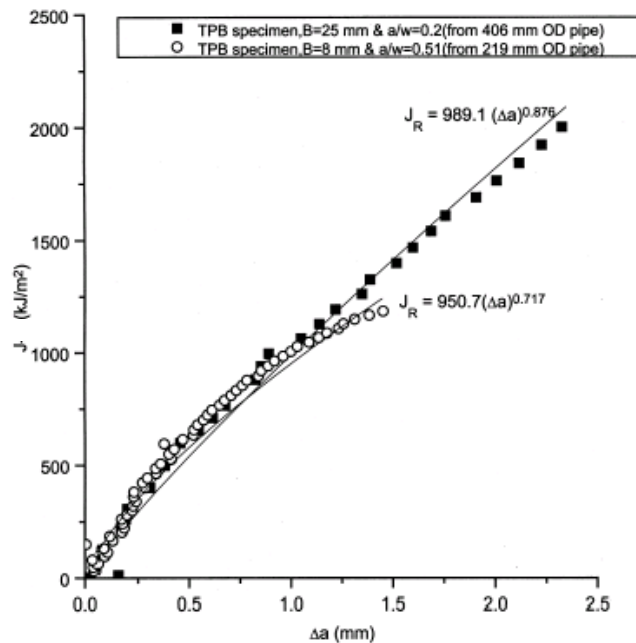


Fig.4.3 Power law fit of J-R curves obtained from TPB specimens

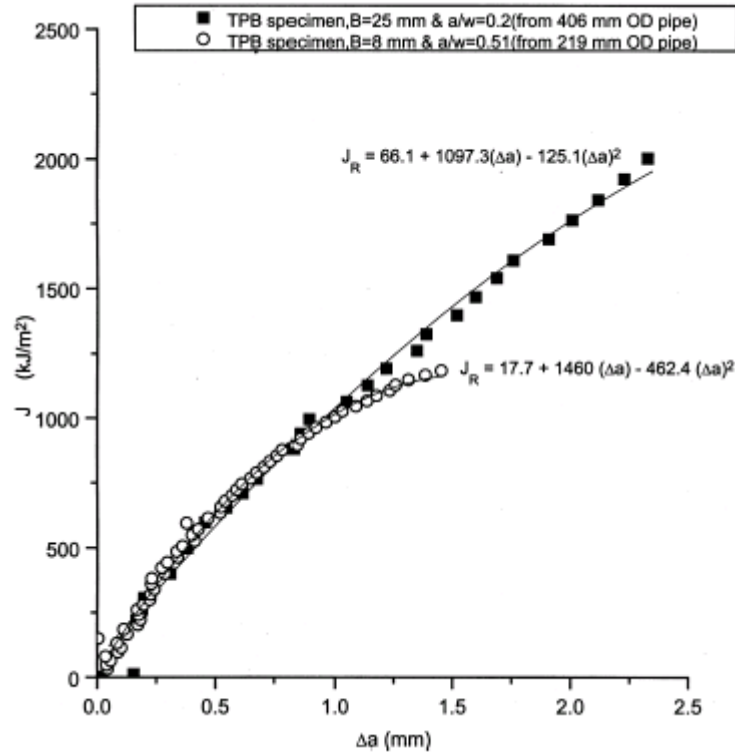


Fig.4.4 Second order polynomial fit of J-R curves obtained from TPB specimens

4.2 FRACTURE EXPERIMENTS ON FULL SCALE PIPING COMPONENTS

4.2.1 Scope of the Work

The transferability of the specimen J-R curve to the component level is an important issue in the field of elastic-plastic fracture mechanics safety assessment procedure. There is also an issue related to the extrapolation of specimen J-R curve beyond test range that requires investigation. Specimen J-R curves generated through the testing of compact tension (CT) or TPB specimens are often limited to very small amount of crack growth ($\Delta a = 2 - 10$ mm). A real component, on the other hand, often undergoes substantial amount of stable crack growth ($\Delta a = 50 - 150$ mm) before instability occurs. The point is how to extrapolate the specimen J-R curve beyond test range so that the extrapolated J-R curve can be used for fracture assessment of real-life components. Presently, specimen J-T_{mat} curve is extrapolated linearly tangent to the last test data where

' T_{mat} ' is the material tearing modulus as defined in eqn. (2.18). However, it requires further experimental investigation to check the adequacy of this extrapolation method. To address these issues, a number of fracture tests are carried out on throughwall cracked pipes and elbows as a part of comprehensive project on *Component Integrity Test Program*. The details of these tests are discussed below.

4.2.2 Fracture Tests on Straight Pipes

4.2.2.1 Test Specimens

Test specimens consist of straight pipes made of SA333Gr6 carbon steel material with through wall circumferential crack at the middle of its length. Figure 3.13 shows the geometry of the pipe specimens. These pipe specimens are subjected to four point bending load. The notched test specimens are fatigue pre-cracked by small amount (~ 2 - 10 mm at each side) prior to performing the experiment. This ensures a sharp crack tip. During the fatigue pre-crack, sinusoidal cyclic load is applied. The maximum cyclic load is approximately 10% of the collapse load and minimum cyclic load is 10% of the maximum load. The geometric details of the test specimens are given in Table 4.3.

Table 4.3 Details of Pipe Test Specimens

Test no.	Outer Dia. (mm)	Thickness (mm)	Outer Span (mm) Fig.3.13	Inner Span (mm) Fig.3.13	Crack angle, 2θ ($^{\circ}$)	
					As machined	After fatigue pre-crack
SP BM TWC8-1*	219	15.15	4000	1480	60.0	65.6
SP BM TWC8-2	219	15.10	4000	1480	90.0	93.9
SP BM TWC8-3	219	15.29	4000	1480	120.0	126.4
SP BM TWC8-4	219	15.11	4000	1480	150.0	157.0
SP BM TWC16-1	406	32.38	5820	1480	90.9	96.0
SP BM TWC16-2	406	32.15	5820	1480	121.4	126.3
SP BM TWC16-3	406	32.36	5820	1480	153.0	157.8

*SP = Straight Pipe, BM = Base Metal, TWC = Through Wall Crack, First number represent the nominal pipe diameter in inch and second number represents the test no.

4.2.2.2 Test Arrangement

Fracture tests are carried out on the fatigue pre-cracked pipe specimens at room temperature. Similar type of tests on pipes and its analysis had been reported by several researchers e.g. Moulin and Delliou [43], Kashima et al, [75], Wilkowski et al [76], Roos et al, [77], Darlaston et al [78], Forster et al [79]. In the present work, tests are conducted on carbon steel pipes under four point bend loading using computer controlled servo-hydraulic actuator of ± 1 MN capacity. Figure 4.5 shows the photograph of the test set up. The pipe is supported over a span of 4 and 5.82 meters in case of 200 and 400 mm NB pipes respectively. Steel pedestals are used to support the pipes. A distribution beam with rollers is used to apply two concentrated loads on the pipe over a distance of 1.48 m. Static (monotonic) load is applied on the pipe specimens under displacement control. The rate of displacement has been fixed as 0.055 mm/sec. Since the actuator has a maximum displacement of 100 mm, the test is programmed to stop after reaching the maximum displacement using the limit switch of the controller. The test is again continued after adjusting the displacement of the actuator using manual control and by providing packing plates at the loading points.

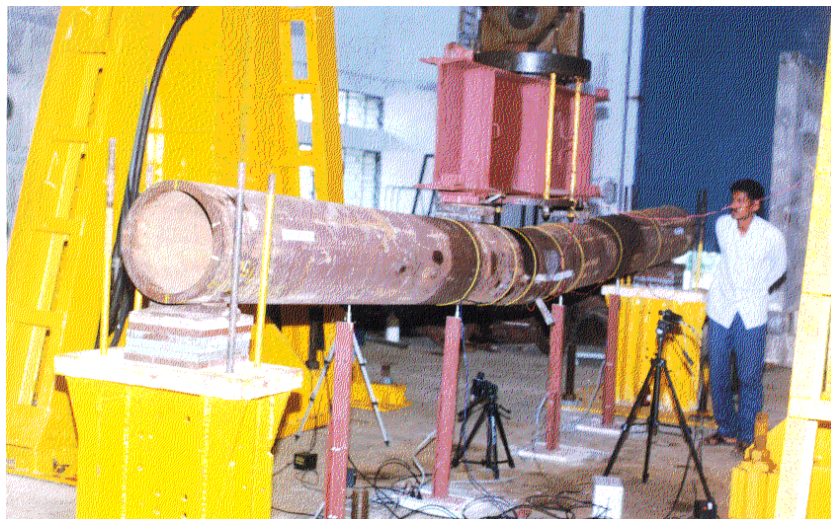


Fig.4.5 Photograph of pipe fracture test set-up

4.2.2.3 Instrumentation and Data Acquisition

During the fracture experiments, instrumentation are mounted to measure the various parameters, namely, total applied load, load line displacement, crack growth at both the tips, crack opening displacement at various locations of the notch, deflection of pipe at typical locations.

The total applied load is measured directly using a strain gauge based load cell of ± 1 MN dynamic capacity connected to the actuator. The load cell output is conditioned by a dc signal conditioner module in the servo-hydraulic control console. The load-line displacement is measured by an in-built linear variable displacement transducer (LVDT) of the actuator. Signal conditioning for the LVDT is accomplished using an alternating current (AC) signal conditioner incorporated into the servo-hydraulic control console.

Crack growth in the present set of pipe fracture experiments is measured by image processing system. It consists of four charged couple device (CCD) cameras connected to a PCI frame grabber (DT 3155) plug-in compatible with computer. Out of the four cameras, two are designated for measuring the crack growth at two crack tips, one is used to measure the crack opening displacements and one for recording the load & load-point displacement from the digital display. Clicking one key captures all the four images with a maximum time delay of around 600 milli-seconds. Considering the very slow rate of quasi-static loading, this delay is tolerable. A grid of 5 mm uniform spacing is made near the crack tips to obtain the crack growth on a 3D surface from the 2D images. The details of the image processing system are described in Ref. [80]. Figure 4.6 shows typical four windows displayed in the image processing system. Crack opening displacements at crack mouth and at various locations along the length of the crack are measured by clip gauges and image processing technique. Finally the deflections of pipe at some selected locations are measured by LVDT.

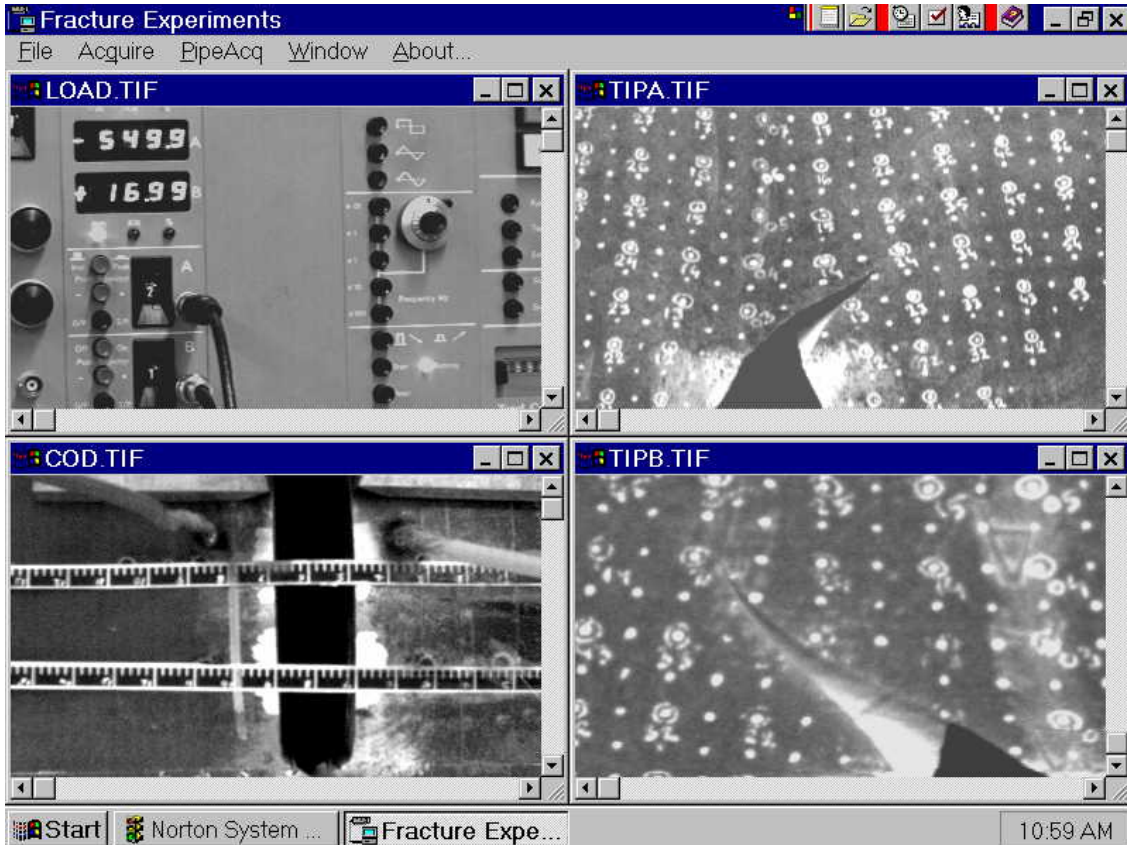


Fig.4.6 Typical Four windows as seen on the PC monitor of image processing system titled LOAD, COD, TIPA, TIPB display the load-displacement reading, crack opening displacement, crack tip A image and crack tip B images respectively

4.2.2.4 Pipe Fracture Test Results

Pipe fracture test results are expressed in the form of load vs. load-point-deflection, crack growth and crack opening displacement curves. Figure 4.7 shows the load vs. load-point deflection curves for various pipes. Crack grows out-of-plane in case of carbon steel pipes. The amount of crack growth is slightly different at two crack tips. To construct the load vs. crack growth (in circumferential direction) curves and generate the component J-R curves, the average projected crack growth in the plane of the initial crack is taken. Figure 4.8 shows the load vs. crack growth curves for various pipes. Figure 4.9 shows the photograph of the typical crack growth in one of the pipes. Figure 4.10 shows the images of complete crack growth process at one tip of the crack for fracture

test no. SPBMTWC8-3. It shows first the blunting of the sharp crack tip that is generated during fatigue pre-crack, its out-of-plane crack growth and taking turn following a zig-zag path.

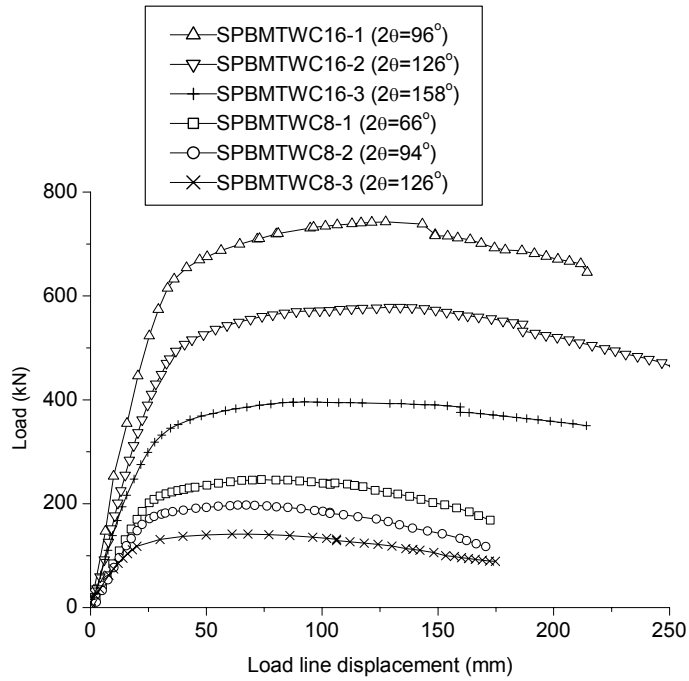


Fig.4.7 Load vs. load-line-displacement curves for various pipes

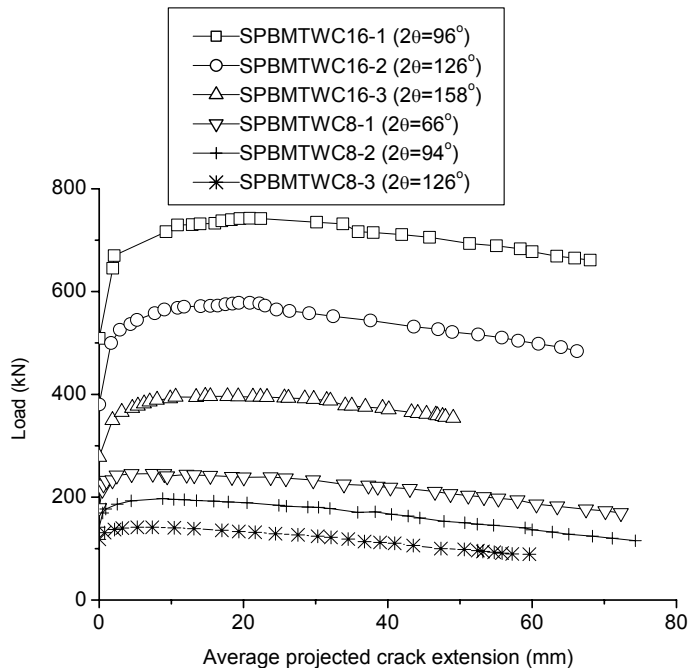


Fig.4.8 Load vs. crack growth curves for various pipes

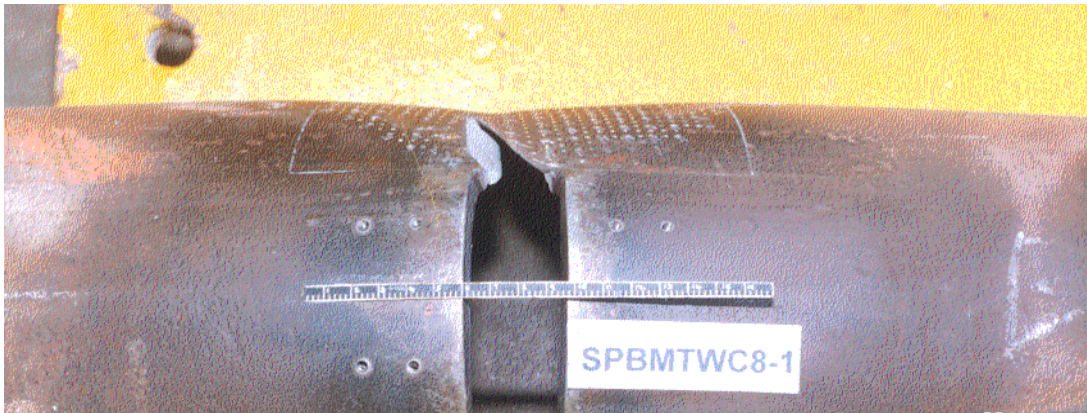


Fig.4.9 Typical crack growth pattern in pipe test specimen no. SPBMTWC8-1

4.2.3 Fracture Tests on Elbows

4.2.3.1 Test Specimens and Set-up

Test specimens consist of 200 mm NB 90° elbows made of SA333 Gr.6 carbon steel material having through wall circumferential crack at elbow (Fig.4.11) and through wall axial crack at elbow crown (Fig.4.12). The thickness of elbows along the circumference of cracked section varies from 15.5 mm to 24.1 mm. For each elbow, wall thickness has been measured at 24 locations along the circumference and an average value is considered in the analysis. The average thickness for three elbows is around 19 mm. The straight pipes of length of 600 mm are welded on both sides of the elbow. The other end of the straight pipe is welded to a 200 mm NB flange, which is bolted to a circular plate. Figure 4.13 shows the schematic drawing of test set-up. Out of three circumferentially throughwall cracked elbows tested, two have cracks at intrados and are subjected to opening bending moment and one has crack at extrados and is subjected to closing bending moment. Cracks have been machined on elbows by milling process. Before carrying out the fracture tests, each elbow is fatigued to a fatigue surface with about 4 - 10 mm on each side of the crack to have sharp crack tips. These fatigue pre-cracked elbows are then subjected to in-plane opening/closing bending moment as shown in Fig.4.13. During the experiments, load, load-point-deflection and crack growth on both the sides are measured.

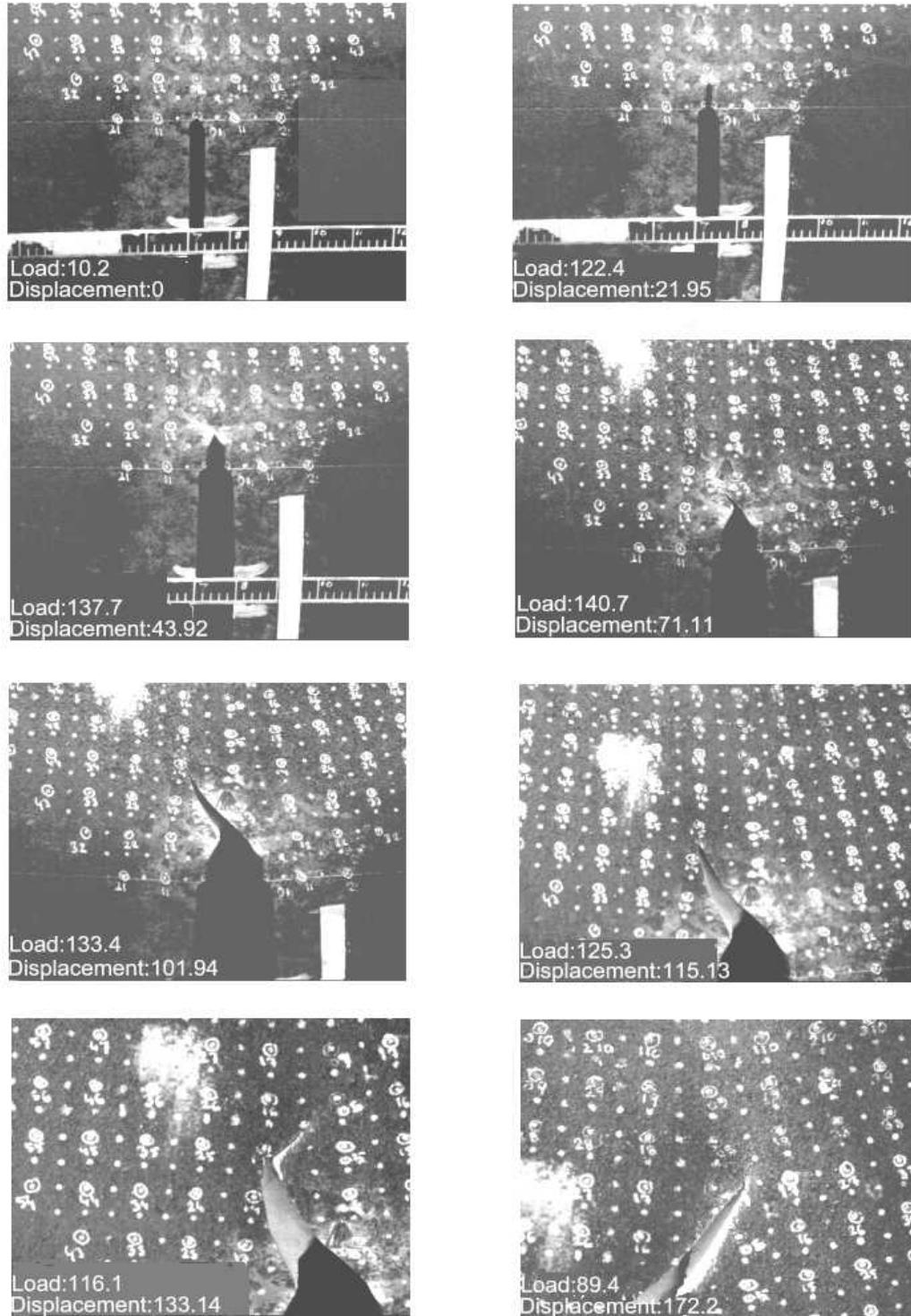


Fig.4.10 Crack growth images at various stages of loading in carbon steel pipe test no. SPBMTWC8-3 (Load in kN and Displacement in mm)

Crack growth is measured by image processing techniques as in case of pipes. Table 4.4 shows the geometric details of the elbows. Figure 4.14 shows the photograph of the test rig.

Table 4.4 Details of Elbow Test Specimens

Test no.	R_b (mm)	OD (mm)	t_{av} (mm)	Crack orientation	Crack location	Bending mode	Semi crack angle (θ)
ELTWIN8-1	207	219	19.1	Circumferential	Intrados	Opening	47.48°
ELTWIN8-2	207	219	18.8	Circumferential	Intrados	Opening	62.58°
ELTWEX8-4	207	219	19.3	Circumferential	Extrados	Closing	49.12°
ELTWCR8-6	207	219	19.0	Axial	Crown	Closing	* $a=54.6$ mm

* 'a' is the semi axial crack length

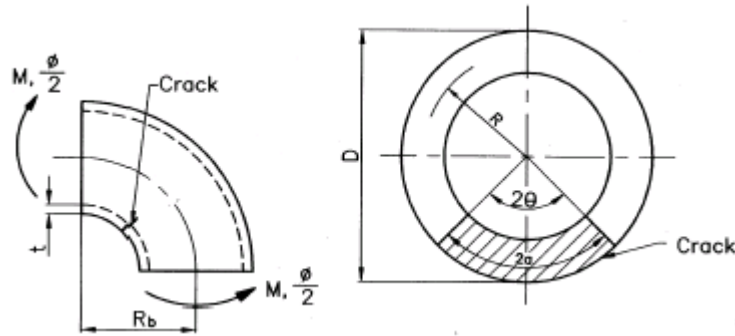


Fig.4.11 Sketch of elbow with through wall circumferential crack at intrados

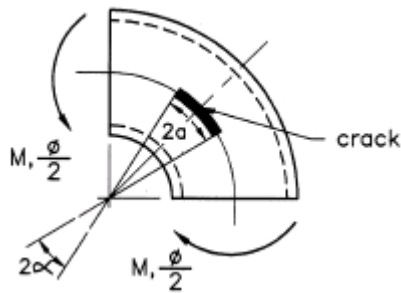


Fig.4.12 Sketch of elbow with through wall axial crack at crown

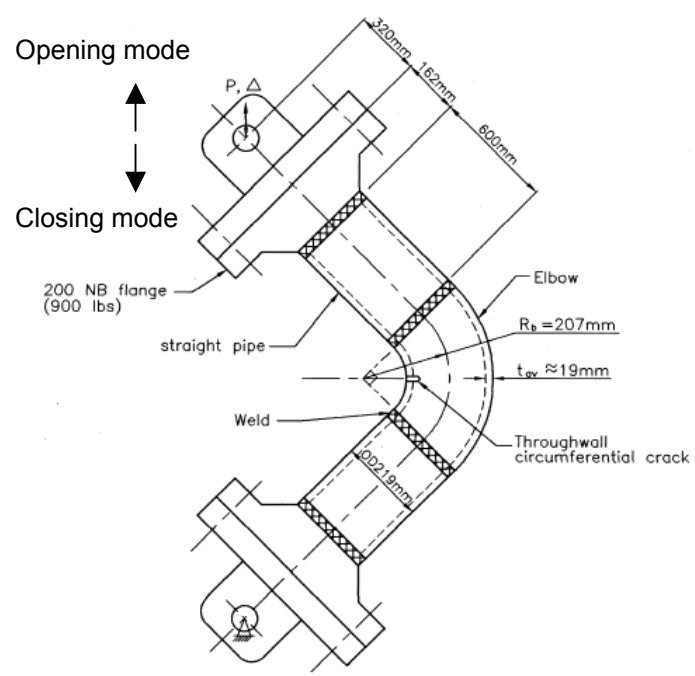


Fig.4.13 Schematic drawing of elbow test set-up



Fig.4.14 Photograph of elbow test set-up

4.2.3.2 Experimental Results

Figures 4.15 and 4.16 show the load vs. total load-line-displacement and load vs. load-line-displacement due to crack only curves respectively for all the elbow specimens. It may be noted from Figs.4.15 and 4.16 that elbow no. ELTWEX8-4 and ELTWCR8-6 under closing moment reached the maximum load and then drops after peak value indicating the instability of the structure. However, elbow nos. ELTWIN8-1 and ELTWIN8-2 under opening moments tried to reach the maximum load asymptotically without showing any dropping behavior. This is compatible with the observations of Kussmaul et al [66]. From the total load-line-displacement, displacements of un-cracked elbow are subtracted to obtain the load-line-displacements due to crack only. Crack grows out-of-plane in case of carbon steel elbows. However, crack growth is measured as the projected value in the initial plane of the crack. The amount of crack growth is slightly different at two crack tips. To construct load vs. crack growth curves, the average value is considered. It may be noted that crack growth, observed by the image processing technique, is on the outer surface of elbow. To get the mean value, crack growth on outer surface has been multiplied by (R/R_o) . This assumes that crack front is radial across the thickness of elbow. No crack growth has been observed during fracture test of axially cracked elbow. Figure 4.17 shows the load vs. mean crack growth curves for the elbow specimens.

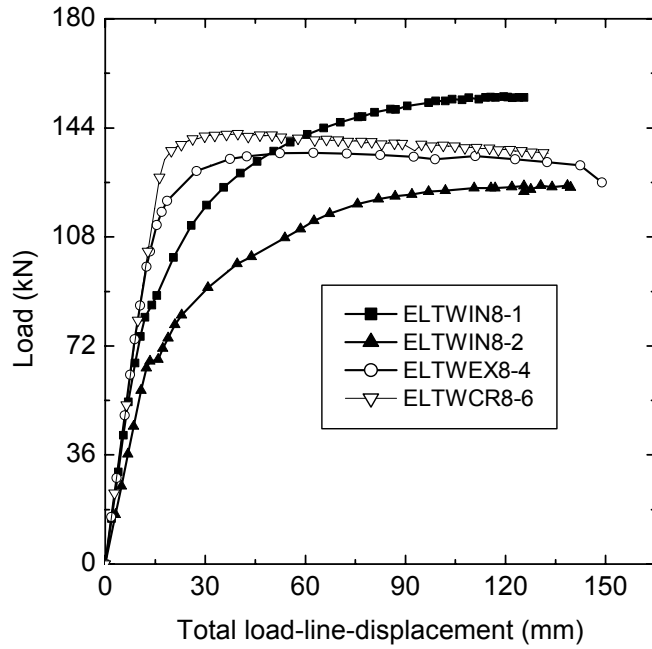


Fig.4.15 Load vs. load-line-displacements for various elbow specimens

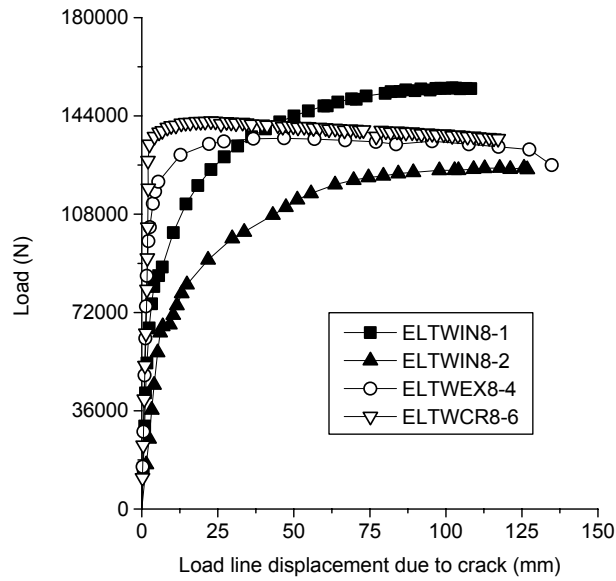


Fig.4.16 Load vs. load-line-displacements due to crack only for various elbow specimens

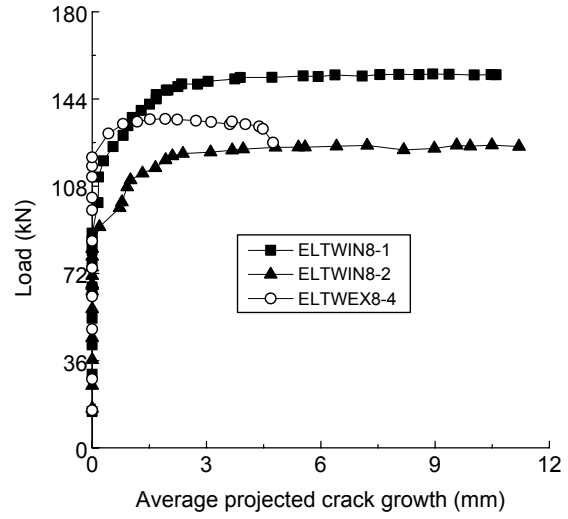


Fig.4.17 Load vs. crack growth curves for various elbow specimens

5. NUMERICAL AND THEORETICAL ANALYSIS OF EXPERIMENTAL RESULTS

5.1 FINITE ELEMENT ANALYSIS OF TPB SPECIMENS, PIPES AND ELBOWS

5.1.1 Finite element model

The 3-D elastic-plastic finite element analyses have been carried out on cracked piping components and the specimens. Due to symmetry in both geometry and the loading conditions only one fourth of the TPB specimen, pipe and elbows are modeled. Fine mesh has been provided near the crack front to obtain the steep stress/strain gradients accurately. The side-groove is also modeled in the case of the TPB specimens. Figures 5.1 - 5.3 show the typical finite element mesh for TPB specimen, cracked pipe and elbow respectively. The finite element mesh for TPB specimen consists of 5606 nodes and 1023 elements, for cracked pipe it is 8231 nodes and 1404 elements and for cracked elbow it is 5763 nodes and 966 elements. The large strain, large displacement relations based on geometry changes are assumed in the analysis. The isoparametric 20-noded elements are adopted in the models. Reduced order of integration (2x2x2) is used to eliminate artificial locking under incompressibility condition imposed by plastic deformation. The analyses are done using the finite element program WARP3D [81]. The finite element models are analyzed under displacement control to simulate the experimental procedure. Nonlinear material behavior is modeled using incremental plasticity with Von Mises yield function associated flow rule and isotropic hardening. The true stress-strain curve obtained from a uni-axial test is given as the input to the material model.

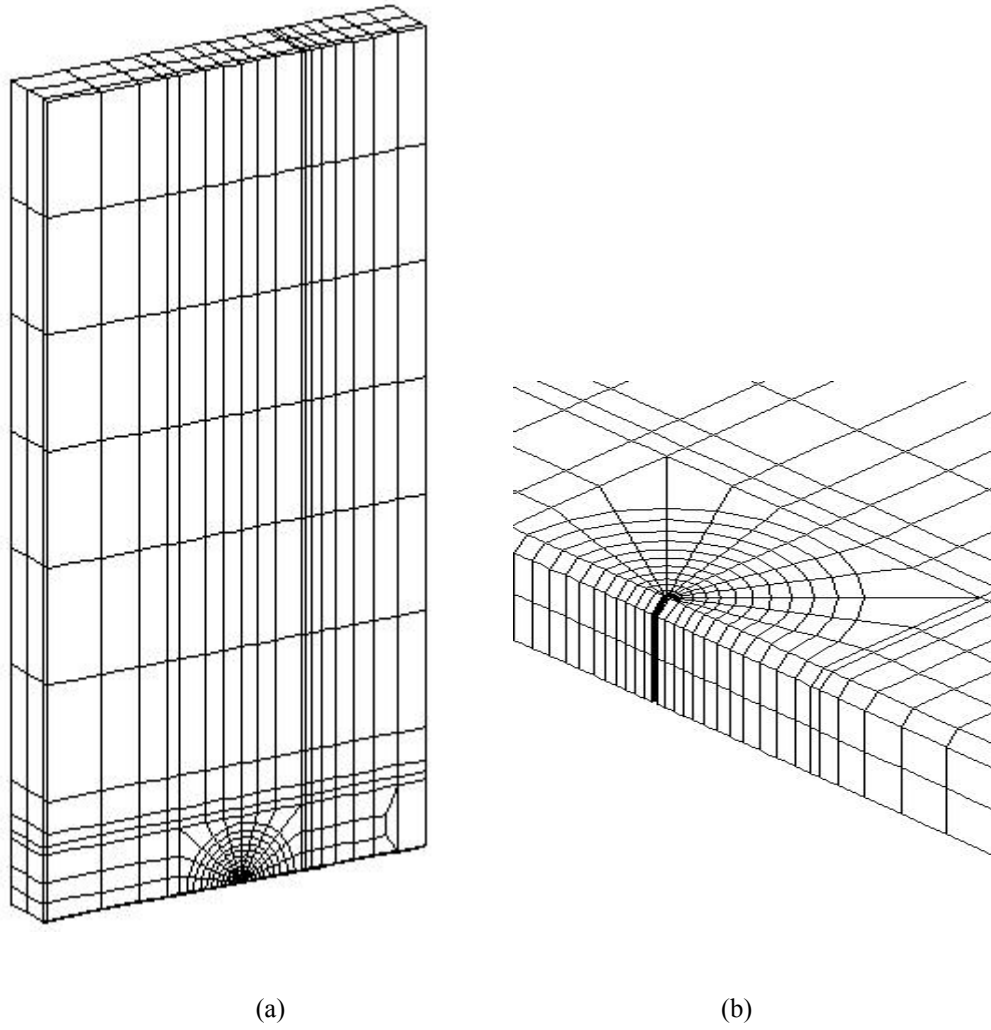


Fig.5.1 Finite element mesh employed to model TPB specimen (a) overall (b) near the crack tip

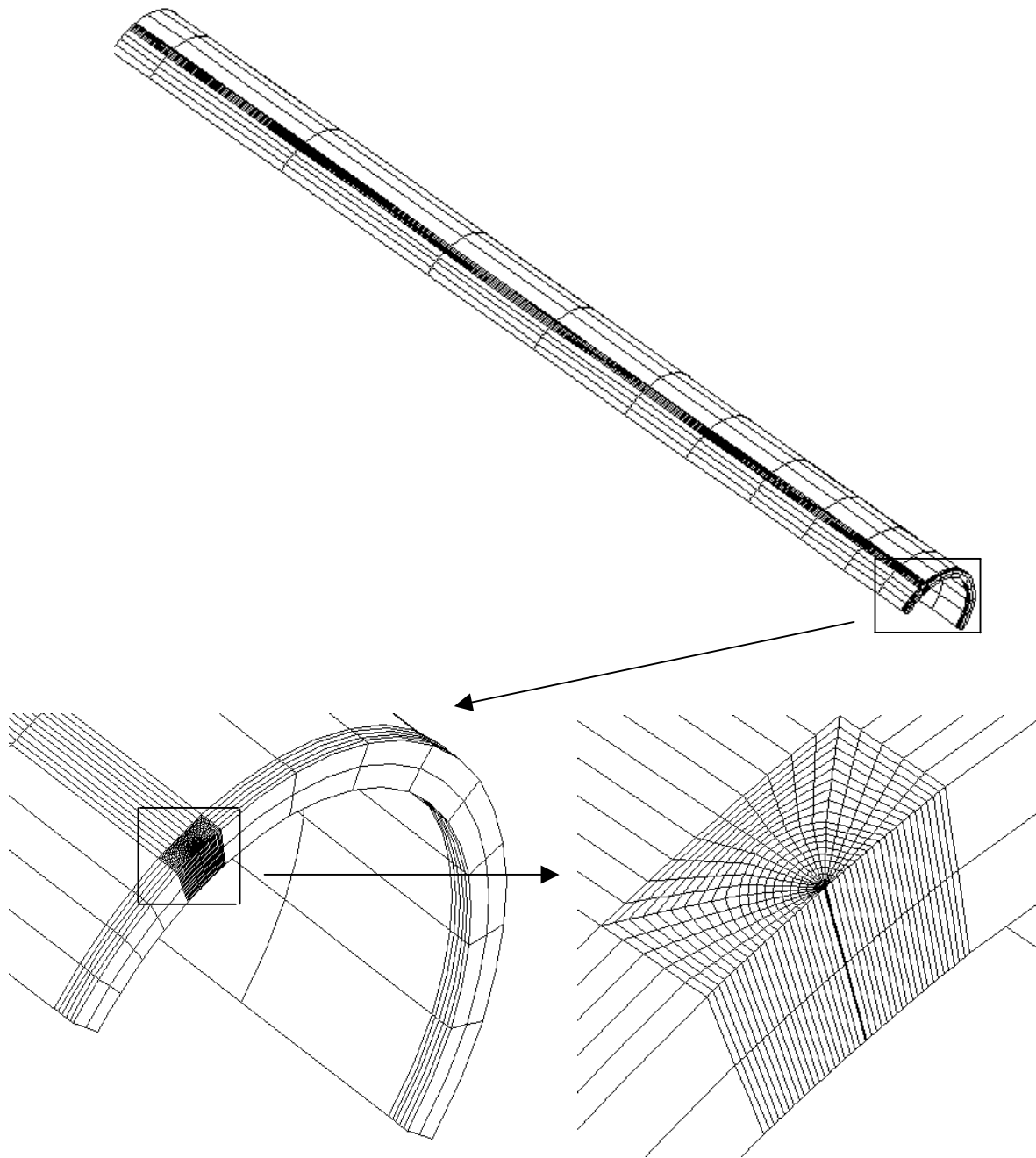


Fig.5.2 Finite element mesh employed to model pipe with throughwall circumferential crack

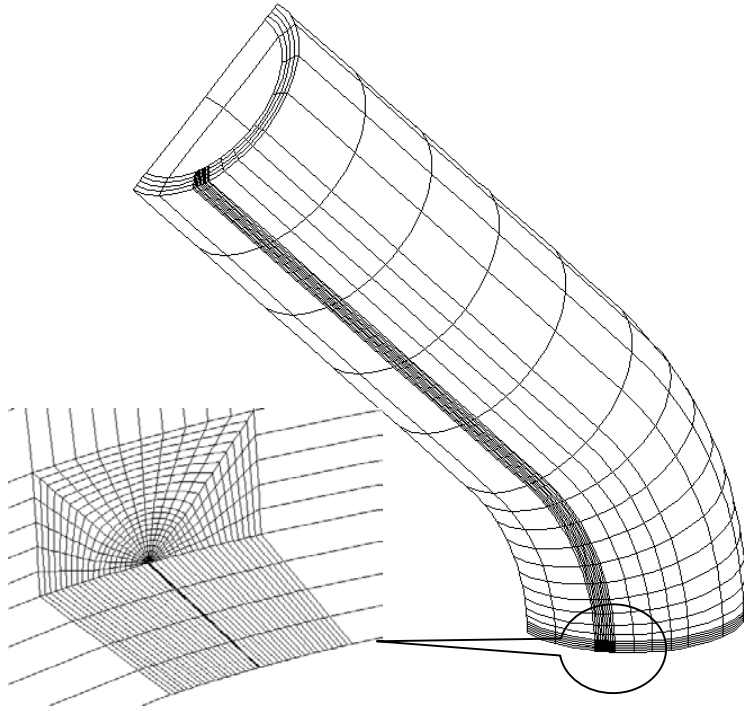


Fig.5.3 Typical finite element mesh used to analyze elbow with throughwall circumferential crack

5.1.2 Material parameters

The tensile specimens have been machined from 200 mm NB pipes made of SA333Gr6 and have been tested as described in section 4.1.3. The uni-axial true-stress-strain curve is modeled in multi-linear fashion as indicated in Fig. 5.4. The data is given up to the ultimate tensile stress level (20% of strain). After this specified point the response assumes perfectly plastic. The material with the extended yield plateau, followed by strain hardening region produced

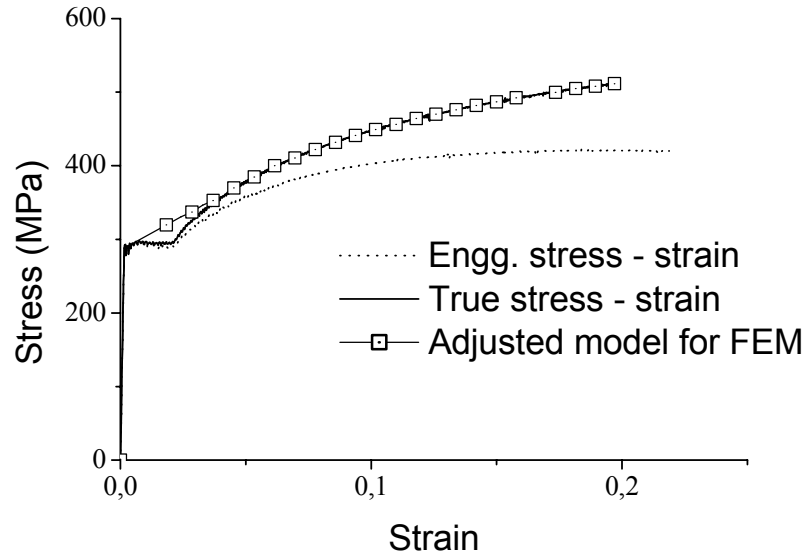


Fig.5.4 Stress-strain input to finite element analysis

numerical instability. The yield plateau is replaced as shown in Fig. 5.4 to eliminate the instability and to allow the use of larger load steps. Solution computed using much smaller load steps and the actual stress-strain curve showed that the results are insensitive to the modification of the stress-strain curve [82].

5.1.3 Finite Element Analysis Results

5.1.3.1 Load Deflection Curve

The comparison of numerical and experimental load-deflection characteristics of the typical TPB specimen, full-scale pipe and elbow is shown in Figs. 5.5 – 5.7. The numerical and experimental results agreed well. The good matching between experimental and numerical results ensures the validation of the numerical model as well as experimental results. As expected, the numerical model shows higher stiffness just before the maximum load occurs. This is because of the assumption of the stationary crack in the model without considering the crack growth.

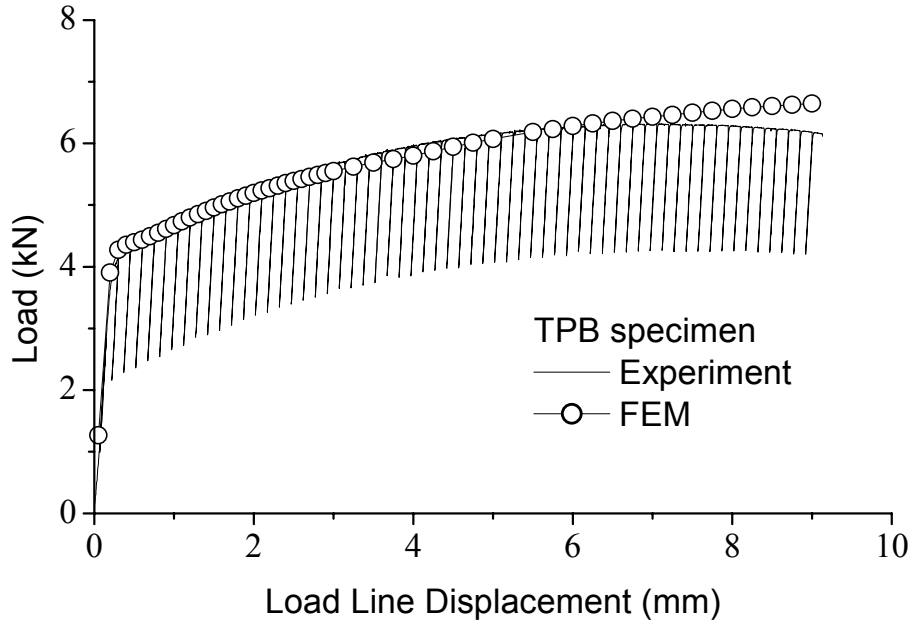


Fig. 5.5 Comparison of load deflection curve for TPB specimen

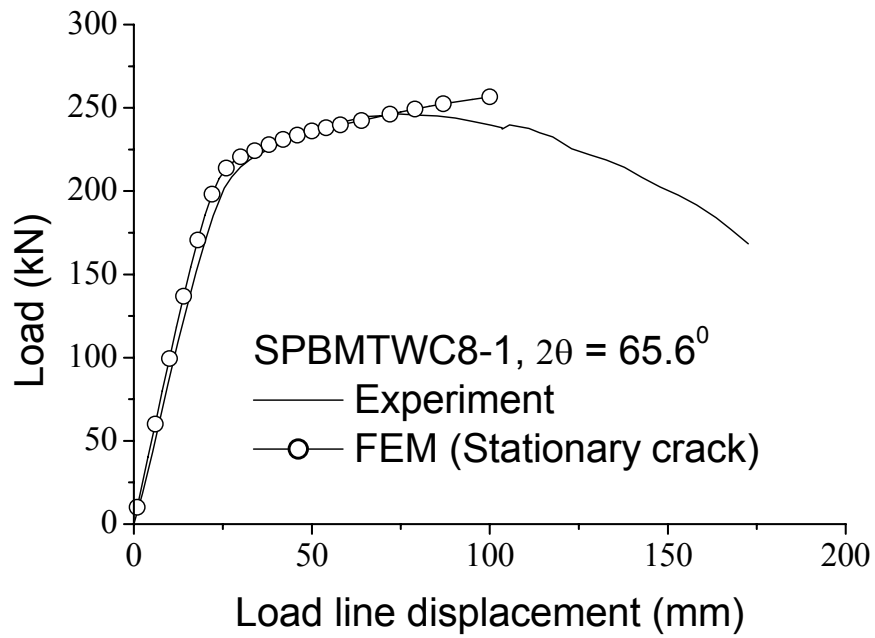


Fig. 5.6 Comparison of load deflection curve for one typical tested pipe

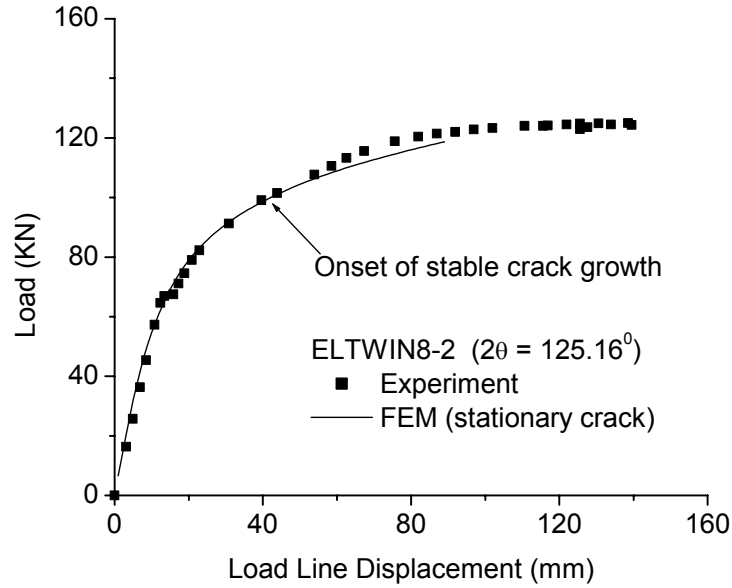


Fig. 5.7 Comparison of load deflection curve for one typical tested elbow

5.1.3.2 Evaluation of stress triaxiality ahead of crack tip and transferability of J-R curve

As mentioned in section 2.3.3, the stress triaxiality ahead of crack tip are compared for the specimen and the cracked component beyond crack initiation. If the triaxial conditions are found to be similar then it is believed that the J-R curves are transferable. Fig.5.8 compares the stress triaxiality quantified by 'q'

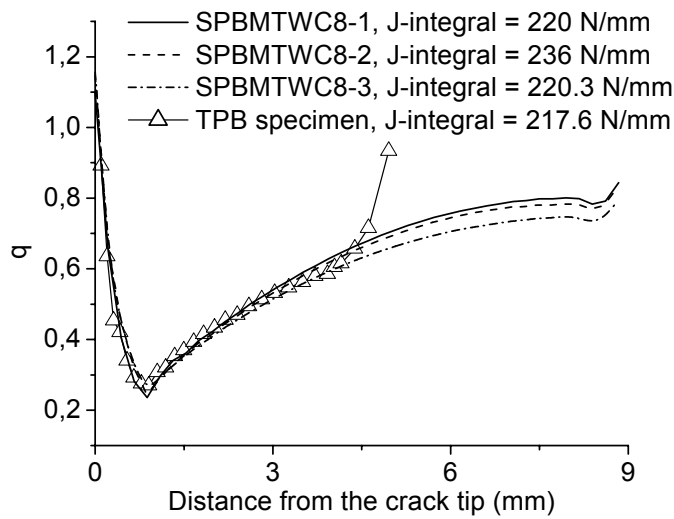


Fig.5.8 Comparison of stress triaxiality between TPB specimen and 200 mm NB pipes

parameter as defined in eqn.2.28 for TPB specimen and 200 mm NB pipes with various sizes of throughwall circumferential cracks. The comparison is made at the J-integral value of 220 N/mm which is the initiation toughness (J_i) based on SZW for the pipe material. It can be observed that the stress triaxial conditions for the specimen and the cracked pipes are similar. Hence, it can be inferred that TPB specimen J-R curve can be transferred to the cracked components. It is indeed shown later in section 5.4 that the TPB specimen J-R curve falls within the band of cracked pipe J-R curves (Fig.5.12). This proves the role of stress triaxiality in transferring the specimen characteristics to the component.

5.2 COMPARISON OF CRACK INITIATION LOAD

The initiation toughness (J_i), obtained from the stretched zone width (SZW) can be used to determine the onset of ductile crack growth (see section 2.3.1). Investigations [47,48,83] have shown that (J_i) is more or less independent of stress triaxiality and can be treated as a material property. Hence, it is possible to predict the crack initiation loads by comparing (J_i) determined from the laboratory specimen with the calculated crack driving force (applied J-integral) of the cracked component. The comparison here is shown for 200 mm NB pipes and elbows. The (J_i) for 200 mm NB pipe and elbow materials (SA333 Gr 6 carbon steel) is evaluated as 220 kJ/m². Figure 5.9 shows the variation of crack driving force (J-integral), obtained from finite element analysis, with the load for 200 mm NB pipes and elbows. It should be noted that the J-integral varies across the thickness. The J-integral is maximum at the mid-thickness and low at the outside/inside surfaces. The average J-integral is calculated using the following equation.

$$J_{ave} = (J_{in} + 4J_{mid} + J_{out})/6.0 \quad (5.1)$$

This average J-Integral is used to predict crack initiation load. In addition to finite element calculation, applied J-integral for throughwall cracked pipe has also

been determined using various analytical J-estimations schemes, for example, GE/EPRI [24,84], LBB.BCL1 and LBB.BCL2 [85] method. Table 5.1 summarizes the experimental and numerical/analytical results. The crack initiation loads predicted by finite element method based on the (J_i) show very good agreement with the experimental results.

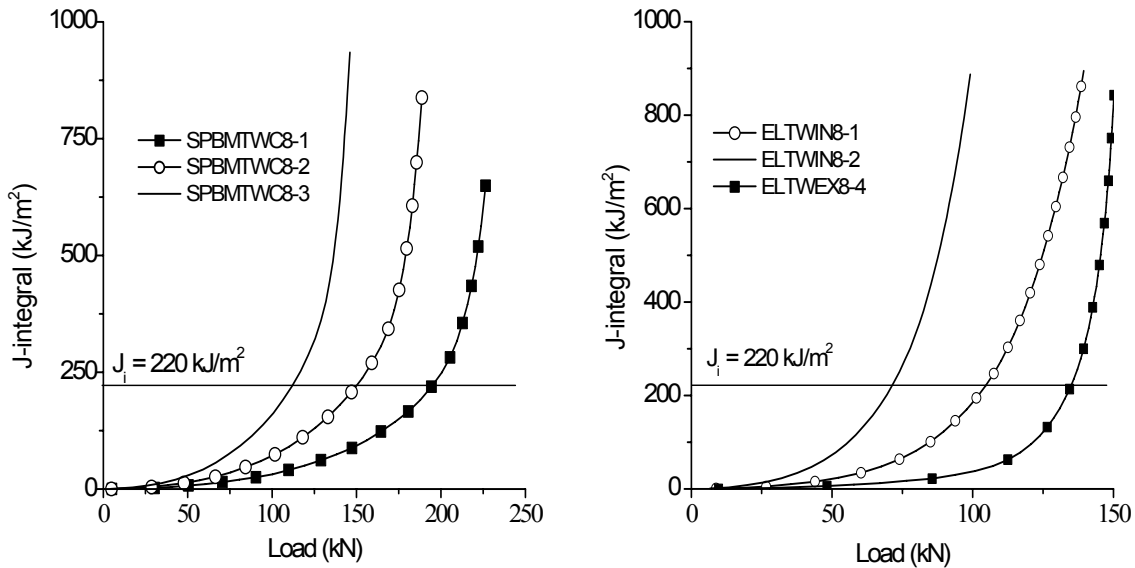


Fig.5.9 Variation of finite element J-integral with load for 200 mm NB pipes and elbows

Table 5.1 Comparison of crack initiation load

Component	Test no.	Crack initiation load (kN)				
		Expt.	Predicted			
			FEM	GE/EPRI	LBB.BCL1	LBB.BCL2
Throughwall Cracked Pipe	SPBMTWC8-1	194	195	142	175	170
	SPBMTWC8-2	148	150	112	131	124
	SPBMTWC8-3	116	114	85	97	96
Throughwall Cracked elbow	ELTWIN8-1	112	105	-	-	-
	ELTWIN8-2	92	71	-	-	-
	ELTWEX8-4	125	135	-	-	-

5.3 J-INTEGRAL – TEARING MODULUS (J-T) ANALYSES OF PIPE FRACTURE EXPERIMENTAL DATA

Crack initiation in ductile material is generally followed by stable crack growth, unless very high stress triaxiality exists in the vicinity of crack. With increasing load, stable crack growth, at one stage, leads to unstable ductile tearing. It has been shown in section 2.3.1 that the unstable ductile tearing load for a given cracked structure can be predicted using the J-integral-Tearing modulus (J-T) approach. In this section, effort has been made to predict the unstable ductile tearing load of 200 mm NB throughwall circumferentially cracked pipes based on the J-T approach. In this analytical prediction, the material J-T curve has been generated from the TPB specimen which were machined from the 200 mm NB pipes and tested to generate the J-R curve (see section 4.1). Power law fit of the specimen J-R curve has been done to get the derivative, dJ_{mat}/da , and hence the material tearing modulus using eqn.(2.18). The J-T curve has been extended beyond test range linearly as per the procedure recommended in [2]. The applied J-integrals for these cracked pipes have been evaluated by three analytical J-estimation schemes, namely, GE/EPRI [24,85], LBB.BCL1 and LBB.BCL2 [86] method. Figure 5.10 shows typical J-T curves to determine the unstable ductile load for pipe no. SPBMTWC8-1 with a throughwall circumferential crack angle (2θ) equal to 65.6° (see Table 4.3). Figure 5.11 shows the same on J - a space through tangency of J - a applied and J - R curves (see section 2.3.1.2). Table 5.2 shows the comparison of experimentally observed maximum load with the instability loads predicted by the J-T approach. A good matching may be observed. Among the three analytical J-estimation schemes, GE/EPRI method predictions are closest to the test data.

Table 5.2 Comparison of maximum experimental load with the unstable ductile tearing loads

Test no.	Expt. maxm. moment (kN-m)	Predicted unstable ductile tearing moment* using J-T approach (kN-m)		
		GE/EPRI	LBB.BCL1	LBB.BCL2
SP BM TWC8-1	154	158	196	189
SP BM TWC8-2	124	127	149	141
SP BM TWC8-3	89	97	109	107
SP BM TWC8-4	60	70	75	72

* In 4-point bending load, moment is converted into load using eqn.(3.117) and Table 4.3

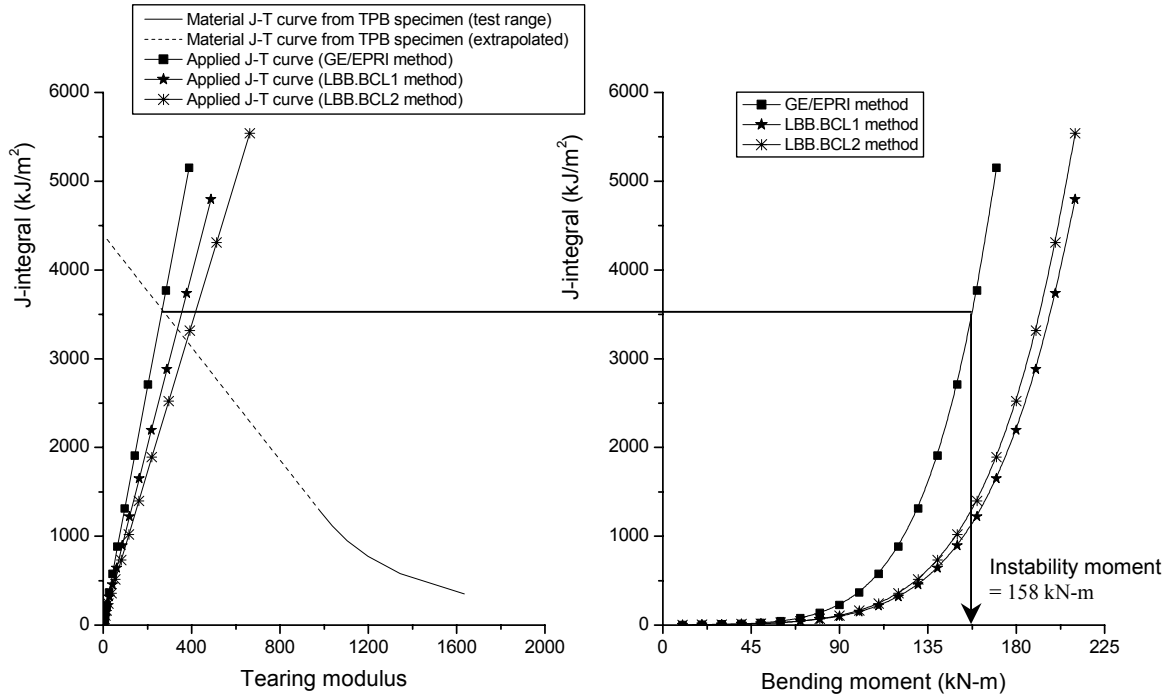


Fig.5.10 Illustration of J-T analysis for one typical 200 mm NB pipe SPBMTWC8-1

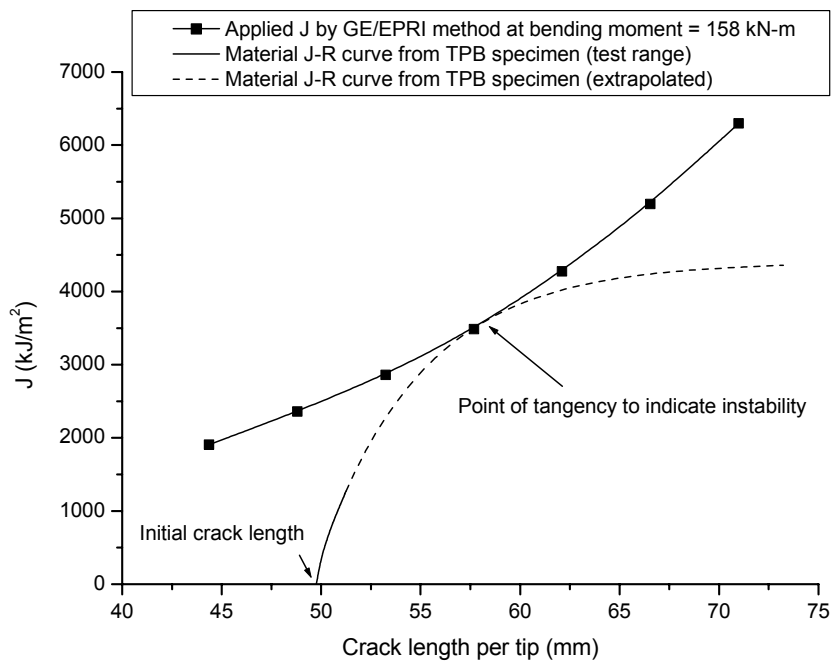


Fig.5.11 Illustration of tangency condition on J-a space to determine instability load for one typical 200 mm NB pipe SPBMTWC8-1

5.4 LIMIT LOAD ANALYSIS

5.4.1 Carbon Steel Pipes

In this section, limit load analyses of fracture test results of through wall circumferentially cracked pipes are performed. The limit loads are calculated using equations (2.19 – 2.24) as described in section 2.3.2. Equation (2.24) to calculate the heat specific 'Z factor' is not truly valid here as the condition of $\sigma_y < 276$ MPa is violated. The pipe materials have yield stress of 288 and 312 MPa for 200 and 400 mm NB pipes respectively (see Table 4.2). However, eqn.(2.24) is still used to calculate the heat specific 'Z factor'. Table 5.3 shows the comparison of the experimentally observed maximum moment with the predictions of critical moments as per 'G factor' approach (eqn.2.21), 'Z factor' approach (eqn.2.24) and also the limit moments (eqn.2.19) and modified limit moments (eqn.2.20). All the moments are normalized with $4R^2t\sigma_f$, where σ_f is chosen as average of yield and ultimate strength. It also shows the percentage difference between the predicted and experimental values where difference is defined as,

$$\% \text{ difference} = (\text{Experiment} - \text{Predicted}) \times 100 / \text{Experiment} \quad (5.2)$$

Therefore, positive difference indicates that the prediction is conservative. Figure 5.12 shows the comparison of experimental maximum moments with the predictions as per eqn. (2.19) and (2.20). It is seen from Table 5.3 that the critical moments by 'G factor' (see eqn.(2.21)) approach match very closely with the experimental data. However, in one case out of seven, the prediction is slightly non-conservative. It is seen from Table 5.3 and Fig.5.12 that, for 200 mm NB pipe, the limit moments and experimentally observed maximum moments are very close whereas in case of 400 mm NB pipe, maximum moments are below the limit moments. This indicates that 200 mm NB pipes have failed in plastic collapse whereas 400 mm NB pipes have failed due to ductile tearing prior to the attainment of limit moment. This is also corroborated by the load *versus* crack growth curves in Fig.4.8 where it is seen that before attainment of maximum

moment, crack growth in case of 200 mm NB pipes is very small compared to 400 mm NB pipes. Figure 5.12 also shows that all the experimental points are conservative with respect to the predictions as per eqn.(2.20).

Table 5.3 Comparison of maximum experimental moments with theoretical predictions for throughwall circumferentially cracked pipes under four point bending load (the numbers in bracket indicate percentage difference as per eqn.(5.2))

Test no.	Expt.	Predicted critical moments			
		$\frac{(M_{\max})_{\text{expt.}}}{4R^2t\sigma_f}$	$\frac{(M_L)_{\text{eqn.}(2.19)}}{4R^2t\sigma_f}$	$\frac{(M_c)_{\text{eqn.}(2.20)}}{4R^2t\sigma_f}$	$\frac{(M_c)_{\text{eqn.}(2.21)}}{4R^2t\sigma_f}$
SPBMTWC8-1	0.6965	0.688 (+1.22)	0.585 (+16.0)	0.681 (+2.22)	0.653 (+6.24)
SPBMTWC8-2	0.559	0.552 (+1.25)	0.469 (+16.1)	0.524 (+6.26)	0.524 (+6.26)
SPBMTWC8-3	0.3977	0.405 (-1.83)	0.344 (+13.5)	0.373 (+6.21)	0.385 (+3.19)
SPBMTWC8-4	0.2702	0.284 (-5.11)	0.241 (+10.8)	0.255 (+5.62)	0.270 (+0.07)
SPBMTWC16-1	0.4626	0.542 (-17.2)	0.461 (+0.34)	0.491 (-6.13)	0.516 (-11.5)
SPBMTWC16-2	0.3622	0.406 (-12.1)	0.345 (+4.75)	0.354 (+2.26)	0.387 (-6.85)
SPBMTWC16-3	0.2468	0.281 (-14.0)	0.239 (+3.04)	0.238 (+3.44)	0.268 (-8.72)

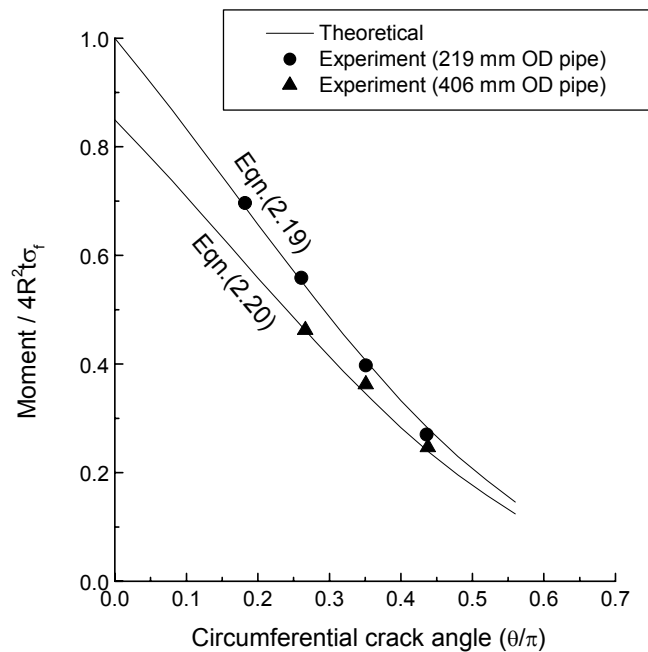


Fig.5.12 Comparison of theoretical limit moment with experimental maximum moment

5.4.2 Carbon Steel Elbows

The experimentally observed maximum load has been compared with the limit loads as predicted by Zahoor [45] through eqns.(2.25 – 2.27). To get the corresponding load, moment is divided by the perpendicular distance between the load line and middle of elbow axis which is 825.72 mm in the present case. Although this distance changes during loading of the elbow, the change has been found to be negligible compared to the initial distance and hence has not been accounted in the calculation. In terms of applicability of eqn.(2.25) and (2.27), although the limits of elbow factor ($h = 4R_b t / D_m^2 \leq 0.5$) and crack length ($a/D_m < 0.8$ or 0.9) are satisfied, the condition of $D_m/t \geq 15$ is violated here. The flow stress (354 MPa) of the material is defined as the average of yield and ultimate strength (see Table 4.2). Table 5.4 shows the comparison of theoretical and experimental load values. The difference is 11.7%, 10.4%, 1.0% and 15.1% of experimental load for tests ELTWIN8-1, ELTWIN8-2, ELTWIN8-4 and ELTWCR8-6 respectively. It may be seen for throughwall circumferentially cracked elbow that the difference is more for opening bending moment compared to the closing mode. It may be noted that eqn.(2.25) does not differentiate between opening and closing mode of bending moment whereas the behavior of elbow under these two bending modes has been reported to be different by many researchers [38-40,66]. It is well-known that an elbow subjected to opening bending moment can sustain higher load compared to when subjected to closing moment. The present experimental results also show this trend. Although, it is not mentioned, according to these results, eqn.(2.25) seems to be for closing moment evaluated, which is conservative and therefore, the predicted and experimental loads for this mode are very close.

Table 5.4 Comparison of predicted and experimental loads for cracked elbows

Test no.	D_m/t	$h = R_b t / R^2$	θ	Bending mode	Predicted limit load (kN)	Experimental maxm. load (kN)
ELTWIN8-1	10.45	0.3948	47.48°	Opening	136.12	154.1
ELTWIN8-2	10.65	0.3881	62.58°	Opening	111.97	125.0
ELTWEX8-4	10.33	0.4014	49.12°	Closing	137.22	135.8
ELTWCR8-6	10.53	0.3930	a=54.6 mm	Closing	163.41	141.9

'a' is the semi axial crack length

5.5 DETERMINATION OF COMPONENT J-R CURVE

5.5.1 Straight Pipe with throughwall circumferential crack

From the experimental load *versus* load-point-deflection and load *versus* crack growth curves, pipe J-R curves have been generated using the expressions given by Zahoor and Kanninen [24,54]. The J-integral of throughwall circumferentially cracked straight pipe under bending can be expressed through eqns. (2.31-2.37) with ' η_{pl} ' and ' γ ' functions as defined in eqn. (2.42-2.43).

Figures 5.13 shows the pipe J-R curves for 200 mm NB pipes. It may be seen from Fig.5.13 that the J-R curves of throughwall circumferentially 200 mm NB pipes and TPB specimen, machined from the same tested pipes, are almost identical. It has been shown earlier in section 5.1.3 (see also Fig.5.8) that this is due to identical stress triaxiality in the vicinity of crack tip. This highlights the role of stress triaxiality in transferring the specimen J-R curve to component.

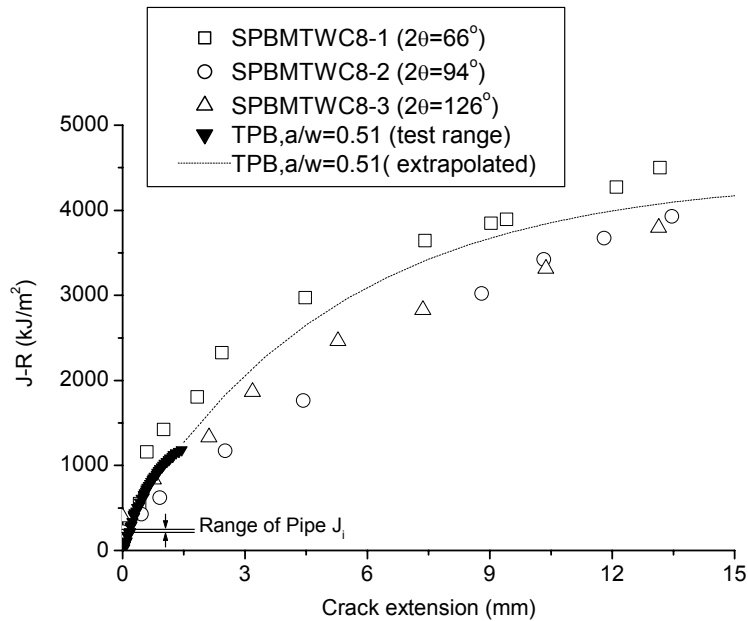


Fig.5.13 J-R curves generated from 200 mm NB pipes and TPB specimen

5.5.2 Elbow with throughwall circumferential crack

From the load *versus* load-line-displacement and load *versus* crack growth curves, component J-R curves have been generated using eqns.(2.31-2.37) where the ' η_{pl} ' and ' γ ' functions as derived in eqns.(3.81) and (3.83) are used. Plane stress conditions are assumed to get the elastic component of the J-integral from the Stress Intensity Factor (SIF) through eqn.(2.32). The SIF equation for throughwall circumferentially cracked elbow under in-plane bending moment, proposed by Chattopadhyay et al [57] , is used here and shown below :

$$K = A_e \sigma \sqrt{\pi a} \quad (5.3)$$

$$\sigma = \frac{M}{\pi R^2 t} \quad (5.4)$$

$$A_e = [(C_1 + C_2.h^{p_1})+(C_3 + C_4.h^{p_2}).(\theta/\pi)^{p_3}] + [(C_5 + C_6.h^{p_4})+(C_7 + C_8^{p_5}).(\theta/\pi)^{p_6}].(t/R)^{p_7} \quad (5.5)$$

$$C_1 = -3.4628, C_2 = 4.446, C_3 = -52.429, C_4 = 52.445, C_5 = -2.2524, C_6 = 1.1102, C_7 = 0.8634, C_8 = 1.7283, p_1 = 0.1366, p_2 = -0.1848, p_3 = 2.6137, p_4 = 0.1216, p_5 = 0.0695, p_6 = 0.4587, p_7 = -0.5119$$

Although the equation of ' A_e ' by Chattopadhyay et al [57] is given for an extrados crack under in-plane closing moment, it is used here for both intrados and extrados cracks under in-plane opening and closing moment. This is because the SIF depends mainly on the elastic behavior of the structure and the elastic response of elbows under closing and opening moments is the same [86]. It may be mentioned here that in the evaluation of plastic strain energy, one should ideally subtract the displacement of the un-cracked elbow from the total displacement of the cracked elbow to get the displacement due to crack only. However, it has been assumed in the present analyses that the contribution of the un-cracked elbow displacements in the plastic strain energy for these deeply cracked elbows is negligible. Figure 5.14 shows the component J-R curve for all the elbows. It may be seen that 'ELTWIN8-2' ($\theta = 62.58^\circ$) has higher crack resistance than 'ELTWIN8-1' ($\theta = 47.48^\circ$) although the plastic strain energy is

more for the latter. This is because the ' η_{pl} ' of 'ELTWIN8-2' is 0.231×10^{-3} (at $\theta = 62.58^\circ$) compared to $\eta_{pl} = 0.126 \times 10^{-3}$ (at $\theta = 47.48^\circ$) of 'ELTWIN8-1'.

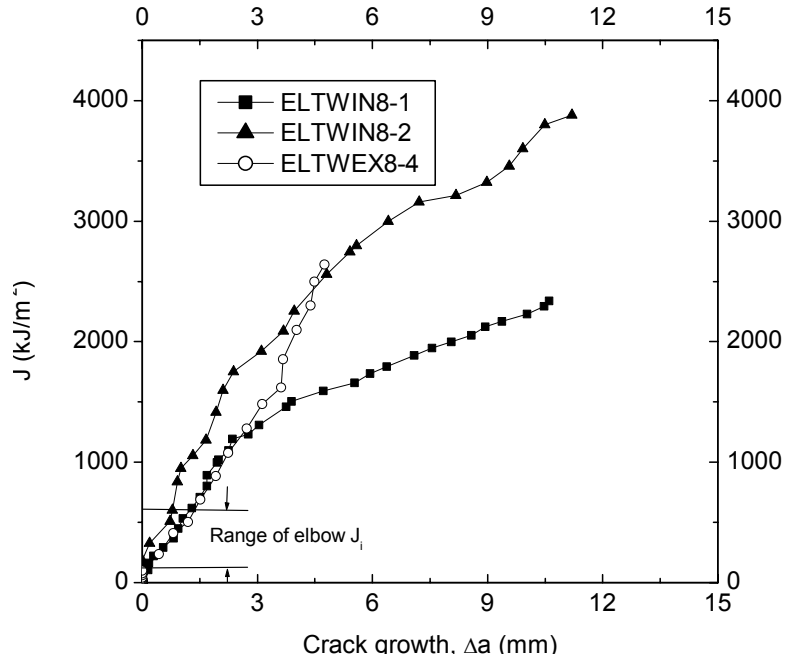


Fig.5.14 J-R curves from throughwall circumferentially cracked elbows

**6. INTEGRITY ASSESSMENT OF PIPES AND ELBOWS
: RECOMMENDED METHODOLOGY**

Based on the investigations conducted in this study, the following methodology for integrity assessment of pipes and elbows is recommended.

1. If the pipe/elbow is defect-free, use Eqns.2.1-2.3 to predict the limit load of pipe and Eqns.3.1-3.2 to predict the limit load of elbow. Eqns.3.1-3.2 have been newly proposed in the present thesis. The applied load must be lower than the limit load with a user-defined factor of safety.
2. If there is a through wall circumferential crack in the pipes/elbows (which has the maximum deleterious effect), the preliminary estimate of load carrying capacity may be made based on limit load. The limit load of a through wall circumferentially cracked pipe under bending moment should be determined using the Eq.2.19 and for elbow, Eq.2.25 should be used. In both the equations, flows stress (σ_f) = yield stress (σ_y) should be used to be on the conservative side. Again the applied load must be lower than the limit load with a user-defined factor of safety.
3. If sufficient safety margins are obtained with limit load approach, there is no need to use the more involved fracture mechanics based approach, especially for lower diameter pipes.
4. However, with limit load approach, if sufficient safety margins are not available or the design has to made more optimum with reduced wall thickness or higher allowable load, the fracture mechanics evaluation methods based on J-integral – Tearing modulus (J-T) approach as described in section 2.3.1 are to be invoked. This is mainly important for large diameter (say, > 600 mm) piping components.
5. In J –T approach, one requires the material fracture resistance data in the form of J-R curve as basic unit. J-R curve is normally evaluated on small laboratory specimens e.g. Compact Tension (CT), Three Point Bend (TPB)

etc. These specimens are preferably to be machined from the same piping components which are being assessed. Also one has to choose the specimen type in such a way that the stress triaxiality ahead of crack tip (quantified by the 'q' parameter as detailed in Eqs.2.28 –2.30) of the specimen and the actual full size component match. The stress triaxiality (or the constraint) ahead of crack tips are to be evaluated by finite element method.

6. If the stress triaxiality of specimen and components do not match, one has to vary the specimen geometry and loading condition to attain various stress triaxialities. The tensile loading and shallow cracked specimen, in general, provide lower constraint whereas the bending load and deeply cracked specimen, in general, provide higher constraint. In the extreme case, the J-R curve evaluated from the test of at least one full-scale piping component should be used.
7. To construct the J-R curve, the J-integral is evaluated from test data using the Eqs.2.31 –2.37. For this evaluation, one requires the ' η_{pl} ' and ' γ ' functions for a particular specimen geometry and loading condition. For conventional deeply cracked CT and TPBB specimens and for through wall circumferentially cracked pipe under bending loads, these functions are already available (see section 2.4 for detail). However, for other geometry and loading conditions, one has to evaluate the ' η_{pl} ' and ' γ ' functions from the limit load based general expressions Eq.3.20 – 3.21 which are newly developed in this thesis.
8. While measuring the crack growth by compliance technique during J-R test, one should consider whether change in basic geometry during deformation alters the compliance correlation in a significant manner or not. It has been brought out in Chapter 3.3 that for some geometry (e.g pipe with through wall

circumferential crack under bending), the deformation of basic geometry causes a significant change in compliance correlation which must be accounted for. It has also been shown here that the deformation of TPB specimen does not cause much difference of its compliance and hence existing ASTM [42] formula, which does not account for the deformation on the compliance, can be used without any error.

9. After the evaluation of suitable J-R curve from a specimen which has same stress triaxiality as that of the actual component, one can transfer the specimen J-R curve to the component level for integrity assessment by J-T approach. This has been brought out in chapter 5.

10. Finally, one can evaluate the critical load at the onset of unstable ductile tearing for the actual piping component using the J-T approach as detailed in section 2.3.1 of this thesis. One has to compare between unstable ductile tearing load and limit load of the structure. The lower of the two should be considered as the governing critical load for integrity assessment of the components. One must ensure that the applied load on the component is lower than this critical load with sufficient safety margins.

7. CONCLUSIONS

Conclusions

Integrity assessment of pipes and elbows is very important for safety and reliable operation of any industrial plant. This is specially important for nuclear power plant because, leak-before-break (LBB) concept is used to design the primary heat transport system piping. The LBB approach essentially consists of detailed integrity assessment of piping with postulated cracks. While a considerable work has already been done in the development of integrity assessment procedure of cracked/un-cracked piping components over the last twenty years, some issues are still unresolved or not fully resolved, especially regarding elbows. Effort has been made in this work to address these issues and in some cases, new formulations have been proposed. The present work can be broadly categorized as theoretical and experimental study.

In the theoretical work, new closed-form collapse moment equations of un-cracked elbows subjected to combined internal pressure and bending moment have been proposed. The predictions of these new equations are consistent with the test data.

Secondly, new limit load based basic general expression of ' η_{pl} ' and ' γ ' have been proposed to evaluate J-R curve from test results of load-deflection and load-crack growth data. The implication of these new basic equations is that for any new specimen geometry and loading condition for which limit load formula is available, specimen/component J-R curve can be obtained from test data. On this basis, new ' η_{pl} ' and ' γ ' functions for piping components with various crack configurations under different loading conditions have been derived.

Then, the effect of deformation on the unloading compliance correlation has been investigated for accurate measurement crack growth during J-R tests. It has been shown that deformation of pipe significantly changes the compliance correlation and must be accounted for. However, it has also been shown that this effect is not so significant for the commonly used ASTM three point bend (TPB) specimen.

In the experimental work, fracture tests have been carried out on full size (200 – 400 mm diameter) pipes and elbows with through wall circumferential cracks. Load, load-line-displacement and crack growth have been measured during these experiments. From these data, component J-R curves have been evaluated using the newly developed ' η_{pl} ' and ' γ ' functions.

Tensile tests have been carried out on small tensile samples machined from these tested pipes to evaluate the pipe/elbow material tensile properties. Small TPB specimens have also been machined from these tested pipes to conduct fracture tests and evaluate the small specimen J-R curve.

With elastic-plastic finite element analyses, the stress triaxiality (quantified by ' q ' parameter) ahead of crack tip has been evaluated on these tested specimens and components. It has been shown that if stress triaxialities of specimen and component match within a certain distance ahead of crack tip, small laboratory specimen J-R curve can be transferred to full size real components.

Based on these studies, the improved integrity assessment procedures of pipes and elbows have been proposed, which may be a reliable basis for leak-before-break (LBB) analysis.

REFERENCES

1. Generic Letter 84-04. Safety evaluation of Westinghouse topical reports dealing with elimination of postulated pipe breaks in PWR primary main loops, US Nuclear Regulatory Commission, Washington DC, 1st February, 1984
2. Report of the United States Nuclear Regulatory Commission Piping Review Committee, Evaluation of Potential for Pipe Breaks, NUREG/CR-1061, Vol.3, 1984
3. Standard Review Plan; Public Comment Solicited. Federal Register, Vol.5.2, No.167, published by the Office of the Federal Register, Washington DC, 28th August, 1987
4. Wichman,K. and Lee,S., "Development of USNRC Standard Review Plan 3.6.3 for Leak-Before-Break Applications to Nuclear Power Plants, *International Journal of Pressure Vessel and Piping*, **43**, 1990, pp 57-65
5. Nathwani,J.S. and Stebbing,J.D., "Ontario Hydro's Leak-Before-Break Approach to Darlington NGS Heat Transport System Piping", *International Journal of Pressure Vessel and Piping*, **43**, 1990, pp 113-127
6. Boiler and Pressure Vessel Code, Sec.III, American Society of Mechanical Engineers, 2000
7. International Atomic Energy Agency, Applicability of the Leak-Before-Break Concept, IAEA-TECDOC-710, Vienna, 1993
8. International Atomic Energy Agency, Guidance for the Application of the Leak-Before-Break Concept, IAEA-TECDOC-774, Vienna, 1994
9. Faidy,C., Bhandari,S. and Jamet,P., "Leak-Before-Break in French Nuclear Power Plants", *International Journal of Pressure Vessel and Piping*, **43**, 1990, pp 151-164
10. RKS Guidelines for Pressurized Water Reactors, 2nd Edition, 24th January 1979, incl. Appendices to Section 4.2; 3rd Edn, 14th October 1981, later changes of RKS Guidelines Sections 21.1. and 21.2, 1983, Gesellschaft für Reaktorsicherheit mbH, Köln
11. Kussmaul,K., German basic safety concept rules out possibility of catastrophic failure, *Nuclear Eng. Int.*, 1984, pp 41-46

12. Bartholome, G., Steinbuch, R. and Wellein, R., "Preclusion of double ended circumferential rupture of the main coolant line", *Nuclear Engineering and Design*, **72**, 1982, pp 97-105
13. Roos, E., Herter, K.H., Julish, P. and Bartholome, G., "Assessment of large scale pipe tests by fracture mechanics approximation procedures with regard to leak-before-break", *Nuclear Engineering and Design*, **112**, 1989, pp 183-195
14. Asada, Y., Takumi, K., Hata, H. and Yamamoto, Y., "Development of criteria for protection against pipe breaks in LWR plants", *International Journal of Pressure Vessel and Piping*, **43**, 1990, pp 95-112
15. Asada, Y., Takumi, K., Gotoh, N., Umemoto, T. and Kashima, K., "Leak-Before-Break verification test and evaluations of crack growth and fracture criterion for carbon steel piping", *International Journal of Pressure Vessel and Piping*, **43**, 1990, pp 379-398
16. Isozaki, T., Shibata, K., Shinokawa, H. and Miyazono, S., "Measurement of leak rates through fatigue cracks in pipes under four point bending and BWR conditions", *International Journal of Pressure Vessel and Piping*, **43**, 1990, pp 399-412
17. Sharples, J.K. and Clayton, A.M., "A leak-before-break assessment method for pressure vessels and some unresolved issues", *International Journal of Pressure Vessel and Piping*, **43**, 1990, pp 317-328
18. Milne, I., Ainsworth, R.A., Dowling, A.R. and Steward, A.T., "Assessment of the integrity of structures containing defects", CEBG Report R/H/R6 – Rev.3, 1986, *International Journal of Pressure Vessel and Piping*, **32**, 1988, pp 3-104
19. Rodriguez, M. and Esteban, A., "Application of leak-before-break to primary loop piping to eliminate pipe whip restraints in a Spanish nuclear power plant", *International Journal of Pressure Vessel and Piping*, **43**, 1990, pp 85-94
20. Czechoslovak Atomic Energy Commission, "Leak Before Break Procedures", ČSKAE Requirements for Safety Case Reports and their Appendices, Prague, 1991
21. Chattopadhyay, J., Dutta, B.K. & Kushwaha, H.S., "Application of leak-before-break concept in the design of high temperature and high pressure primary heat transport piping", Bhabha Atomic Research Centre (India), BARC external report, BARC/1992/E/033, 1992

22. Chattopadhyay, J., Dutta, B.K. & Kushwaha, H.S., "Leak-Before-Break qualification of primary heat transport piping of 500 MWe Tarapur Atomic Power Plant", *International Journal of Pressure Vessel and Piping*, **76**, 1999, pp 221 – 243
23. Kanninen, M.F., Zahoor, A., Wilkowski, G.M., Abousayed, I., Marschall, C., Broek, D., Sampath, S., Rhee, H. and Ahmad, J., "Instability Predictions for Circumferentially Cracked Type 304 Stainless Steel Pipes Under Dynamic Loading", EPRI-NP-2347, Vol. 1 & 2, Electric Power Research Institute, Palo Alto, CA, 1982
24. Zahoor, A., "Ductile Fracture Handbook", Vol.1, EPRI-NP-6301-D, N14-1, Research Project 1757-69, Electric Power Research Institute, 1989
25. Electric Power Research Institute, *Evaluation of Flaws in Ferritic Piping*, EPRI-NP-6045, 1988
26. Miller, A.G., "Review of Limit Loads of Structures Containing Defects", *Int. J. of Pres. Ves. and Piping*, **32**, pp 197 - 327, 1988
27. Kanninen, M.F., Broek, D., Marschall, C.W., Rybicki, E.F., Sampath, S.G., Simonen, F.A. and Wilkowski, G.M., EPRI-NP-192, *Mechanical Fracture Predictions for Sensitized Stainless Steel Piping with Circumferential Cracks*, Electric Power Research Institute, USA, 1976
28. Marcal, P.V., "Elastic-Plastic Behavior of Pipe Bends With In-Plane Bending," *Journal of Strain Analysis*, **2**, No. 1, 1967, pp.84-90.
29. Spence, J. and Findlay, G.E., "Limit Load for Pipe Bends Under In-Plane Bending," *Proc. 2nd Int. Conf. on Pressure Vessel Technology, San Antonio*, 1-28, 1973, pp.393-399
30. Calladine, C.R., "Limit Analysis of Curved Tubes," *Journal of Mechanical Engineering Sciences, Institute of Mechanical Engineers*, **16**, No.2, 1974, pp 85-87
31. Goodall, I.W., "Large Deformations in Plastically Deforming Curved Tubes Subjected to In-plane Bending", Research Division Report RD/B/N4312, Central Electricity Generating Board, UK, 1978.
32. Griffiths, J.E., "The Effect of Cracks on the Limit Load of Pipe Bends Under In-plane Bending : Experimental Study", *Int. J. of Mech. Sciences*, **21**, 1979, pp 119-130

33. Touboul, F., Ben Djedidia, M. and Acker, D., "Design Criteria for Piping Components Against Plastic Collapse : Application to Pipe Bend Experiments", *Pressure Vessel Technology, Proceedings of 6th International Conference held in Beijing, 11-15th Sept., 1988*, Edited by Cengdian, Liu and Nichols, R.W., 1989, pp 73-84.
34. Drubay, B., et al., "A16 : Guide for Defect Assessment and Leak-Before-Break Analysis", Third Draft, Commissariat A L'energie Atomique, Rapport DMT 96.096, France, 1995
35. Goodall, I.W., "Lower Bound Limit Analysis of Curved Tubes Loaded by Combined Internal Pressure and In-plane Bending Moment", Research Division Report RD/B/N4360, Central Electricity Generating Board, UK, 1978
36. Rodabaugh, E.C., "Interpretive Report on Limit Load Analysis and Plastic Deformations of Piping Products", *Welding Research Council Bulletin*, No.254, 1979, pp 65-82.
37. Hilsenkopf, P., Boneh, B. and Sollogoub, P., "Experimental Study of Behaviour and Functional Capability of Ferritic Steel Elbows and Austenitic Stainless Steel Thin-Walled Elbows", *Int. J. of Pres. Ves. And Piping*, **33**, No.2, 1988, pp 111-128.
38. Shalaby, M.A. and Younan, M.Y.A., "Limit Loads for Pipe Elbows with Internal Pressure Under In-plane Closing Bending Moment", *J. of Pres. Ves. Technology, Transactions of the ASME*, **120**, No.1, 1998, pp 35-42.
39. Shalaby, M.A. and Younan, M.Y.A., "Limit Loads for Pipe Elbows Subjected to In-plane Opening Moment and Internal Pressure", *Paper Presented at the 1998 ASME/JSME Joint Pressure Vessels and Piping Conference held at San Diego, California, July 26-30, 1998*, PVP-Vol.368, 1998, pp 163-170.
40. Chattopadhyay, J., Venkatramana, W., Dutta, B.K. and Kushwaha, H.S., "Limit Load of Elbows Under Combined Internal Pressure and Bending Moment", *Proceedings of the 15th International Conference on Structural Mechanics in Reactor Technology, SMiRT, Vol.V, Korea, 1999*, pp 281 – 288
41. Paris, P.C., Tada, H., Zahoor, A. and Ernst, H., "The Theory of Instability of the Tearing Mode of Elastic-Plastic Crack Growth", *Elastic-Plastic Fracture*, ASTM STP 668, J.D.Landes, J.A. Begley and G.A. Clarke, Eds., American Society for Testing and Materials, Philadelphia, 1979, pp 5-36
42. ASTM E 1820 - 99, "Standard Test Method for J-integral Characterization of Fracture Toughness", American Society for Testing and Materials, Philadelphia, 1999

- 42a. International Standard, ISO 12135, Metallic materials-Unified method of test for the determination quasistatic fracture toughness, Reference no. ISO 12135:2002(E), 2002
43. Kastner, W., Rohrich, E., Schmitt, W. and Steinbuch, R., "Critical Crack Sizes in Ductile Piping", *Int. Journal of Pressure Vessel and Piping*, **9**, 1981, pp 197 - 219
44. Moulin, D. and Delliou, P., "French Experimental Studies of Circumferentially Through-Wall Cracked Austenitic Pipes under Static Bending", *Int. Journal of Pressure Vessel and Piping*, **65**, 1996, pp 343 – 352
45. Zahoor, A., "Ductile Fracture Handbook", Vol.3, EPRI-NP-6301-D, N14-1, Research Project 1757-69, Electric Power Research Institute, 1991
- 45a. Williams, M.L., "On the stress distribution at the base of a stationary crack", *J. of Applied Mechanics*, **24**, 1957, pp 109-114
- 45b. O'Dowd, N.P. and Shih, C.F., "Family of crack tip fields characterized by a triaxiality parameter-I: Structure of fields", *J. of Mechanics and Physics of Solids*, **39**, 1991, pp 989-1015
46. Clausmeyer, H., Kussmaul, K. and Roos, E., 'Influence of stress state on the failure behavior of cracked components made of steel' ASME, *Applied Mechanics Rev.*, **44**, no.2, 1991, pp77-92
47. Schuler, X., Blind, D., Eisele, U., Herter, K.H., Stoppler, W., 'Fracture mechanics evaluation of cracked components with consideration of multiaxiality of stress state, *Nuclear Engineering and Design*, **151**, 1994, pp291-305.
48. Eisele, U., Herter, K.H. and Schuler X., 'Influence of the multiaxiality of stress state on the ductile fracture behaviour of degraded piping components', ECF 10, Structural Integrity: Experiments, Models and Applications, Vol.1, Ed. Schwalbe, K.H. and Berger, C., 1-10, 1994
49. Rice, J.R., Paris, P.C. and Merkle, J.G., "Some Further Results of J-integral Analysis and Estimates", *Progress in Flaw Growth and Fracture Toughness Testing*, ASTM STP 536, American Society for Testing and Materials, Philadelphia, 1973, pp 231 – 245
50. Hutchinson, J.W. and Paris, P.C., "Stability Analysis of J-Controlled Crack Growth", *Elastic-Plastic Fracture*, ASTM STP 668, American Society for Testing and Materials, Philadelphia, 1979, pp 37 - 64

51. Ernst, H.A., Paris, P.C., Rossow, M. and Hutchinson, J.W., "Analysis of Load Displacement Relation to Determine J-R Curve and Tearing Instability Material Properties", *Fracture Mechanics*, ASTM STP 677, C.W. Smith, Ed., American Society for Testing and Materials, Philadelphia, 1979, pp 581 - 599,
52. Ernst, H.A. and Paris, P.C., "Techniques of Analysis of Load-Displacement Records by J-integral Methods", NUREG/CR-1222, US Nuclear Regulatory Commission, 1980
53. Ernst, H.A., Paris, P.C. and Landes, J.D., "Estimations of J-integral and Tearing Modulus T from a Single Specimen Test Record", *Fracture Mechanics: Thirteenth Conference*, ASTM STP 743, Richard Roberts Ed., American Society for Testing and Materials, Philadelphia, 1981, pp 476 - 502
54. Zahoor, A. and Kanninen, M.F., "A Plastic Fracture Mechanics Prediction of Fracture Instability in a Circumferentially Cracked Pipe in Bending - Part I : J-integral Analysis", *J. of Pressure Vessel Technology*, Transactions, American Society of Mechanical Engineers, **103**, 1981, pp 352 – 358
55. Zahoor, A., "Ductile Fracture Handbook", Vol.2, EPRI-NP-6301-D, N14-1, Research Project 1757-69, Electric Power Research Institute, 1990
56. Tada, H., Paris, P.C. and Irwin, G.R., *Stress Analysis of Cracks Handbook*, Del Research Corporation, Hellertown, Pa, 1973
57. Chattopadhyay, J., Dutta, B.K., Kushwaha, H.S., Mahajan, S.C. and Kakodkar, A., "A Database to Evaluate Stress Intensity Factors of Elbows with Throughwall Flaws under Combined Internal Pressure and Bending Moment", *Int. J. of Pres. Ves. and Piping*, **60**, pp 71 - 83, 1994
58. Zahoor, A. and Norris, D.M., "Ductile Fracture of Circumferentially Cracked Type 304 Stainless Steel Pipes in Tension", *J. of Pressure Vessel Technology*, Transactions, American Society of Mechanical Engineers, **106**, 1984, pp 399 – 404
59. Miura, N. and Wilkowski, G.M., "J-R Curves From Circumferentially Throughwall Cracked Pipe Tests Subjected to Combined Bending and Tension - Part I : Theory and Numerical Simulation", *J. of Pressure Vessel Technology*, Transactions, American Society of Mechanical Engineers, **120**, 1998, pp 406 – 411
60. Miura, N. and Wilkowski, G.M., "J-R Curves From Circumferentially Throughwall Cracked Pipe Tests Subjected to Combined Bending and Tension - Part II : Experimental and Analytical Validation", *J. of Pressure*

Vessel Technology, Transactions, American Society of Mechanical Engineers, **120**, 1998, pp 412 – 417

61. Baker, A., "A DC potential drop procedure for crack initiation and R curve measurements during ductile fracture tests", ASTM STP 856, American Society of Testing and Materials, Philadelphia, 1985, pp 394 – 410
62. Schwalbe, K-H., Hellmann, D., Heerens, J., Knaack, J. and Muller-Roos, J., "Measurement of stable crack growth including detection of initiation of growth using the DC potential drop and partial unloading methods", ASTM STP 856, American Society of Testing and Materials, Philadelphia, 1985, pp 338 – 362
63. Anderson, T.L., "*Fracture Mechanics: Fundamentals and Applications*", Second Edition, CRC Press, 1995
64. Roos, E., MPA, University of Stuttgart, Germany, Private communication, 1999
65. NISA, 1997, A General Purpose Finite Element Program, Windows NT/95 Production Version, Engineering Mechanics Research Corporation, Michigan, USA.
66. Kussmaul, K., Diem, H.K., Uhlmann, D. and Kobes, H., "Pipe Bend Behaviour at Load Levels Beyond Design" Proceedings of 13th International Conference on Structural Mechanics in Reactor Technology, SMiRT. Brazil. Vol.G., 1995, pp 187-198.
67. Roos, E., Eisele, U. and Silcher, H., "A Procedure for the Experimental Assessment of the J-integral by Means of Specimens of Different Geometries", *Int. J. of Pres. Ves. and Piping*, **23**, 1986, pp 81 – 93
68. Sharobeam, M.H., Landes, J.D. and Herrera, R., "Development of Eta Factors in Elastic-Plastic Fracture Testing Using a Load Separation Technique", *Elastic-Plastic Fracture Test Methods : The User's Experience (Second Volume)*, ASTM STP 1114, J.A. Joyce, Ed., American Society for Testing and Materials, Philadelphia, pp 114 - 132, 1991
69. Chattopadhyay, J., Dutta, B.K., Kushwaha, H.S., "Leak-Before-Break Qualification of 500 MWe PHWR PHT Straight Pipes by J-integral – Tearing Modulus and Limit Load Method", BARC External Report, BARC/1997/E/017, 1997
70. Chattopadhyay, J., Dutta, B.K., Kushwaha, H.S., "Leak-Before-Break Qualification of Primary Heat Transport Elbows of 500 MWe Tarapur Atomic Power Plant", BARC External Report, BARC/1998/E/015, 1998

71. Kumar,V., German,M.D. and Shih,C.F., "An Engineering Approach for Elastic-Plastic Fracture Analysis", EPRI-NP-1931, Project 1287 - 1, Topical Report, Electric Power Research Institute, Palo Alto, CA, 1981
72. Kanninen,M.F., et al, "Towards an Elastic-Plastic Fracture Mechanics Predictive Capability for Reactor Piping", *Nuclear Engg. and Design*, **48**, pp 117 - 134, 1978
73. ASTM E 8M - 89b, "Standard Test Methods for Tension Testing of Metallic Materials [Metric]", American Society for Testing and Materials, Philadelphia, 1989
74. Sumpter, J.D.G., "J_c Determination for Shallow Notch Welded Bend Specimens", *Fatigue and Fracture in Engineering Materials and Structures*, **10**, No.6, 1987, pp 479-493
75. Kashima, K., Matsubara, M. and Miura, N., "Prediction of the Failure Stress From Japanese Carbon Steel Pipe Fracture Experiments", Proceedings of the Seminar on Assessment of Fracture Prediction Technology Piping and Pressure Vessels, NUREG/CP-0037, Nashville, Tennessee, 1990, pp 2.22 - 2.50
76. Wilkowski, G.M., et al., Degraded Piping Program - Phase II, "Summary of Technical Results and Their Significance to Leak-Before-Break and In-Service Flaw Acceptance Criteria", March 1984 - January 1989, NUREG/CR-4082, BMI - 2120, Vol.8, 1989
77. Roos,E., Herter,K.-H. and Otremba,F., "Testing of Pressure Vessels, Piping, and Tubing", ASM Handbook, Vol.8, *Mechanical Testing and Evaluation*, Eds: Howard Kuhn and Dana Medlin, American Society of Metals, 2000,
78. Darlaston, B.J., Bhandari, S., and Franco, C., "Predictions of Failure for Several of the International Pipe Tests Using the R6 Method", Int. Conf. Pressure Vessel Tech. Proc., Vol.1 Design Analysis, Paris, May/June, 1992
79. Forster, K., Gruter,L., Setz,W., Bhandari,S., Debaerie,J.P., Faidy,C. and Schwalble, K.H., "Crack Resistance of Austenitic Pipes with Circumferential Through-Wall Cracks", *Int. J. of Pressure Vessel and Piping*, **65**, 1996, pp 335 – 342
80. Joshi, D.G., Kumar,V., Kar,S., Chadda,V.K., Nigam,R.K., Chattopadhyay,J., Sunil,K.P., Dutta,B.K. and Kushwaha,H.S., "Image Processing System for Fracture Experiments of Piping Components", BARC Internal Report, 1999

81. Kopenhoefer, K., Gullerud, A.S., Ruggieri, C., Dodds, R.H., Jr., WARP3D-RELEASE 10.8, 'Dynamic nonlinear analysis of solids using a preconditioned conjugate gradient software architecture', User's manual, University of Illinois, Urbana, Illinois, USA, 1998.
82. Pavankumar, T.V., Chattopadhyay, J., Dutta, B.K. and Kushwaha, H.S., "Transferability of specimen J-R curve to straight pipe with through wall circumferential flaw", *International Journal of Pressure Vessels and Piping*, **79**, 2002, pp 127 – 134
83. Joyce, James A. and Link, Richard E., "Application of two parameter elastic-plastic fracture mechanics to analysis of structures", *Engineering Fracture Mechanics*, **57**, 1997, pp 431-436
84. Kumar, V., et al, "Advances in Elastic-Plastic Fracture Analysis", EPRI-NP-3607, Electric Power Research Institute, 1984
85. Brust, F.W., "Approximate Methods for Fracture Analysis of Throughwall Cracked Pipes", NUREG/CR-4583, United States Nuclear Regulatory Commission, 1987
86. Chattopadhyay, J., Nathani, D.K., Dutta, B.K. and Kushwaha, H.S., "Closed-Form Collapse Moment Equations of Elbows Under Combined Internal Pressure and In-plane Bending Moment", *J. of Pressure Vessel Technology*, Trans., American Society of Mechanical Engineers, **122**, 2000, pp 431 - 436

Curriculum Vitae

Personal Data

Name : Jayanta Chattopadhyay
Date and Place of Birth : 4th August, 1966 at Canning Town, West Bengal (India)

School Education

1972 to 1975 Primary education at St. Gabriel School at Canning Town, West Bengal (India)

1976 to 1982 Secondary Education at David Sassoon High School at Canning Town, West Bengal (India)
Passed Secondary Examination under West Bengal Board of Secondary Education in June, 1982

1982 to 1984 Higher Secondary Education in Science Discipline at David Sassoon High School at Canning, West Bengal (India)
Passed Higher Secondary Examination under West Bengal Council for Higher Secondary Education in July, 1984

University Education

1984 to 1988 Bachelor of Mechanical Engineering from Jadavpur University, Kolkata (India)
Passed final examination in 1988

1993 to 1995 Master of Technology in Mechanical Engineering with specialisation in Design Engineering from Indian Institute of Technology, Bombay
Passed final examination in 1995
(Sponsored by BARC)

Work Experience

1988 to 1989 One year training at Bhabha Atomic Research Centre (BARC)

1989 to 2004 Working in BARC as Scientific Officer
Specialisation : Fracture Mechanics, Finite Element Analysis